NASA TECHNICAL MEMORANDUM

NASA TM-76953

AUTOMATIC EVALUATION OF INTERFEROGRAMS

F. Becker

Translation of "Zur automatischen Auswertung von Interferogrammen, Max-Planck Institut fuer Stroemungsforschung, Goettingen, West Germany, Mitteilungen No. 74, (ISSN 0374-1257), 1982, pp 1-106

(NASA-TM-76953) AUTOMATIC EVALUATION OF INTERFEROGRAMS (National Aeronautics and Space Administration) 77 p HC A05/MF A01
CSCL 20F

N84-21291

Unclas
G3/74 18446

NATIONAL AERONAUTICS AND SPACE ADMINISTRATION

WASHINGTON, D.C. 20546

SEPTEMBER 1982

STANDARD TITLE PAGE

1. Report No. NASA TM-76953	2. Government Accession No.	3. Recipient's Catalog No.
4. Title and Subtitle: Automatic Evaluation of Interferograms		5. Report Date: Sept. 1982 6. Performing Organization Code
7. Author(s): Friedhelm Becker, Max Planck Institute, Göttingen		8. Performing Organization Report No. 10. Work Unit No.
9. Performing Organization Name and Address: Leo Kanner Assoc., Redwood City, CA 94063		11. Contract or Grant No. NASw-3541 13. Type of Report and Period Covered: Translation
12. Sponsoring Agency Name and Address: NASA, Washington D.C. 20546		14. Sponsoring Agency Code

15. Supplementary Notes: Translation of "Zur automatischen Auswertung von Interferogrammen," Max Planck Institut fuer Stroemungsforschung, Goettingen, West Germany, Mitteilungen No. 74, (ISSN 0374-1257), 1982, pp 1-106

16. Abstract: A system for the evaluation of interference patterns has been developed. For digitizing and processing of the interferograms from classical and holografic interferometers a picture analysis system based upon a computer with a television digitizer has been installed. Depending on the quality of the interferograms, four different picture enhancement operations may be used: Signal averaging, spatial smoothing, subtraction of the overlayed intensity function and the removal of distortion-patterns using a spatial filtering technique in the frequency spectrum of the interferograms. The extraction of fringe loci from the digitized interferograms is performed by a floating-threshold method. The fringes are numbered using a special scheme after the removal of any fringe disconnections which appeared if there was insufficient contrast in the holograms. The reconstruction of the object function from the fringe field uses least squares approximation with spline fit. Applications are given.

17. Key Words (Selected by Author(s))	18. Distribution Statement: Unclassified-Unlimited		
19. Security Classif. (of this report): Unclassified	20. Security Classif. (of this page): Unclassified	21. No. of Pages	22. Price

NASA-HQ

CONTENTS

1. Introduction

Interferometric measuring methods achieved an important place in the area of length, elongation and surface-measuring techniques several decades ago, especially when dealing with measuring accuracies in the lightwave range. For physical-streaming investigations, interferometers are used for the analysis of the behavior of gas flows, especially instationary transsonic flows, since they cause no distortion of the flow due to probes and register the entire measured range. With the introduction of holographic methods, interference methods have penetrated primarily into the area of industrial laboratory and production inspection.

With the increasing use of such methods the problem of the evaluation of interferograms becomes evident, especially when we are dealing with continuous quality inspections in industry, with large interferogram series in the investigation of instationary processes, when high accuracy requirements exist or the reconstruction of three-dimensional density fields from several interferograms taken in various directions is to be performed via tomographic methods. The qualitative evaluation of the interferograms has been usually done by hand by tracking and counting off the fringes or direct interpolation at support points and it is thus very time-consuming.

In order to permit the scientific, technical and economical utilization of interferometric methods on a quantitative level, an automation of the evalaution of interference patterns is desired.

For the analysis of simple interference fringe-field characterized by a small number of similar-shaped fringes running perpendicular to the scan direction and having good contrast, as generally occur in the quality testing of optical components, automation of evaluation has already been described in the literature [1,2], or in the form of test instruments on the market (ZYGO interferometer system) which are not suitable for the evaluation of complex interferograms due to the prerequisites of the interferograms and to the systems being tailored for specific purposes (manual input of additional information is required, resolution insufficient).

In the area of the holographic analysis of diffusely-reflecting surfaces, like the non-destructive testing of materials, several papers on automated evaluation are found in the literature [3-7]. The described systems are largely still under development and apparently will not be used in automatic testing operation. In all cases, holographic methods with several reference beams are used; these have several advantages for automatic evaluation.

In [3] and [4] several reconstructions of the object photographed with two reference beams are used to calculate the object phase at each point; the reconstructions are produced with a programmable phase difference between the reference beams. In [3] the phase at each point of the object is determined by photographs of four reconstructions and solution of a system of equations, whereas in [4], the counting direction of the strips is determined by consideration of the shift-direction

after introduction of a phase difference of the one reference beam. In the last case however, only the intensity profile along a manually specified fringe is evaluated. A deep-pass filter is used for signal enhancement and this limits the fringe density significantly.

In [5] a method is described with which distance changes of the fringes are determined in the scan direction by adapting sine-functions in sections, to the intensity distribution in the line direction in order to have the fringe extrema more precisely. Here as also in [6] an image subtraction of two reconstructions of the object for a 180 degree shifted reference beam phase, is performed for interference suppression and for background delimitation. In [6] the fringes are determined as zero-points of the intensity distribution after image subtraction, and based on knowledge of the deformation properties of the object, the object phase along an evaluation line can be determined there by ascending numbering of the nearly parallel field.

To determine the three components of the deformation vector, in [7] three interferograms obtained by different directions of the illumination beam, were taken with a video camera. After subtraction of the background brightness and a picture smoothing, the fringes have to be numbered manually and incorrect fringe points have to be eliminated by hand and corrected.

In all these methods, properties of special holographic photography are used in part to determine the direction or absolute fringe shift; the fringe fields are limited to very simple structures or the methods are considered semi-automatic due to the need for manual inputs and corrections, so that the evaluation steps performed there cannot be used for the automatic evaluation of classical interferograms desired here, and the tire-test holograms taken with a reference beam cannot be used, since both interferogram types are characterized by the appearance of random fringe loci which can yet be distrubed by certain object properties (like e.g. compression jolts in flow interferograms).

In this paper an interferogram evaluation method is described which can be applied to nearly any fringe loci and which conducts a reformation of the fringe field into an object function via 2-dimensional polynomial approximations after presentation of the fringes as polygon sections and numbering of these lines.

The selection of a TV scan method with line-by-line digitalization for acquisition of interferograms is favored by the speed and plentiful supply of video cameras with special picture tubes and by the attainable resolution which can be achieved with the image storage systems available on the market at the beginning of the project which are in a reasonable price range. Several devices since appearing on the market have improved resolution (Matrox, Hamamatsu, Quantex) and can indeed be used with the system, especially if they are suitable for a specific picture pre-processing (e.g. picture smoothing) after suitable hardware modification. In this paper, no special hardware was developed for picture-data pre-processing, since the emphasis was on the evaluation of interferograms and their processing.

After a brief discussion of interferometric measuring methods and of object reconstruction from interferograms, the system components of the evaluation system, like computer hardware, input and manipulation of graphic data, digitalizing of interferograms and picture preprocessing, interference fringe recognition and numbering, elimination of any occurring evaluation errors, presentation of object function via polynomial approximation and the final evaluation are described and an application to the analysis of double-illumination holograms of vehicle tires made by Continental Rubber works [8] is given, together with an evaluation of Mach-Zehnder interferograms of instationary jet streams by the MPI for flow reasearch [9-11].

1.1 Interferometric Measurement Methods

Interferometric measurement methods serve for the determination of distances, surface-deviations and changes in refractive index from path differences of two coherent monochromatic light bundles. In the case of classical interferometry, these light bundles are produced by beam splitting. Interference results due to the combining of both beams after passing one beam through the object and diverting the other beam around the object along another path.

Whereas with classical interferometry, only phase objects or deformations of reflected surfaces can be measured, by using holographic interferometry, deformations or shifts of diffusely-reflecting surfaces are measurable with lightwave accuracy, which is an important prerequisite for application of such methods in industrial quality control (QC)[3,5,8]. In holographic interferometry, both wave fields (the one disturbed by the object and the reference field) are overlapped on a hologram plate by double illumination or application of real-time methods. Since both wave fields transit the same path and also large coherence lengths are present when using laser light, the quality demands of the optical components are not so extreme as in classical interferometry, which means that holographic methods are being used increasingly in the investigation of large object fields [8, 12].

1.1.1 Interference Methods in Gas Dynamics

The use of interferometric methods in gas dynamics refers back to the change in refractive index of compressible media, known as the Gladstone-Dale relation:

$$n - 1 = K\rho \qquad (1.1.1)$$

Here, n is the refractive index of the medium, ρ is the density and K a proportionality factor which is constant for the particular gas over a broad range of pressure and temperature. Incompressible media can also be investigated interferometrically, if e.g. sufficiently large density gradients occur due to temperature fields or mixing of various media.

The optical path of a light beam spreading out in the z-direction which passes into the medium at point (x,y,0) and leaves it at point (x,y,1)(neglecting a deflection of the beam due to a change in refrac-

tive index perpendicular to the beam direction) is:

$$Q(x,y) = \int_0^{l(x,y)} n(x,y,z)\, dz. \qquad (1.1.2)$$

By using an interferometer, e.g. a Mach-Zehnder interferometer, this path is measured by comparison with a reference path and measurement of the phase change as a shift of the interference pattern.

If $n_o(x,y)$ is the reference refractive index and λ is the wavelength of light, then the fringe shift N is obtained at point (x,y) by

$$N(x,y) = \frac{1}{\lambda} \int_0^{l(x,y)} [\, n_o(x,y) - n(x,y,z) \,]\, dz \qquad (1.1.3)$$

From this follows that only one refractive index $\bar{n}(x,y)$ averaged over the integration path can be determined from the interference fringe-shift function N(x,y) and that this is only possible when the function l(x,y) is known. From this definition of N(x,y) it follows that the fringe shift is taken positively when the refractive index and thus the density are reduced. If equation (1.1.1) is converted into the form below through introduction of the stationary quantities ρ_o and n_o,

$$\rho/\rho_o = (n - 1) / (n_o - 1) \qquad (1.1.4)$$

then by means of equation (1.1.3) the density change for planar flows of depth l can be computed:

$$\bar{\rho}(x,y) / \rho_o = 1 - \frac{1}{n_o - 1} \frac{\lambda}{l} N(x,y) \qquad (1.1.5)$$

In order not to have to recompute the rest refractive index n_o for each measurement, equations valid within broad limits are used for a gas for the change in refractive index, as a function of pressure and absolute temperature [13]:

$$n_o(T_o, \rho_o) - 1 = [\, n_o(T,\rho) - 1 \,] \frac{T}{\rho} \frac{\rho_o}{T_o} \qquad (1.1.6)$$

and for the relative density in the flow field [11] the expression below is obtained:

$$\bar{\rho}(x,y)/\rho_o = 1 - \frac{1}{n_o(T_o, \rho_o) - 1} \frac{\rho_o}{T_o} \frac{T}{\rho} \frac{\lambda}{l} N(x,y) \qquad (1.1.7)$$

A fringe shift N of the interference field at point (x,y) is thus proportional to the change in density. If the interferometer is set to fringe width of infinite length, i.e. in the rest-state the optical path length at all points (x,y) is the same, then the density on the interference lines is constant. But often a parallel fringe field (wedge field) is overlapped to increase sensitivity and to detect a reversal of fringe order in the investigation of small phase objects and naturally, this must be taken into account in the evaluation.

For three-dimensional flows, the density can then be computed from the fringe shift, if certain symmetry properties (axial symmetry, conical streaming) are present.

1.1.2 Holographic Interferometry

In a holographic photograph, that interference pattern generated at the location of the hologram plate is registered which results from overlapping of the object beam U_O --which is either diffusely reflected from the object or has passed through it, in the case of transparent objects--with the reference beam U_R. Thus, not only the amplitude, but also the relative phase of the object wave to the reference beam is registered. It is thus possible to reconstruct the wavefield of the object by means of the reference beam.

The complex amplitude U at distance r from a spherical wave is defined by:

$$U(r) = \frac{|A_p|}{r} \exp i(k r + \phi) \qquad (1.1.8)$$

where A_p is the amplitude, ϕ is the phase of the wave and $k = 2$ is the wave vector.

Thus, the intensity at point (x,y) of the hologram [14] results as:

$$\begin{aligned} I(x,y) &= |U_o + U_R|^2 \\ &= |U_o|^2 + |U_R|^2 + U_o^* U_R + U_o U_R^* \\ &= |U_o|^2 + |U_R|^2 + 2|U_o||U_R| \cos(k(r_o - r_R) + \phi_o - \phi_R) \end{aligned} \qquad (1.1.9)$$

For incoherent light, only the first two terms of the intensity distribution are left, since through statistically occurring phase changes, the last term (so-called interference term) is zero on the average, in all observed time intervals. During the exposure time, the hologram plate receives the energy $E = I \cdot t$. After development, the transparency of the plate is proportional to E if the recording is made in the linear section of the transparency curve $T = f(E)$ of the film material, which is approximately the case when the amplitude of the reference beam is much greater than that of the object beam. If the amplitude of the reference beam is nearly constant over the hologram plate, then according to [14] we have the following expression for the transparency of the plate:

$$T(x,y) \simeq T_o - \beta t (U_o^* U_R + U_o U_R^*). \qquad (1.1.10)$$

If this plate is now illuminated during reconstruction by a wave $\hat{U}_R$, then the following wave distribution results directly behind the plate:

$$\begin{aligned} T\hat{U}_R &= T_o \hat{U}_R && \text{(transiting light)} \\ &- \beta t\, U_o U_R^* \hat{U}_R && \text{(wave front of the direct image)} \\ &- \beta t\, U_o^* U_R \hat{U}_R && \text{(wave front of the conjugated image)} \end{aligned} \qquad (1.1.11)$$

If we take the reference wave itself for the reconstruction, then the second term in (1.1.11) generates the same wave front (except for an amplitude factor) behind the hologram as the original object, i.e. an observer sees, when looking through the hologram at the location of the object, a virtual image of it. In double-illumination holography, two wave fronts corresponding to two states of the object, are registered in chronological sequence on a hologram plate. In the reconstruction, the wave fronts now released simultaneously, interfere with each other and produce an interference pattern which is superimposed on the intensity distribution of the object.

The real-time method operates similarly: The hologram is developed after the first photograph, but remains installed in the beam path. The interference pattern results through viewing the object through the hologram where dynamic object changes are observed directly and e.g. can be registered photographically [15].

For the double illumination (exposure), the intensity distribution I'

$$I' = |U_o'|^2 + |U_R'|^2 + U_o'^* U_R' + U_o' U_R'^* \qquad (1.1.12)$$

of the second object state U_o' with the second reference beam U_R' is added to the intensity distribution I corresponding to the first object state. Now in the reconstruction there results nine different terms, analogous to (1.1.11), four of which correspond to conjugated wave fronts [14]. If both reference beams are the same and equal to the reconstruction beam, then the sum of the two object waves results as a fraction of the wave field.

$$-2\beta t\,|U_R|^2 (U_o + U_o') \qquad (1.1.13)$$

In the case of real-time holography, the reference state stored on the plate is compared directly with the picture of the changed object. Due to the negative sign of the term in (1.1.11) which represents the virtual image, the waves more or less cancel each other out (depending on amplitude of object illumination), so that only the interference fringes are seen for an object change. For this reason, the dark fringes here have the same orders as the bright fringes in the double illumination.

If we are working with two different reference beams in the double illumination, then the fringes can still be changed upon reconstruction. This property is used by Lanzl and Schlüter [7, 16] for an elimination of the background intensity and of fixed disturbances, by taking two pictures of the interference pattern with 180^o-shifted phase of the reference waves and then subtracting them from each other.

From (1.1.10) and (1.1.12) results for the term appearing for the reconstruction, the following expression (instead of 1.1.13):

$$-2\beta t\,|U_R|^2 (U_o - U_o') \qquad (1.1.14)$$

if the phase of the reference beam U_R is shifted by 180^o. The intensity on the camera registering the interference field is ($|U_o| = |U_o'|$, $\Delta\phi$ = phase difference of U_o and U_o')

$$I_1(x,y) = |U_o|^2 + |U_o'|^2 + 2|U_o|\,|U_o'| \cos \Delta\phi(x,y) \qquad (1.1.15)$$

$$= 2|U_o|^2 (1 + \cos \Delta\phi(x,y))$$

Difference-formation with image I_2 taken with phase shifting of the reference beam:

$$I_2(x,y) = 2|U_o|^2 (1 - \cos \Delta\phi(x,y))$$

gives:

$$I(x,y) = 4|U_o|^2 \cos \Delta\phi(x,y) \qquad (1.1.16)$$

By searching for zero points of this intensity change--now possible through a threshold-value analysis with fixed threshold [7]--the fringes can be determined very accurately.

The order of an interference fringe is defined by the optical path difference of the two overlapped fringes emanating from the same object point before and after deformation of the object and appearing in the same hologram point. This observation is justified according to [14] since light emitted from other points is incoherent due to the surface roughness, and thus only the light emanated from equivalent object points generates visible interference.

Let the object point P be illuminated by a light source in S, then at the observation point K the optical path difference D results when moving the object point P to P':

$$D = (\overline{SP} - \overline{KP}) - (\overline{SP'} - \overline{KP'}) \qquad (1.1.17)$$

If we introduce the shift vector $\bar{u}$ which moves the object point P to P' and the unit vectors $\bar{h}$ in direction SP and $\bar{k}$ in direction PK and also take into account that the shift $\bar{u}$ is small, then the optical path difference D can be expressed as the first term of a series expansion as [14]:

$$D = \bar{u} \cdot (\bar{k} - \bar{h}) = \bar{u} \cdot \bar{g} \qquad (1.1.18)$$

The fringe order $N(x,y) = D(x,y/\lambda$ thus depends not only on the shift of the object point, but also on the observation and illumination direction. Several methods for evaluation of the object-shift vector $\bar{u}(x,y)$ from the interference-fringe field are based on this method.

According to the static method [17] the interference field is registered from three different directions. The shift vector is then known with respect to one of the coordinate systems specified by the three directions $\bar{g}_i$ and can be converted into object coordinates by a transformation. Since it may be difficult to use three sufficiently different observation directions, the object can be illuminated by three different illumination beams [17] which is equivalent to a

variation of the vector $\bar{h}$. A second difficulty is the determination of the absolute fringe order. The fringe order N = 0 exists where $\bar{u} = 0$, i.e. no object deformation occurred. Thus, at this point, no affect on the fringe system occurs through changing the object illumination or the observation direction. If there are no such points on the object, then additional information about the absolute fringe order must be obtained through additional measurements at several object points, by the introduction of known physical criteria, or by taking several photographs with different object deflections.

In the method of Dändlicker et al. [18] in the reconstruction, the frequency of the one reference beam is changed by the amount which leads to an electronically measurable intensity modulation:

$$I \simeq I_o + 2|U_o|\,|U_o'| \cos\left(\frac{2\pi}{\lambda} D - 4\pi \Delta\nu\, t\right) \qquad (1.1.19)$$

The interesting quantity D--the phase shift of the two waves--can now be measured by comparison with a reference signal derived from an unchanged position between the photographs, from the phase relation of the two signals. The accuracy is to ~1/1000 fringes. If the location of the derivation of the reference signal is fixed, then for D we have the absolute phase shift.

The dynamic evaluation method [3, 17, 19] uses the change of fringe order at point P, when the observation direction is changed from $\bar{k}_{oi}$ to $\bar{k}_i$. With three of these measurements, we obtain [14]:

$$\lambda \Delta N_i = \Delta D_i = \bar{u} \cdot (\bar{k}_i - \bar{k}_{oi}) = \bar{u} \cdot \bar{f}_i \qquad (i = 1, 2, 3) \qquad (1.1.20)$$

In this case, the absolute fringe orders need not be known for a calculation of $\bar{u}$, only the sign of the fringe shift and the vectors $\bar{f}_i$ are needed.

1.2 Topology of an Interferogram and Object Reconstruction

Through the interferometric imaging process (sec. 1.1) the object function, i.e. the function of the optical path-length difference at the object point (x,y) $D(x,y) = N(x,y) \cdot \lambda$ is imaged subjectively on the interval $[0.2 \cdot I_o]$ by a periodic function:

$$I(x,y) = I_o \left[1 + \cos(2\pi N(x,y))\right] \qquad (1.2.1)$$

whereby I(x,y) is the intensity distribution in the interferogram. The calculation of the object function which first needs the interference ordering function N(x,y) comes from the formation of the inverse function of (1.2.1) which is generally not possible in closed form due to the ambiguity of the imaging. To reverse the imaging the interference fringes must be numbered in accord with the optical path length at the location of the fringe. The numbering criteria are derived in part from the profile of the fringes and from external, boundary conditions.

The lines of an interferogram where the intensity or blackening has a maximum, are the contour lines of the interference ordering function $N(x,y)$, i.e. on a contour line i, $N(x,y) = n_i$ is constant.

If we presume the function $N(x,y)$ is continuous, then for the contour lines, we have:

1) For constant spacing of contour lines in the z-direction, i.e. $\Delta n = n_i - n_{i-1}$ for all i, the following expression applies for the difference of function values $N(x,y)$ on two neighboring contour lines:

$$\Delta N = 0 \qquad (1.2.2)$$

or

$$|\Delta N| = \Delta n.$$

If we select whole numbers as contour-line constants n_i, then the contour lines represent the dark and bright interference fringes. From (1.2.2) it follows that the difference of fringe order of two neighboring interference fringes can only be 0 or $\pm$ 1. If we know the local ascent behavior of the function $N(x,y)$, then from a knowledge of the constants of a contour line, the constants of the other contour lines can be determined.

2) Contour lines can never intersect when they are not imaged by the same constant n_i; for interference fringes, this means when they do not have the same order.

3) A contour line can not end except at the edge of the considered region. An exception is the annular, closed contour lines or peaks generated by convolution. (But in theory, an annular line can degenerate to a single (double)-line, it must then nevertheless be treated as an annular line).

If the local ascent-behavior of the function $N(x,y)$ is not known, then in general not all constants of the contour lines or numbers of the interference fringes can be determined precisely. For example, in a region with annular fringe profile, under some circumstances we cannot determine whether the order increases or decreases. Even for a fringe profile in the direction of a discontinuity or in the direction of a line where the sign of the gradient of the object function changes, the fringe order generally cannot be determined from the neighboring fringes.

Through suitable selection of photographic technique it is generally possible that the interferograms have two other properties:

4) The function $N(x,y)$ is very flat in a region crossed by several contour lines and under some circumstances, even monotonous (i.e. the contour-line difference is adjusted accordingly, e.g. through overlapping a wedge-field, by tipping an interferometer mirror or changing one beam path for double-exposure holography, perhaps by using a hollow prism filled with different gases).

5) For a string of time-dependent, continuous functions $N(x,y,t)$ with $\Delta_n(x,y) = N(x,y,t_n) - N(x,y,t_{n-1})$; $n = 1, 2, \ldots$ we have $|\Delta_n(x,y)| \ll 1$ for almost all locations (x,y) of the interferogram (i.e. we select $\Delta t = t_n - t_{n-1}$ accordingly).

With the properties 1-5 all contour lines of the function $N(x,y)$ can be designated--except for multiplicative and additive constants which have to be determined through physical criteria or additional measurements--if all annular contour lines can be allocated by comparison with chronologically preceeding or following interferograms.

For the interferograms of instationary, transsonic flows (see fig. 31) the continuity of the function $N(x,y)$ required above cannot be maintained over the entire measured range since discontinuities can occur here due to compression shock.

As for the annular lines, property 5 must be used again and proceed or return to an interferogram in which no discontinuity occurs.

But if a designation of the contour lines should not be possible by utilization of property 5 in certain regions of the interferogram, e.g. due to a stationary ring-structure or a stationary compression shock, then physical criteria must be used (like additional pressure measurements) in order to specify the fringe designation in an interferogram of this series.

The object function $z(x,y)$ is obtained through reconstruction of the function $N(x,y)$ about which we now know only the profile of its contour lines, by means of a two-dimensional interpolation (see also sec. 3.4), possibly by subtraction of a superimposed wedge field and subsequent conversion into the interesting physical quantity, like the density function for flow-interferograms (sec. 1.1.1) or the surface deformation for double-illuminated holograms (sec. 1.1.2).

2. Description of the Evaluation System

The system for evaluation of interferograms consists of the computer hardware and software, input and output of graphic data, picture halftone input, picture halftone output, film projector control and hologram reconstruction device. These components are described in more detail below. Figure 1 shows the configuration of the system.

2.1 Type of Interference Patterns to be Evaluated

The image patterns used at present are Mach-Zehnder interferograms of instationary transsonic flows [9-11] taken with high-speed cameras on 16 mm film and filmed double-illuminated holograms of holographic vehicle tire investigations of Continental Rubber Works Co., Hannover [8]. Figures 2a and 3a show typical examples. The tire-test holograms are reconstructed in a reconstruction device with a He-Ne-laser and imaged with a wide-angle lens on the receiving tube of the video camera. The wide-angle lens is needed because each hologram has a ca. 100° cut-out of the tire tread registered from the inside.

But fundamentally, patterns of other formats can be evaluated with the system, since by replacement of the camera lens, the imaging scale can be adjusted within a large range. For the evaluation of other formats, the automatic feed (film projector) would only have to be adjusted; in a series evaluation this is indespensible.

The picture quality of the Mach-Zehnder interferograms is characterized by relatively good contrast and by a quite uniform illumination of the test object. In addition, in most cases no interfering objects lie in the measured field. In some cases where markings are present in the measured field, they are of fixed location and can be easily accounted for.

The tire-test holograms have a greatly variable, sometimes very low contrast which drops off quickly toward the picture edges.

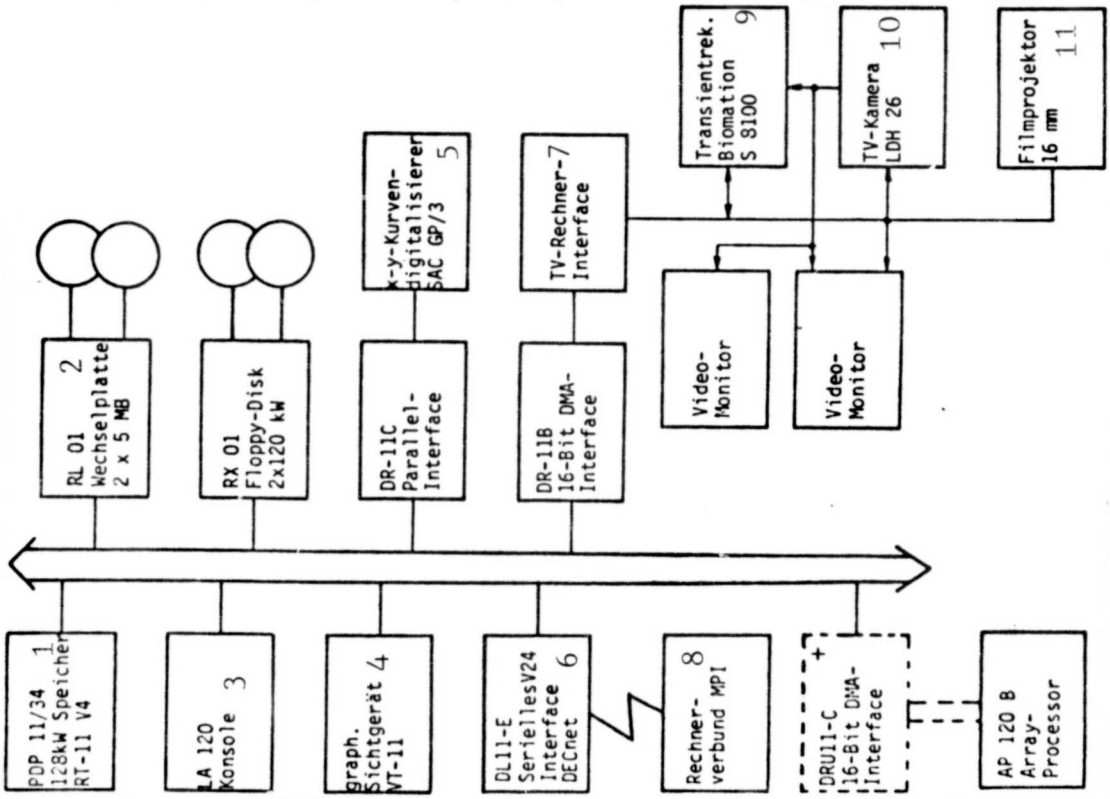

\+ planned, fast data line for use with an array processor which is already used with another project.

Fig. 1a: Configuration Sketch of the Computer System

Key: 1-memory 2-changeable disk 3-console 4-graphic video terminal 5-curve digitizer 6-serial V24 interface 7-TV-computer interface 8-computer link 9-transient rec. 10-TV camera 11-film projector

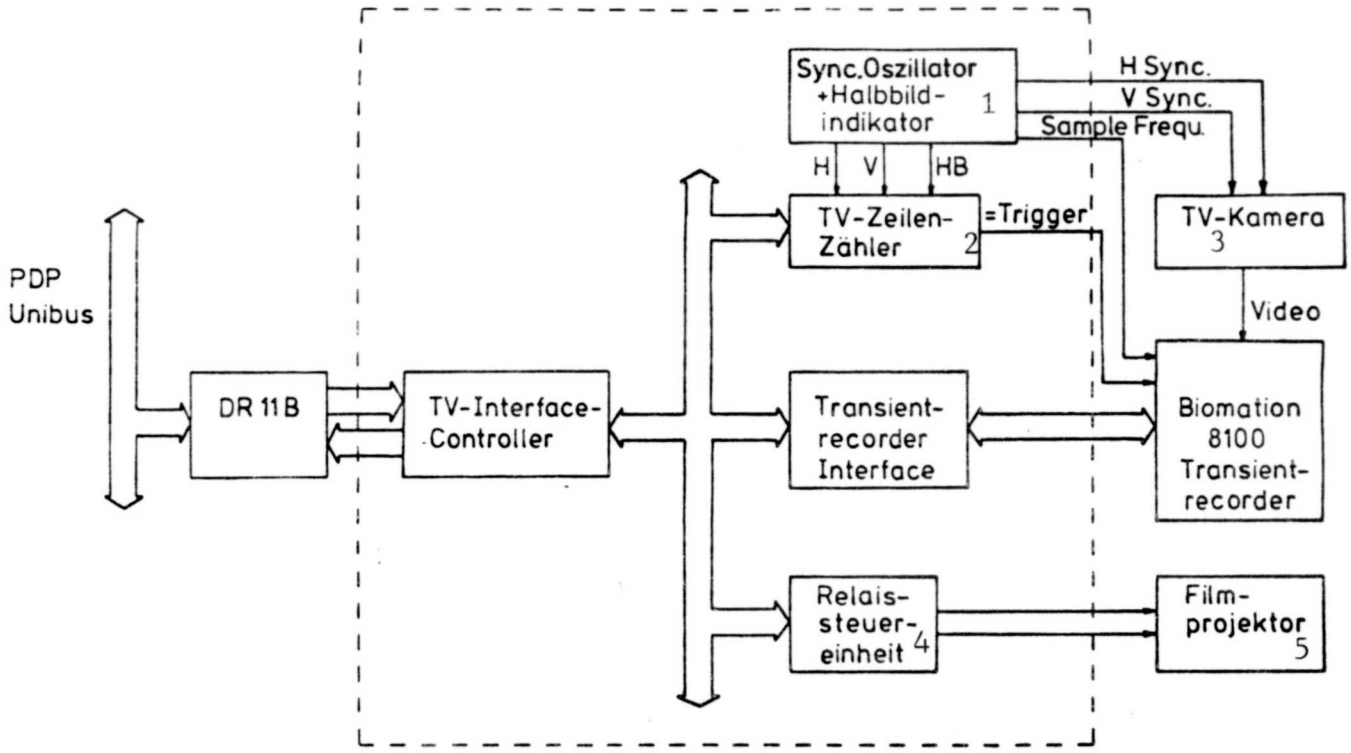

Fig. 1b: Overview Sketch of TV Interface

Key: 1-sync. oscillator & picture halftone indicator 2-TV line counter 3-TV camera 4-relay control unit 6-film projector

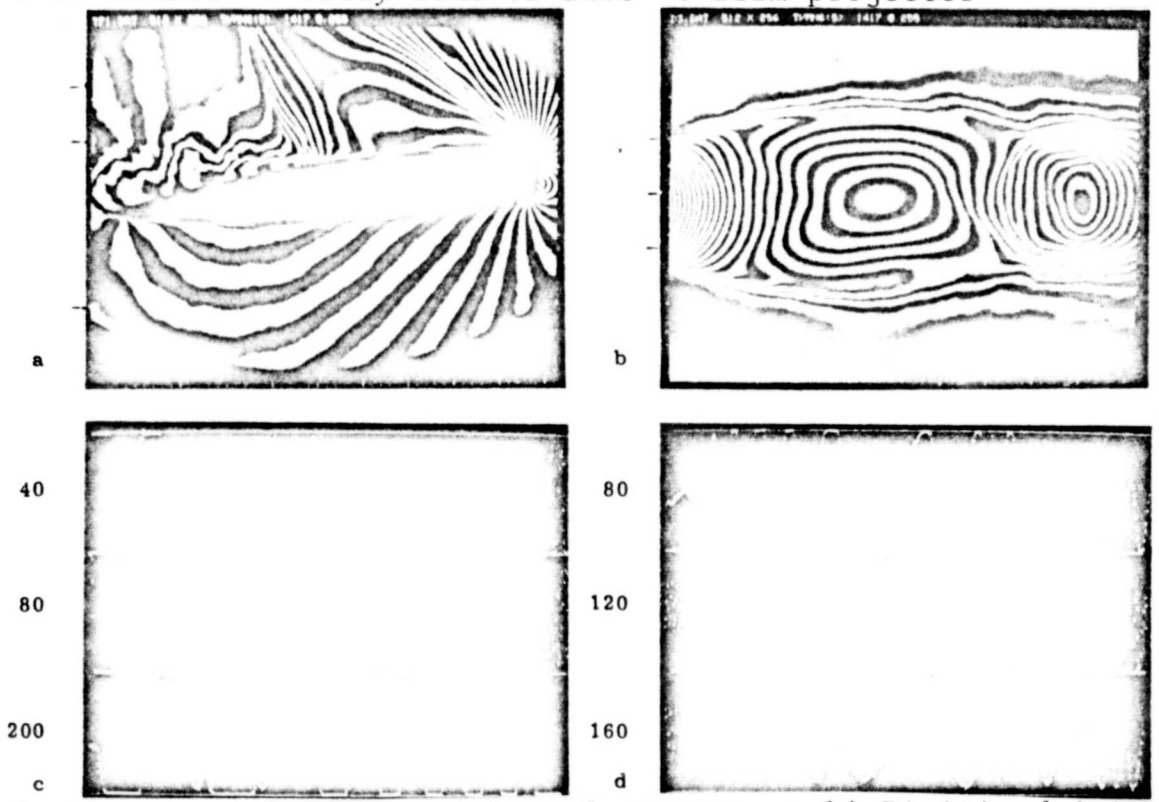

Fig. 2: Examples of Evaluated Interferograms. a,b) Digitized interferograms (resolution 512 x 256 points); c,d) Profile of intensity in line direction using the example of several lines

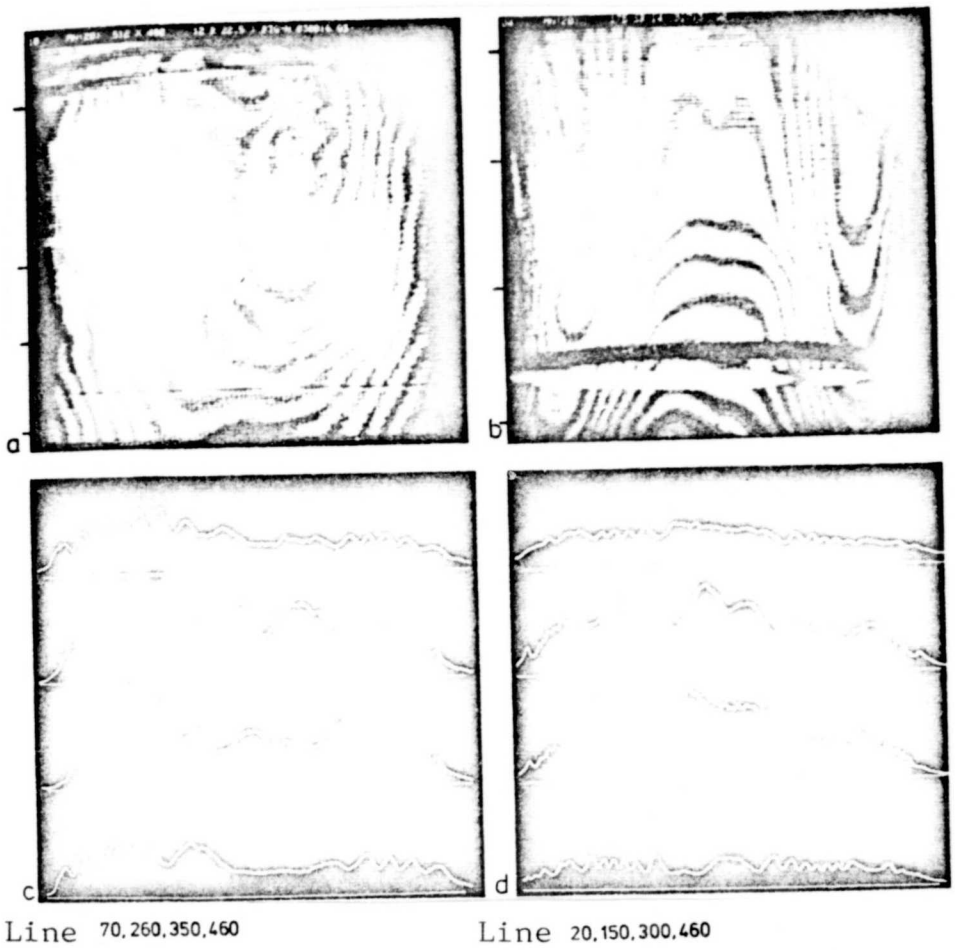

Fig. 3: Examples of Tire Test-Holograms to be Evaluated.

a,b) Digitized holograms, no. 18 or 04 (resolution 512 x 480 points, averaging over 20 TV-pictures

c,d) Profile of the intensity in the line direction using the example of several lines.

Through non-uniform illumination during the hologram photograph and scattering phenomena which lead to an interference pattern on the hologram film, a strong modulation of the background intensity results. Furthermore, hot-bellows impressions are sometimes very prominent. These hot-bellows impressions are narrow compressions running diagonal to the tire-roll direction; they are generated during tire production and are unavoidable. The interference pattern is pushed onto these hot-bellows impressions, sometimes up to one-half the fringe width (see also sec. 4.1) which in some circumstances can lead to wrong interpretations in later evaluation. Since the object is also imaged by the photographic principle, all objects lying in the measured range, like so-called spreaders (the rods which hold the tires apart) and irregular reflections from the tire surface, lead to additional interference. Figures 2b and 3b show typical contrast profiles of interferograms and tire-test holograms.

2.2 Computer Configuration

The computer component consists of a PDP 11/34 computer (Digital Equipment) which is equipped with a 256 kilobyte (KB) MOS memory. As external memory media there is a floppy disc double drive (240 KB each) and two alternating-disc drives RLO1 (5 MB each). In addition, the computer is equipped with a 16 bit parallel interface for connecting a curve-digitizer for input of graphic data, with a 16 bit DMA interface for connection of the image digitizer and with a serial interface (V 24) for communication with a computer-link system (see configuration sketch in fig. 1). For output of graphic data, a graphic video terminal VT-11 (image-repeat type) with light stylus is available. As operating system, the real-time operating system RT-11 is used and as communication software, DECnet/RT by Digital Equipment is used.

The system will have access to an array processor (AP 120 B by Floating Point Systems) after installation of a fast data-link; this processor is already being used in another project. An array processor is a fast, special computer can be perform vector and matrix operations very fast and is suitable for the throughput of large quantities of data. By shifting a large part of the evaluation program, especially the computer-intensive program segments to the array processor, the evaluation time can be reduced (by a factor of 10-50) drastically (see also sec. 3.7).

2.3 Input and Output of Graphic Data

The input of graphic data uses a curve-digitizer (Graf/Pen GP3 by SAC Co.) having a resolution of 4000 x 4000 points. The curve digitizer is connected to the computer via a linkage unit and a 16-bit parallel interface.

The graphic data input is used for the acquisition of interference fringe profiles in the semi-automatic interferogram evaluation where the fringes of the interferograms projected onto the tablet of the digitizer are tracked manually by an evaluator, and for the input of edge contours of objects to be evaluated.

The input of data takes place with the data acquisition program FAW2 with which functions like input of fringe coordinates and designations, display of input data on the screen in the form of polygon sectors, coordinate transformations, execution of a redundance reduction of fringe coordinates, cancellation of data points and polygon sections, and storage of data and display of acquired data structures on the screen, are possible in an interactive mode.

The output of graphic data structures is possible via a plotter (Calcomp 565) at the large computer center of the University (UNIVAC 1100/82, Gesellschaft fuer wissenschaftliche Datenverarbeitung, Göttingen (GWDG)), which can be accessed via a computer-link network.

2.3.1 Redundance Reduction

A method for redundance reduction of a point sequence by U. Ramer [20] will be discussed briefly; it can be used for fringe input by hand, but also for the polygon-section presentation of fringes to be discussed later in connection with automatic evaluation, and also for performing fringe numbering.

A random two-dimensional curve is presumed to be defined by an ordered quantity C of N + 1 points p_i. These points form a polygon P with N sides I_i. The problem of redundance reduction is to find a subset $C' \in C$ of points p'_k so that the corresponding polygon P' fits the curve as well as possible. The set C' of points p'_k splits the quantity C into ordered subsets S_k of the form:

$$S_k = \{p_i, p_{i+1}, \cdots, p_j\} \quad ; p_i = p'_{k-1} \; ; p_j = p'_k \tag{2.3.1}$$

One possible criterion for the formation of quantity C, is a minimum-spacing criterion:

$$f(S_k) \leq \alpha = \text{const.} \tag{2.3.2}$$

with

$$f(S_k) = \max_{p_i \in S_k} \{ \text{DIST} (p_i, \overline{\langle p'_{k-1}, p'_k \rangle}) \},$$

this the max. distance of a curve point p_i to a side of the polygon $\overline{p'_{k-1}, p'_k}$ of the reduced polygon (see fig. 4a).

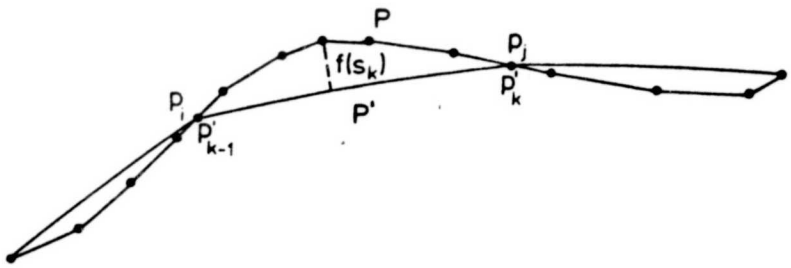

Fig. 4a: Spacing Criterion f (S_k).

A reduction to the minimum number of points for a given bound α is difficult, time-consuming and sometimes impossible. However, if we drop the "Minimum Points requirement", then a simple solution is obtained by an iterative method. The quantity C is split into two subsets and each is tested to see if it meets the spacing criterion. If the distance is greater than the specified bound, then the corresponding subset is again split into two subsets and tested for the distance criteria. If it is met, the corresponding points p'_{k-1} and p'_k become points of the reduced polygon; if the criterion is not met, the subdivision continues. To determine the place where a quantity of points is split into two subsets, the point with max. separation $f(S_k)$ can be used for instance.

The computation of the distance of a curve-point from a line is decisive for the speed of the algorithm. In order to find the point with max. spacing, it will suffice to determine the distance in one coordinate direction.

In order to calculate the point with max. distance to segment $\overline{AB}$ in the curve section (AB) of fig. 4b for example, the maximum of the difference Δy between (AB) and $\overline{AB}$ is determined in the y-direction. The Euclidian distance d_m then results from the cosine of the angle φ between the x-axis and $\overline{AB}$.

$$d_m = \Delta y_{max} \cdot \cos\varphi \quad . \qquad (2.3.3)$$

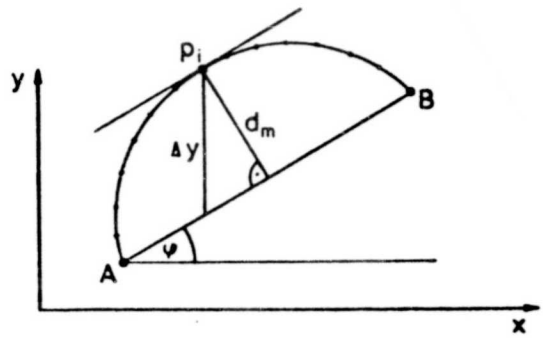

Fib. 4b: Determination of the Spacing

In order to prevent $\cos\varphi$ from becoming too small, the distance is computed in the x-direction if $|\tan\varphi| > 1$.

To shorten the computation time, the calculation of the max. distance in the x- or y-direction is further simplified. We have:

$$\Delta y = y(p_i) - y(A) - (x(p_i) - x(A)) \cdot \tan\varphi \quad . \qquad (2.3.4)$$

To avoid a REAL-multiplication at this point, the quantity $\tan\varphi$ is converted into an INTEGER-number by multiplication with 256 and the REAL-multiplication is replaced by an 8-bit INTEGER multiplication (the point coordinates are INTEGER-quantities. Thus the speed of the algorithm could be increased significantly, since the used computer is not equipped with a hardware-Floating -Point-Processor and thus all REAL-operations have to be performed by the software.

The reduction-speed of a curve depends not only on the number of points, but also on the size of the specified tolerance bound. For small bounds, the polygon section is accordingly split into more subsections for each of which the distance-criterion has to be tested, so that for one point of the polygon section, a distance to a line has to be computed several times. For a small bound (2 raster-point spacing), a speed of ca. 150 points per second results.

2.4 Input and Output of Picture Halftones

The input of the interferograms and holograms into the computer is done by means of a picture digitizer which processes the video signal of a standard video camera. Two video cameras with different receiving tubes are available (LDH 26 and LDH 150 of Philips Co.). One of them is equipped with a 1" Plumbicon tube and the other with a more sensitive 2/3" Newvicon tube; the latter is used for pick-up of relatively weak-light hologram reconstructions. The picture digitizer consists of a programmable transient recorder (Biomation model S 8100) which is connected to the computer via a control interface. This control interface consists of a bus-system to which the individual control elements like synchronization unit, TV-line counter and relay control unit for film-projector control (film projector DF 16B of NAC Co.) are connected. The control interface is of modular design and could easily be expanded by additional units (like e.g. camera positioning etc.). A sketch of the TV-interface is shown in fig. 1b.

The video signal of the TV-camera is taken with the transient recorder with preset frequency (up to 25 MHz) with a voltage resolution of 8 bit, digitized, and then fed to the computer via DMA-transfer. The transient recorder is started by the synchronizatoin pulse of the TV-line where the digitizing is to begin. Depending on selected scan frequency, between 1 and 10 TV-lines are taken per transient recorder burst. The resolution in the line-direction is up to 1600 points for max. ca. 600 lines, but with the video camera currently available, a line resolution of over 1000 points per line cannot be attained.

Since after the scan of a line-sequence until the scan of the next line-sequence, one must wait 20 ms or 40 ms due to the line-return (advance) process, enough time is left for a data transfer into the computer and for simple computation operations (like e.g. picture halftone transformations, signal averaging).

For the resolution of 512 columns and 256 lines or 512 columns and 512 lines normally used by us, scan times of ca. 5 sec. or ca. 10 sec, respectively, result. These times could be reduced to about one-third if three line-sequences were scanned in one TV-frame; this is possible in ca. 5 ms due to the data-transfer time into the computer, but sequential processing would not be possible.

After pick-up of the memory content from the transient recorder, the individual picture lines have to be copied off since the line-beginning of each line in the transient recorder memory and the line-length are governed by the specified scan frequency. The recopying process runs simultaneously via an imaging table in order to attain any desired picture-halftone transformation, e.g. a correction of the film gamma-value or a negative reversal of the digitizing of negative film. The 8-bit values of the digitized lines are taken as the address for an imaging table which contains a mathematically random complicated image. The newly stored picture-halftone is the value which stands in the table at this address:

$$GW_{neu} = \text{Tabelle}\,(GW_{alt}). \qquad (2.4.1)$$

This operation requires appoximately the same amount of time as the imaging of one memory cell into another, if it is programmed in Assembler Code and is thus implemented without time loss.

The subprograms to control the picture digitizer and projector, and those for fast picture-data manipulations like addition, picture-halftone transformation and data transfer into the Virtual-Memory region (memory region of 56 - 248 KB, not normally used by the operating system) are compiled in the TVLIB program library. These programs are written mostly in Assembler in order to keep processing times as small as possible and to simplify creation of some hardware-related programs. All Assembler subprograms can be called up from FORTRAN programs, so that the implementation of complex picture-evaluation programs can be done in the simpler FORTRAN language, without having to take time losses into account.

The output of picture-halftone or binary pictures is needed primarily only in the development phase of the system in order to investigate effects of certain picture-processing algorithms and for documentation purposes.

The picture-halftone output proceeds via the VT-11 video terminal. Of course, 1024 x 1024 points can be addressed on the terminal, but only ca. 2000 points can be displayed simultaneously. The picture output thus occurs through sequential display of individual picture lines, where the impression of a standing picture results through the afterglow of the cathode-ray tube. The terminal can display eight intensity steps, but they are not linearly adjustable nor by a power law and are thus not suitable for the generation of picture-halftones. For this reason, halftone pictures are generated through repeated display of picture points on the screen--depending on brightness--and superimposition of the intensities on a photographic film. The photography occurs in an otherwise darkened room with a Polaroid camera with an open shutter. In order that the output times do not become too long (a point with intensity 256 would have to be displayed 256 times for a linear picture-halftone progression), the 8-bit picture halftones are imaged linearly onto 4-bit values as per the transformation:

$$g_4(x,y) = a\,(g_8(x,y) - g_o) \qquad (2.4.2)$$

where g(x,y) is the picture halftone at point (x,y). The values 'a' and g_o which can be obtained e.g. from the picture-halftone histogram (the percentage distribution of individual halftones), can be preset to permit utilization of the dynamic regions. Now from these 4-bit values, 4 binary output lines $z_n(x_i)$ are generated through the imaging:

$$z_n(x_i) = \begin{cases} 1 \text{ if } g_4(x_i, y_o) \oplus 2^n > 0 \\ 0 \text{ otherwise} \end{cases} \qquad (2.4.3)$$

$n = 0, \ldots, 3$

($\oplus$ logic AND-linkage)

and displayed 2^n-times at the location of line y_o. The output of a picture-halftone of 512 x 512 points with 16 shades of gray lasts ca. 2 min.; the display of a binary picture of the same size lasts ca. 20 seconds.

Since the points of the video terminal are arranged in a square raster, the picture elements of the digitized pictures are not square--depending on the selection of scan frequency and line spacing--a picture bottleneck can occur via the VT-11 terminal upon picture-halftone output, but this will not interfere with the analysis of interferograms.

For the output of picture-halftone and binary pictures, and for the calculation of gray-value histograms, the programs TVDS6, TVDS7A and TVHIS, and subroutines in the TVLIB program library are used.

3. Automated Interferogram Evaluation

The goal of the evaluation of interferograms is the reconstruction of object functions, i.e. the density function for the flow-interferograms and deformation function for the tire-test holograms. In addition, specific structures in the interference patterns are to be recognized and located, through which conclusions can be drawn about the presence of corresponding tire-production defects. For both types of evaluation the acquisition of interference fringe profiles is necessary. For the reconstruction of the density function or deformation function, the relative numbering of the fringes is needed, i.e. the determination of relative light wavelength of each fringe is needed in order to obtain the absolute magnitude of the density or deformation.

The acquisition of interference fringes occurs in the semi-automatic evaluation by means of a curve-digitizer through tracking the fringe profiles by hand [21](see also sec. 2.3). In the fully-automatic evaluation, the fringe profile of interference fringes must be extracted from the digitized picture-halftone, possibly after application of suitable picture preparation steps, by the computer.

After this step, the interferograms or their interference ordering functions, are present in the form of a graphic data structure in the computer and each fringe is represented by two polygon segments which represent the profile of its two flanks. This representation is now checked and corrected as necessary, for the presence of fringe interruptions and misconnections which can originate through weak contrast or through excessive local fringe densities in the holograms.

Then comes the fringe-numbering phase which is designed so that any fringe misconnections not recognized in the preceeding steps, will be detected and resolved.

Interference lines have the same properties as grid lines on a map. Due to this property several important rules result for fringe numbering; other rules arise from the nature of the object (see also sec. 1.2).

From the comparison of the interference fringes with grid lines it follows that the data structure in which the interferograms exist after this step, is not suitable for further numeric-mathematic evaluation. Among the flow-interferograms for example, time-series of the density should be formed from a series of interferograms at specific locations of the measured field in order to compute cross-correlations and phase-plans from this. In the case of turbulent flows, an averaging over several interferograms is also needed to attain comparisons with theoretical results and to eliminate statistical fluctuations. In the case of the tire-test holograms, an investigation of gradients and curvatures of the deformation function, and the determination of a standard deformation surface and the formation of difference interferograms, are provided.

All these operations require that the interference ordering functions be present in a form $F = f(x,y)$. To implement this transformation, a method of weighted two-dimensional polynomial approximation with subsequent spline interpolation is used, which causes the interference ordering functions to be expressed as a set of polynomial coefficients at suitably-selected support points.

In the following sections, the individual process steps like picture preprocessing, interference fringe extraction, fringe numbering and polynomial approximation are presented in more detail. Furthermore, there is a section on Elimination of Distortion from Object Geometries, and a section on computation times needed by the individual steps.

3.1 Preliminary Picture Processing

After the digitalizing of the patterns in many cases it is necessary to perform a picture pre-processing before the extraction of the interference fringes. Spatial and time-averaging methods, gradient formation, subtraction of the averaged intensity distribution, application of two-dimensional filter procedures are all counted in this.

3.1.1 Spatial and Chronological Averaging

The digitized interferograms contain a certain amount of noise which is generated in the hologram preparation and reproduction through speckle formation and scattering, and by the electronic components during interferogram photography and digitizing.

The noise portion due to the camera noise and digitizing is of normal distribution and has an S/N-ratio of ca. 36 dB (for 0.4 V input sensitivity). Thus, an improvement of the signal can be obtained, especially for very low-contrast holograms, through averaging over several chronologically sequential line signals (so-called picture stacking). For the holographic interferograms, the S/N-ratio could be improved by ca. 13 dB through signal averaging. The location- and time-fixed noise (speckles) is reduced by use of a spatial averaging, where the gray-value at each point of the picture is replaced by the

arithmetic average of its 8 neighboring points (program TVMN6, TVMN7A and SMO8). When using spatial averaging methods however, the local resolution is reduced and this is important for high fringe densities. An example of the time and spatial averaging is shown in fig. 5 using two lines from one hologram.

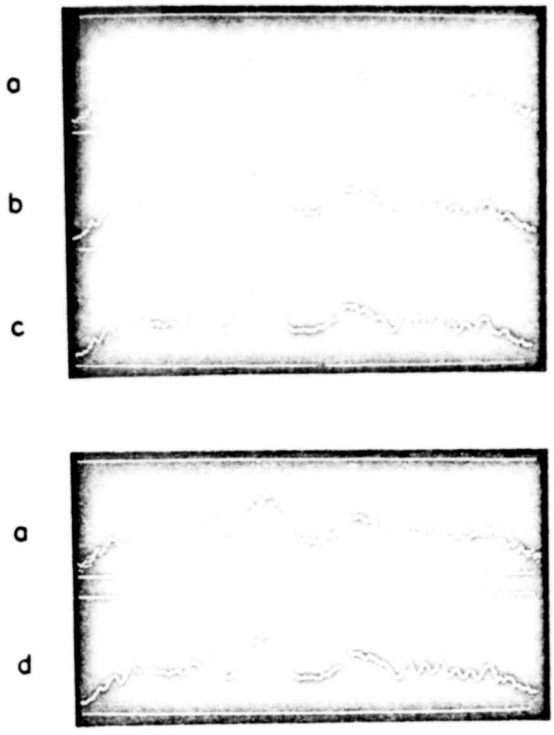

Fig. 5: Line Profile to Demonstrate the Spatial and Chronological Averaging

a) Unaveraged line from a hologram (512 picture points)
b) The same line after averaging over 5 chronologically sequential signals
c) Like b), but averaged over 20 signals
d) Line 'a' after spatial averaging (over 8 neighboring points).

3.1.2 Picture Halftone Transformation

Frequently the actual useful interference pattern is superimposed by a background intensity which preventsuse of threshold-value operations with constant threshold. Thus, the tire-test holograms for instance, have a Gaussian background brightness, caused primarily by the intensity distribution in the laser beam, which is superimposed on the brightness distribution of the object. But a more or less uneven background intensity is present for the interferograms due to the illumination of photography and due to the photographic lens. There are several potentials for eliminating this background intensity. Since the local frequencies of this distortion are very low, they could be eliminated e.g. by a high-pass filter, i.e. by zeroing the corresponding spectral components after a Fourier transformation of the interferogram (see also sec. 3.1.3). The computation effort for

a two-dimensional Fourier transformation is quite high, so that this possibility should only be taken into consideration if a Fourier transformation is required for other reasons.

If we can prepare a "zero picture" for a series of interferograms, i.e. a photograph of the object without interference fringes, and when it is assured that the background intensity distribution does not change in space or time, then the background elimination through subtraction of this zero-picture is performed directly after digitizing after being smoothed somewhat. A similar result could be achieved by averaging a sufficient number of interference patterns, if this "zero picture" is not available.

If no picture-independent basic brightness distribution is present--as is the case for the holograms--it can be obtained from the particular picture by a rough averaging. In order to do this, the picture is split into a regular array of subpictures which may intersect (e.g. with edge lengths of 32 x 32 points) and in the center of these subpictures, the average value of the intensities of all points within the subpicture is written. Through a bilinear interpolation in the meshes of four of these support points, a surface is generated which represents the profile of the background intensity for a suitable selection of subpicture size.

Hologram no. 04, line 350

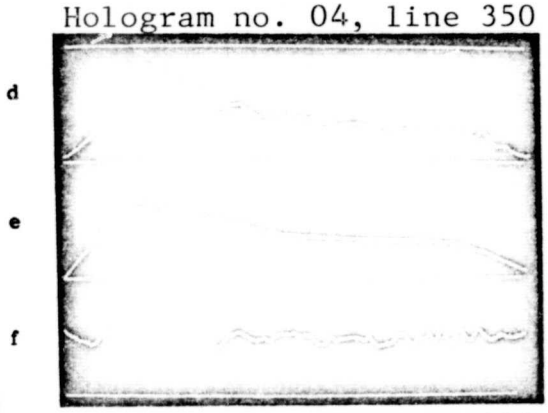

Hologram no. 18, line 100

Fig. 6: Line Profile to Demonstrate The Subtraction of Background Intensities (SUBMF3 program)
a,d) Line from a hologram b,e) Line from the computed surface of average intensity c,f) Hologram line after subtraction of the average-intensity surface

If a subpicture size was too small, then an undesired effect on the obtained background intensity can occur at points with a large-area interference fringe profile.

Figure 6 shows an example of subtraction of the average gray-value surface. A subpicture size of 32 x 32 points was chosen here; it lay over the max. occurring fringe width. Figures 6a and d show line profiles from two holograms. In fig. 6b,e, the corresponding lines of the background intensity are presented, and in fig. 6c,f, the intensity profiles after the subtraction. The subtraction of the average gray-value surface is executed with the SUBMF3 program. An attempt was also made to produce the average gray-value surface after determination of the support values by means of a cubic spline interpolation [22] (SUBMF program), which led to a smooth function profile. The computation times for the evaluation of this 2D spline function--which had to be performed at each point of the picture--are quite high which is why the bilinear interpolation is preferred; it relies essentially on MX INTEGER-divisions and M additions per picture line (MX is the number of subpictures per line, M is the number of points per line). As experience has shown, the discontinuities of the gradient of this function at the mesh boundaries have no disadvantageous effects on interference fringe extraction.

If a method using two or more different reference beams were to be used for photographing and reproduction of the holograms, then the suppression of the background intensity and of scattering phenomena from dust particles could also be computed by forming the difference of two interferograms, which, as discussed in sec. 1.1.2, are obtained by a phase shift of the reference beams in the reconstruction of the hologram. For the tire-test holograms, such methods were not feasible since fundamental changes in the holography system would have been needed.

3.1.3 Interference Removal through Two-Dimensional Filtering

An interference occurring in the tire-test holograms is the interference pattern generated by the hot-bellows impressions, which is probably attributable to a slight shift of the object between the two photos of the double-exposure. This interference is sometimes quite large (shifts of the fringe system up to one-half a fringe width, see fig. 7) and leads to errors even in fringe extraction and impedes a subsequent tire-error analysis since size and shape of the structures generated by the interference pattern do not differ from those structures attributable to tire defects. Thus, it is important to eliminate this disturbing pattern before fringe extraction. The hot-bellows impressions are parallel structures running on a slant to the tire rolling direction; they appear due to the type of hologram photo and reconstruction in the digitized picture approximately as a straight, parallel fringe system which is superimposed on the actual interference pattern.

Due to this regular structure, the 2D Fourier analysis is one possibility for eliminating the disturbing pattern.

As is known from the theory of Fourier optics, the bending of parallel light observed in the distant-field of a 2D structure corresponds to a Fourier transformation of this structure [23].

Optically, the distant-field can be observed through imaging with a lens in the focal plane of the lens. If parallel light is bent at a grid with line spacing 'a', then the diffraction pattern is composed of points with a spacing proportional to 1/a lying on a line oriented perpendicular to the grid lines. The intensity of the points corresponds to the transmission curve of the grid and represents a sin(x)/x-distribution for a rectangular transmission.

If we have a picture of the form f(x,y) where f(x,y) is the gray value at point (x,y), then the Fourier transformation F(u,v) is defined as:

$$F(u,v) = \int_{-\infty}^{\infty}\int_{-\infty}^{\infty} f(x,y)\, \exp(-i2\pi(ux + vy))\, dxdy \qquad (3.1.1)$$

and the retransformation:

$$f(x,y) = \int_{-\infty}^{\infty}\int_{-\infty}^{\infty} F(u,v)\, \exp(i2\pi(ux + vy))\, dudv \qquad (3.1.2)$$

In the 2D Fourier analysis the coefficients of one expansion are computed by two-dimensional sine or cosine functions which represent the relative portion of base functions of the form exp(i2 (ux + vy)) at the affected picture. Thus, F(u,v) is called the space-frequency spectrum of the picture f(x,y). High space frequencies in the picture generate spectral components which lie at places with large u or v in the spectral or Fourier plane. By changing certain spectral components in the Fourier plane, the portions corresponding to certain structures in the picture plane, can be filtered out.

If after digitization, the picture is present in the form of a discrete point-matrix, then formulas (3.1.1) and (3.1.2) are transformed into summations:

$$F(u,v) = \sum_{m=0}^{M-1}\sum_{n=0}^{N-1} f(m,n)\, \exp\left[-i2\pi\left(\frac{mu}{M} + \frac{nv}{N}\right)\right] \qquad (3.1.3)$$

with $u = 0, 1, 2, \ldots, M-1;\ v = 0, 1, 2, \ldots, N-1$ and

$$f(m,n) = \frac{1}{MN}\sum_{u=0}^{M-1}\sum_{v=0}^{N-1} F(u,v)\, \exp\left[i2\pi\left(\frac{mu}{M} + \frac{nv}{N}\right)\right] \qquad (3.1.4)$$

with $m = 0, 1, 2, \ldots, M-1;\ n = 0, 1, 2, \ldots, N-1.$

The indices u and v are called the space frequencies analogous to the continuous form of the Fourier transformation (3.1.1 - 2). To perform the 2D Fourier transformation, the formula (3.1.3) can be rewritten:

$$F(u,v) = \sum_{n=0}^{N-1} \left[\sum_{m=0}^{M-1} f(m,n) \exp\left(-i2\pi \frac{mu}{M}\right) \right] \exp\left(-i2\pi \frac{nv}{N}\right) \qquad (3.1.5)$$

and we see that we have to compute M + N one-dimensional Fourier transformations. First, the lines of the picture matrix are transformed:

$$\hat{F}(u,n) = \sum_{m=0}^{M-1} f(m,n) \exp\left(-i2\pi \frac{mu}{M}\right) \qquad (3.1.6)$$

$$u = 0, 1, 2, \ldots, M/2; \; n = 0, 1, 2, \ldots, N-1$$

Since the picture matrix represents gray-values or intensities, f(m,n) is a positive function. The real portion of the Fourier transformation of a line is thus symmetrical about the point M/2, whereas the imaginary portion is antisymmetric. For this reason, the real and imaginary values are stored in $\hat{F}$ only up to the index u = M/2.

After the transformations of the line, the columns of the interim matrix $\hat{F}$ are Fourier-transformed:

$$F(u,v) = \sum_{n=0}^{N-1} \hat{F}(u,n) \exp\left(-i2\pi \frac{nv}{N}\right) \qquad (3.1.7)$$

$$v = 0, 1, 2, \ldots, N-1; \; u = 0, 1, 2, \ldots, M/2$$

The components F(u,v) for $u > M/2$ do not have to be figured out because they are conjugated, rotation-symmetrical about the point u = M/2 and v = N/2 due to the mentioned symmetries [24].

That is:
$$F(M-u, N-v) = F^*(u,v). \qquad (3.1.8)$$

In order to present the amplitude spectrum of a picture in the standard form where the lower-frequency portions lie in the center of the spectrum, a reordering of components is necessary as per:

$$A(u,v) = \left| F(\mathrm{mod}(u + M/2, M), \mathrm{mod}(v + N/2, N)) \right|^2 \qquad (3.1.9)$$

In addition, a cut-off of components with high amplitude is advisable since the dynamic range of the components far exceeds the illumination play of photographic film.

Fig. 7a shows a digitized tire-test hologram which contains a severe disturbance pattern. In fig. 7b the amplitude spectrum is presented. Here, the portions of the disturbing pattern are clearly seen as bright specks lying on a line perpendicular to the disturbing pattern. The relatively strong frequency components on the v-axis are largely due to the expansion of the 480 lines of the digitized picture to 512 lines; this is necessary due to the use of Fast-Fourier

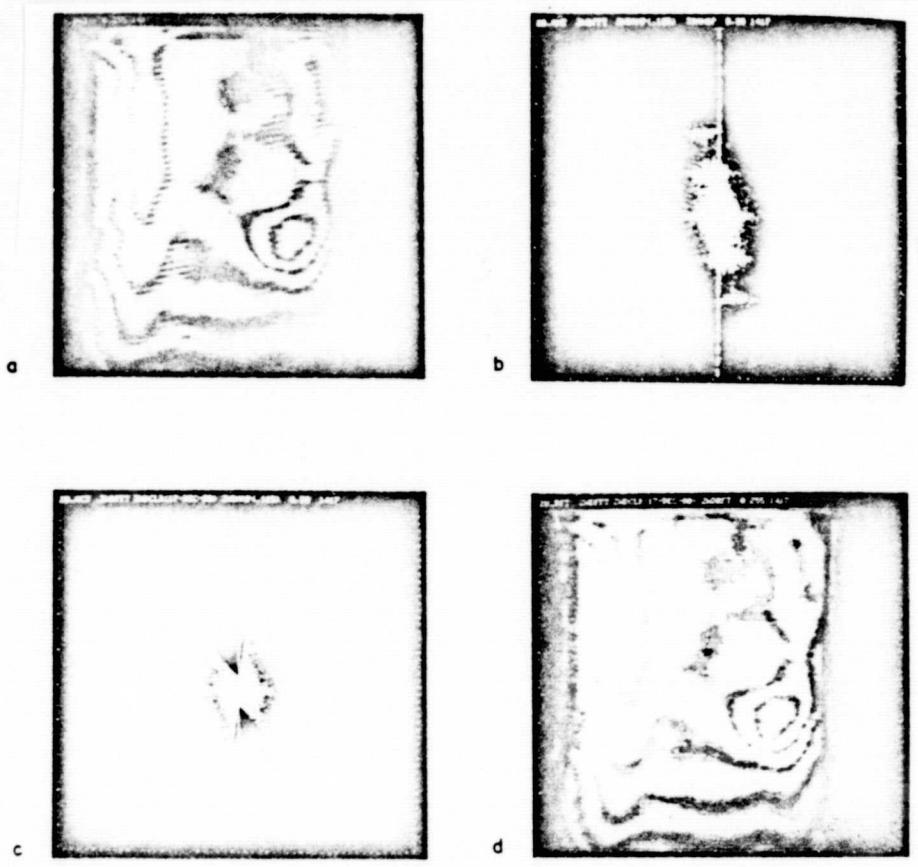

Fig. 7: Interference Elimination by Filtering in the Fourier Plane (Hologram no. A4 8007228)

a) Hologram with superimposed disturbing-interference pattern due to hot-bellows impressions
b) Spectrum of the hologram
c) Filtered spectrum
d) Retransformation of the filtered spectrum

Transform-Algorithms [25] and was done arbitrarily at first after zeroing the additional lines. Thus, in the y-direction there is naturally a discontinuity at line 480 which leads to strong spectral components in this direction. Through multiplication of the spectral plane with a suitably selected filter function and retransformation of the modified spectrum, we obtain the filtered picture. The filter function is created first, after zeroing the appropriate spectral components. Here again, the spectral components corresponding to the high space frequencies, are set to zero to attain picture-smoothing; otherwise, this would have to be done by application of averaging operators in the picture plane.

Fig. 7d shows the hologram after retransformation from the modified spectrum of fig. 7c. The original hologram is obtained, but the disturbing pattern is mostly eliminated.

To execute the Fourier filtering, the programs ZWDFFT, ZWDCLR, ZWDRFT, ZWDAMP are used.

In addition to cutting-off the high space frequencies, it is also possible to influence the low space frequencies which represent essentially the background brightness in the holograms.

Such two-dimensional filter methods require quite high computation times is they are performed with the process computer (ca. 20 min. for one transformation and re-transformation). By using the array-processor, this time can be reduced to a few seconds, which allows the use of such filter methods in the series evaluation.

3.2 Segmentation of the Interference Strips

The extraction of the fringes from the digitized gray-value presentation takes place in two steps: First, the objects which can be interpreted as interference fringes must be pulled out from the local gray-value distribution by an appropriate contrast enhancement, next the locations of fringes which can be derived both from the intensity extrema and from the flanks, are linked together into cohesive lines. For locally large fringes, the extrema cannot be determined accurately in some cases, so that the coordinate sequences of the rising and falling flanks more accurately define the fringes (see also [16]). Furthermore, in the flank representation, more simple graphic data structures result, since no line branchings can occur.

3.2.1 Picture Halftone Transformation

The local operators normally used in digital picture processing for sharpening edges and line recognition, like gradient, Laplace or Sobel operators, and others of a more complex nature [26-28], are not suitable in the case of interference picture evaluation, since they respond only to sharp halftone steps and do not operate satisfactorily for the cosine-squared modulated interferograms normally occurring. In addition, the expected computation times, like e.g. for the so-called Hueckel operator [27] are too long for this type of use.

Fischer et al. [5] use sine functions adapted by sections to the line-by-line extrema determination of the interference fringes (after elimination of noise); their extrema are then taken as fringe locations. Another method which postulates parallel fringes with constant spacing running perpendicular to the scanned line, has been described by Schindler et al. [29]. A Fourier transformation of the intensity is performed in the line direction here, in order to determine the local frequency and phase position of the fringe field. As a minimum number of fringes in the line, ten fringes are posited so that a definite peak will appear in the frequency spectrum.

These methods too, cannot be used for our evaluation since they generally require uniformly echeloned interference fringes running mostly perpendicular to the scan direction.

Therefore, a line-by-line operating method of extrema determination and noise suppression was developed by means of a variable threshold. With this method, first those extrema are sought in the line having a certain halftone difference to the last-found extremum, which is greater than a bound derived from the average noise amplitude. For adaptation to the locally-dependent contrast distribution in the holograms, instead of a fixed bound, a location-dependent bound is used which ran from the picture middle out to the edges (STREX3 and STREX4 programs). Now the extrema are used to define a staircase threshold-value function which assumed the average amplitude between neighboring extrema. At the line beginning or end, the trigger threshold of the first or last two extrema is used. The threshold comparison of the intensity values with this staircase function then gives a binary representation of the lines under consideration (see fig. 8).

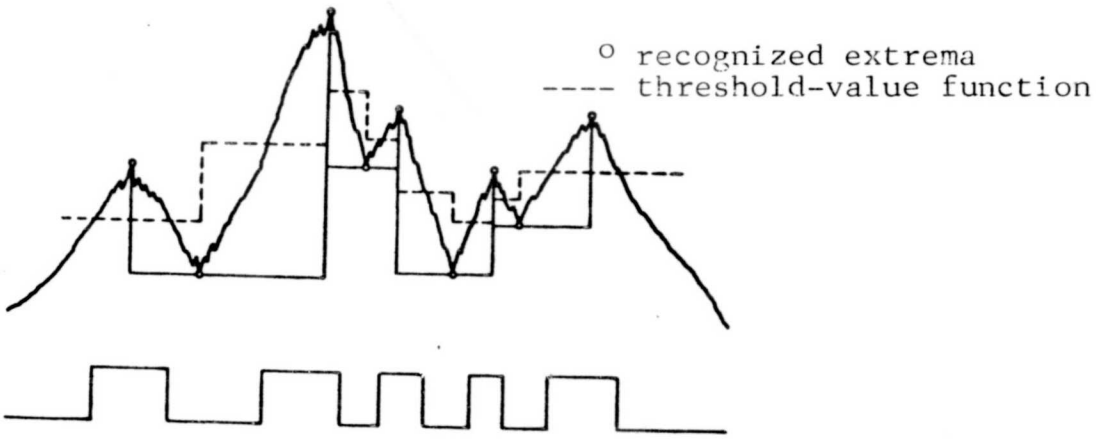

Fig. 8: The Picture-Halftone Transformation (top: gray-value line) (bottom: binary line derived from it).

Figure 9 shows a sequence-plan of the method. This type of contrast enhancement corresponds in effect to a flank-triggering of the fringes with a fixed threshold after an appropriate elimination of background intensity, as can be attained through the use of the program SUBMF3 (sec. 2.1.2).

The results of the last-discussed contrast enhancement are generally much better than for simple elimination of background intensity by the SUBMF3 program. The best results were attained by using the contrast enhancement after application of the SUBMF3 program. Figure 10 shows an application of the STREX3 program to two holograms. We see that the method itself gives a good separation of interference fringes from the background, even for highly variable background brightness and weak contrast. In spite of very good noise suppression, even small structures are still fully contained in the interferogram.

3.2.2 Polygon Segment Illustration

The halftone transformation enhances the contrast and afterward, the interferogram is present as a binary picture which is converted

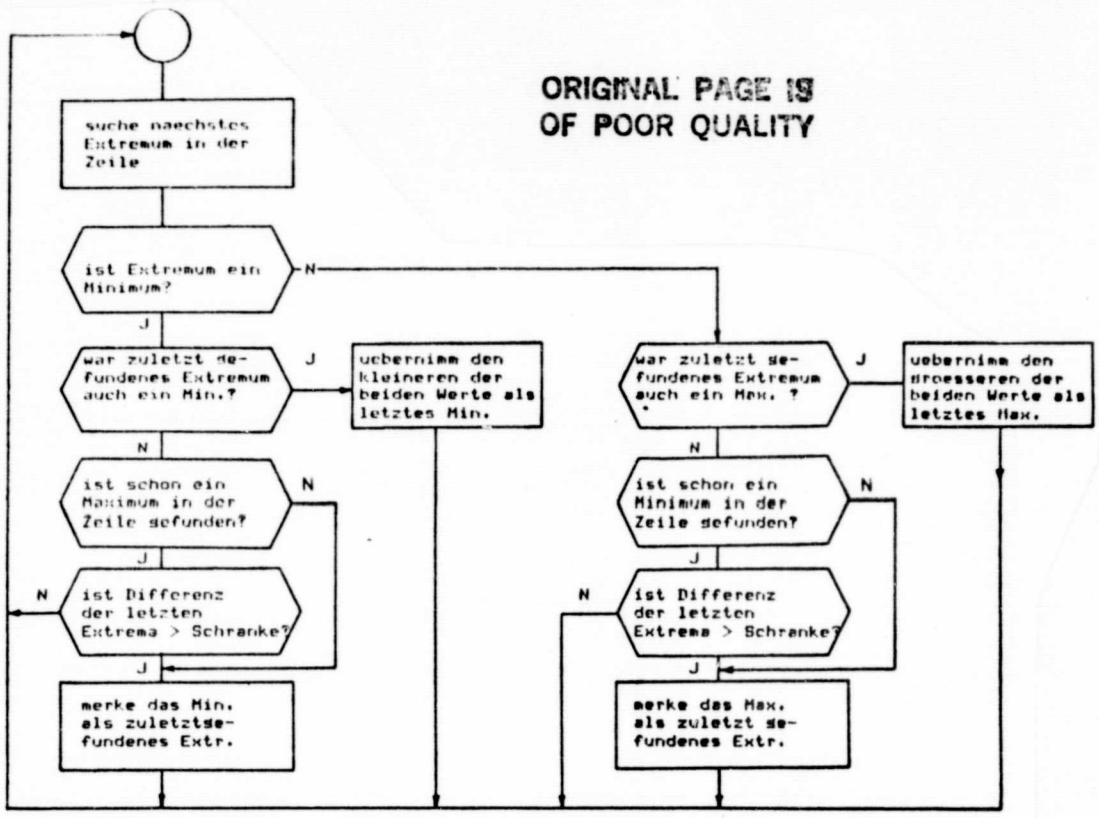

Fig. 9: Sequence Plan for Line-by-Line Extrema Search

Key: 1-seek next extremum in the line 2-is extremum a minimum? 3-was last-found extremum also a minimum? 4-has a maximum already been found in the line? 5-is the difference of the last extrema greater than the bound? 6-mark the min. as the last-found extremum 7-take the smaller of the two values as the last min. 8-was the last-found extremum also a max.? 9-has a minimum already been found in the line? 10-is the difference of the last extrema greater than the bound? 11-mark the max. as the last-found extremum 12-take the larger of the two values as the last max.

into a polygon-segment representation. Each polygon segment represents the coordinate sequence of an interference fringe edge. The polygon-segment representation permits a data reduction of ca. 30:1 to 100:1 compared to the point-representation, in addition to other advantages.

Due to the representation of the interferogram by two halftones, it breaks down into regions with gray-value "0" (bright) and those with value "1" (dark). The cohesive dark regions are called the "object" here.

The extraction of polygon segments from the binary picture is accomplished by the use of a sequential technique (see Agrawala and Kulkarni [30]), where each two sequential lines of the picture are compared. Thus, without further testing it is assured that all objects in the binary picture are recognized--a significant event in the edge-tracking of individual objects. Furthermore, there only needs to be a

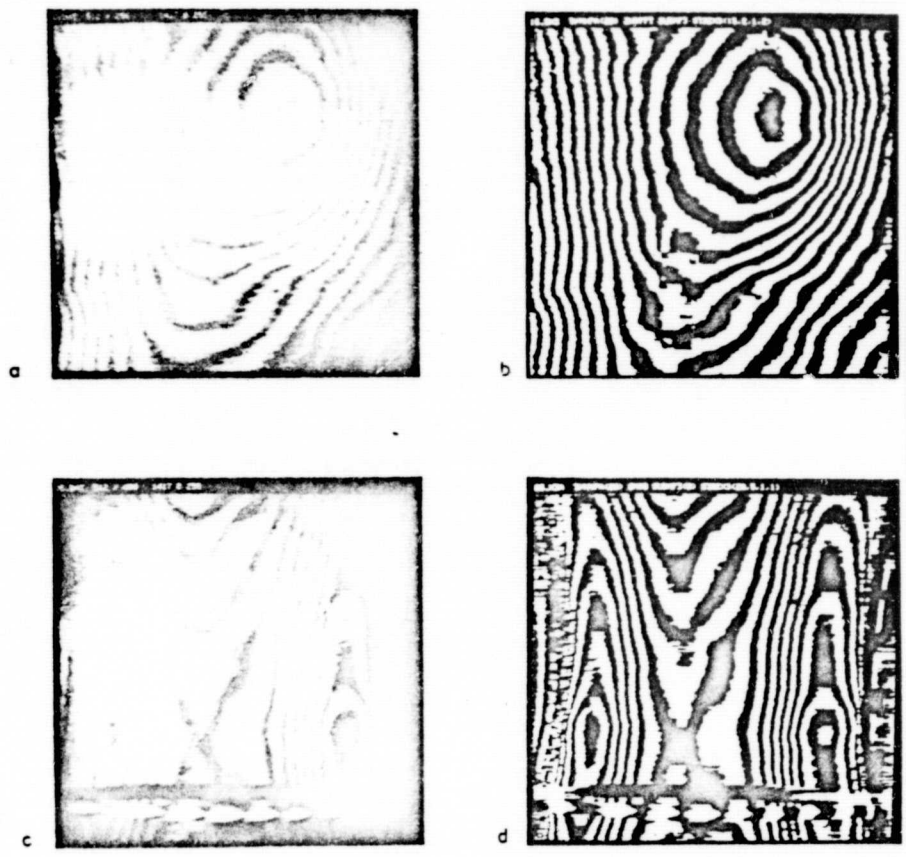

Fig. 10: Examples of the Picture-Halftone Transformation

a) Halftone representation of the digitized hologram no. 16 on the graphic terminal
b) Binary representation of the hologram after picture enhancement and use of the STREX3 program
c) Like a), hologram no. 05
d) Like b), hologram no. 05

single access to each picture line (i.e. to each picture point), thus storage of the entire picture is unnecessary. Therefore, this processing step can be implemented directly in connection with the digitizing and picture-halftone transformation.

With regard to the line direction, an object has a left edge (halftone transition from 0 to 1) and a right edge (halftone transition from 1 to 0). The sequence of edge coordinates of an object is determined by analysis of the continuation-conditions of the left and right object edges from one line to the next.

As continuation-conditions of an object j in line n to the object i in line n+1, the following relations apply for the left (x_l) and right(x_r) object limits (see also fig. 11a):

$$
\begin{aligned}
&\text{I)} \quad x_r(i-1) < x_l(j) \\
&\text{II)} \quad x_l(j) \leqq x_r(i) \\
&\text{III)} \quad x_r(j-1) < x_l(i) \\
&\text{IV)} \quad x_l(i) \leqq x_r(j)
\end{aligned}
\qquad (3.2.1)
$$

If one or more of these conditions does not apply, then the object j ends in the old line, object j-1 is linked with object i in the new line, object j splits into two new objects in the new line, or a new object i is begun in the new line. The cases occurring in case the continuation conditions do not apply, are presented in fig. 11b.

If a new object begins in line n + 1, then its coordinates of the left and right edge are stored in an interim memory under a number issued for the left and right edges of the object. If objects in line n + 1 are linked which had formerly been carried as two different objects (naturally this cannot be avoided due to the sequential process), then these coordinate sequences are linked into a new coordinate sequence. If an object or a "hole" in the object is closed, then the coordinate sequence is eliminated from the interim memory and placed in the permanent memory after a redundance reduction. This reduction is also performed during the coordinate pick-up in the interim memory if the space there has become too small. The redundance reduction (see sec. 2.3.1) replaces the quasi-continuous coordinate sequence by a polygon section with minimal number of coordinates. The accuracy of presentation of the original coordinate sequence is provided with a tolerance bound.

The sense of direction of the coordinate sequence is specified upon storage in the permanent memory so that when running through the coordinate sequence in the sense of the storage, the dark region lies on the right side of the polygon segment.

By means of these "directed" line segments, several difficulties are avoided which arise later during the numbering when comparing two interferograms.

By tracking of left and right fringe edges, the fringe density in the interferograms can be doubled, which has a favorable effect on further processing (calculation of object function), especially for broad fringe-systems. If the profile of extrema is determined in addition to the profile of the flanks, then the interferogram could be presented even more accurately by means of a four-fold line density. When we are speaking of left and right fringe edges, this is always with respect to the scanned lines. For closed fringes of those cut several times by one line, the left fringe edge is transformed into the right, and vice-versa.

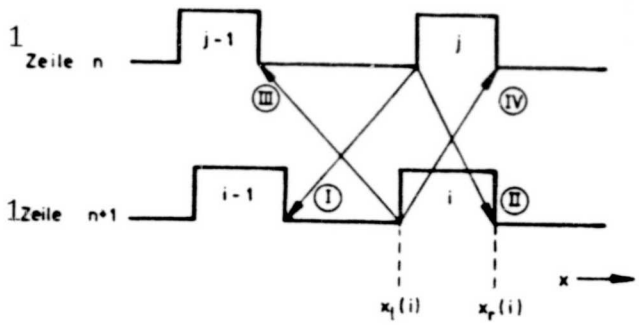

Fig. 11a: Sketch of the Arrangement of Continuation Conditions (3.2.1)
Key: 1-line

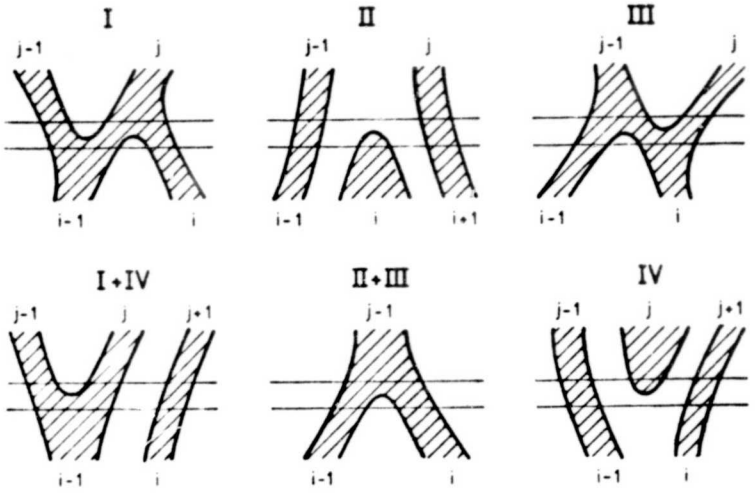

Fig. 11b: Sketch to Illustrate Cases Occurring when the Individual Continuation Conditions are not Met (3.2.1).

A problem which occurs in fringe tracking, is the recognition and handling of the picture edge. If an object of the binary picture ends at the edge, then the two affected edges may not be linked together since they can be lines of different order. The same linkage problem arises when objects end in the picture. If the object represents a closed interference fringe, then the two edges are to be linked. If an object representing a very narrow fringe ends because e.g. the resolution limits are too high, then the edges may not be linked. This problem is a fundamental difficulty which cannot be explained from the analysis of local halftone distribution in the vicinity of the location alone, rather, the global information about the profile of the fringe field must also be included in the decision on the cohesion of such regions. For the case of picture edging, the problem is solved by specification of the geometry of the object edge and a corresponding edge-test for fringe tracking. In order to do this, the coordinate sequence of the edge contour or contours--which can be input manually with the FAW2 program via graphic data input--are converted into a point-image with binary halftones. The imaging of the

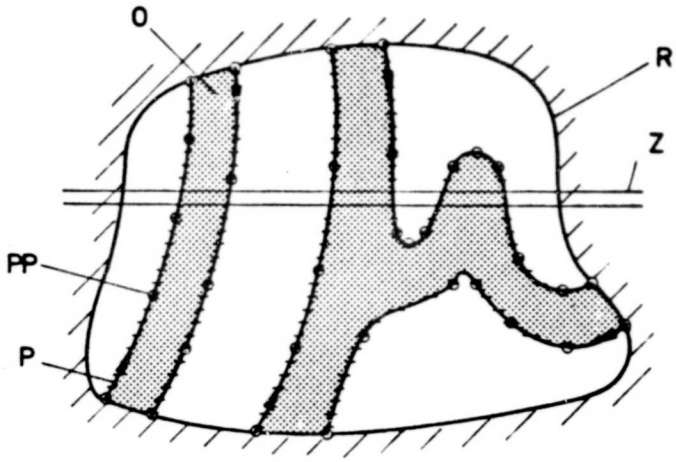

Fig. 12: Sketch of the Polygon Representation of Fringe Edges
o Dark object (interference fringe)
R Picture edge
P Directed polygon segment of the object edge
PP Polygon points remaining after redundance reduction
Ż Picture line

edge contour in the coordinate system of the scanned interference picture occurs with the MASKO1 program. A sketch of the polygon representation of the interference fringes is shown in fig. 12.

The edge contour used for the fringe extraction must overlap somewhat, the physical edge of the measured field in order to prevent the bound of a fringe of the edge from being interpreted as a flank line and to prevent edge effects as can occur especially in the evaluation of flow-physical interferograms in the region of the boundary layer. Examples for the polygon-segment presentation of interferograms are shown in fig. 13 and 18 ff.

3.2.3 Handling of Fringe Misconnections

The fringe misconnections addressed in the preceeding section can appear in the interferogram at those places having insufficient contrast or where the fringe density is so high that the resolution of the scan system is insufficient to separate the fringes.

Examples of such fringe misconnections are shown in fig. 14 and 15 where some interference fringes are broken up in the edge region of a tire-test hologram due to contrast weakness, or in the region of the boundary layer and of the flow cavitation of the interferogram of a transsonic, planar laval jet opening, due to lack of contrast and resolution problems, or fringes are linked with the neighboring fringe.

Now it is desirable to correct the majority of these misconnections before application of the numbering method. Therefore, the BVSF program was developed which specifically seeks places where interference fringes end within the picture. An attempt is made to stretch these strips and touch another, likewise prematurely-ending interference fringe and to eliminate the fringe interruption through linkage of corresponding flank lines.

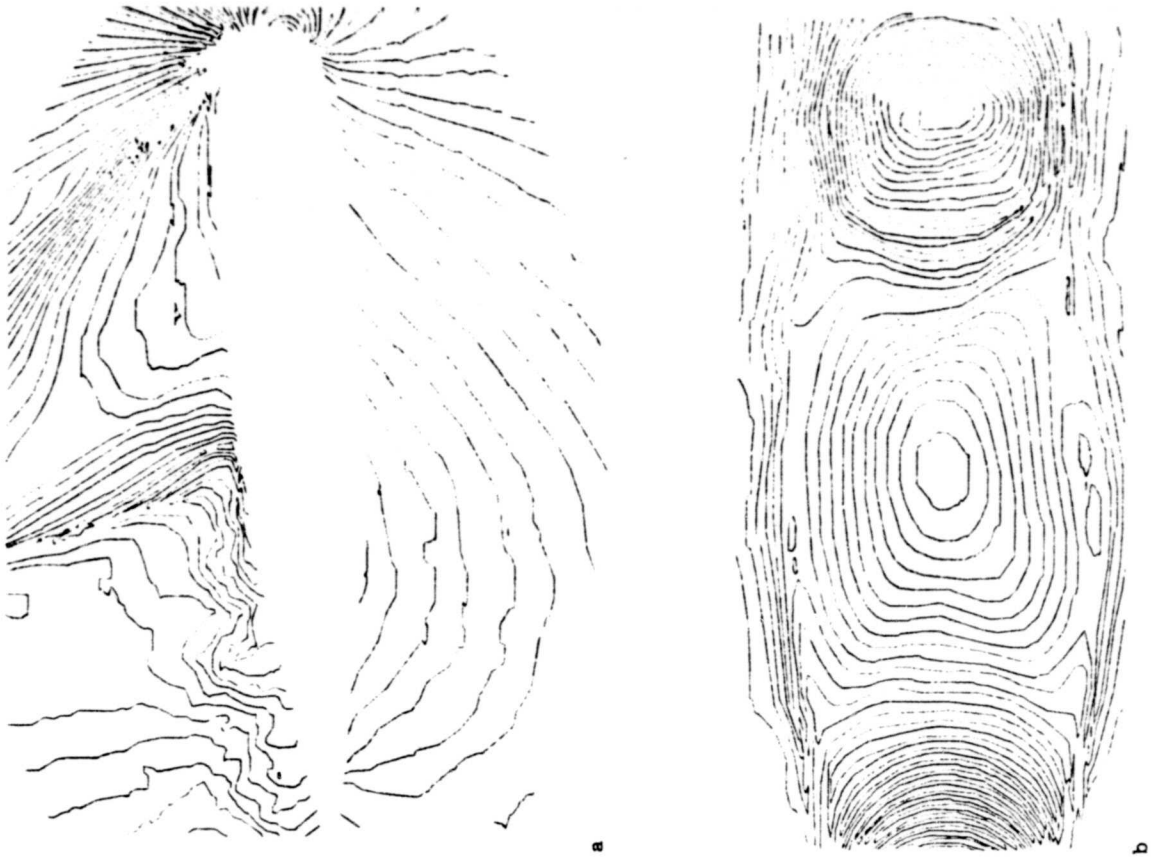

Fig. 13: Example for the Polygon-Segment Representation of Interference Fringes
a) for interferogram of fig. 2a
b) for interferogram of fig. 2b

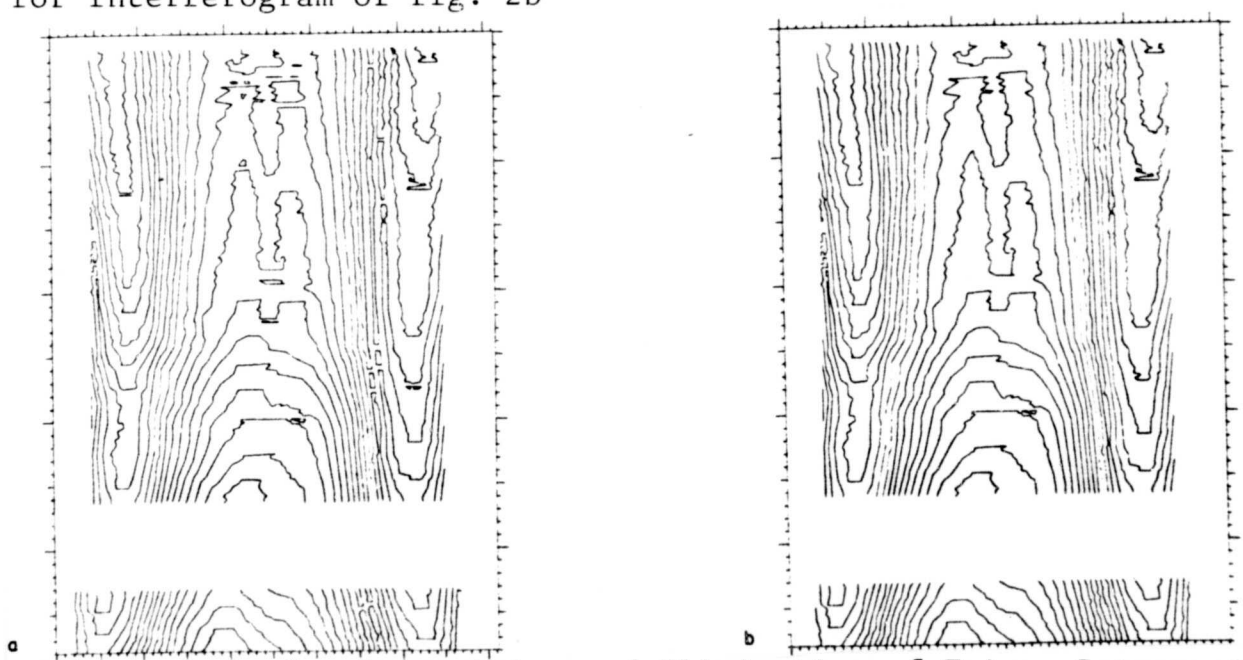

Fig. 14: Example for Recognition and Elimination of Fringe Interruptions
Hologram no. 04 (see also fig. 3).
a) Line image of a hologram with defectively-recognized fringes.

Now it is assumed here, that interference fringes (and thus also their flank lines) must end at the edge, unless we are dealing with closed fringe systems.

As we see in fig. 14, most fringe interruptions in a field with predominately parallel fringe profiles, can be eliminated in this way.

Another method for localization of incorrectly extracted flank lines uses the geometric parameters of a line, like form-factor, fringe length, spacing of end points and the directions of line segments (program BVSF2). The form-factor FF is defined as the ratio of the area A enclosed by the fringe, to the square of the fringe length U (for unclosed lines, the linkage distance of the end points is also included).

$$\text{(3.2.2)} \qquad FF = \frac{4\pi A}{u^2} \tag{3.2.2}$$

With the form factor, the roundness of a line can be expressed; for a circular object, it is 1 and goes to zero for elongated objects. Since the interference fringes as a rule represent elongated objects, the flank lines with wrong linkages can be recognized since they have small form factors and also the ratio of the end-point spacing to the line length EPADL is small. In order to determine the location of the misconnection in the line, the change in direction of the line segment is considered. In order to keep the computation time low and to prevent disturbances through local, small-area changes in direction of line segments, the considered line is approximated by the redundance reduction discussed in sec. (2.3.1) by means of a very rough polygon segment. The considered line is now separated at those places where the segments of the approximated polygon segment enclose small angles. Figure 15 shows an example. The recognized flank lines of the fringes of the interferogram of fig. 15a are presented in fig. 15b and two of the lines recognized as defective are presented in fig. 15c. The corner points of the rough polygon approximation are identified by squares. The places where a separation of lines occurs, are identified by a plus-sign. Experience has shown that for a setting of threshold values of:

$$FF < 0.27 \text{ and } EPADL < 0.4 \tag{3.2.3}$$

most of the misconnections are found and eliminated. Any missed misconnections will have to be localized and eliminated during the numbering of the line field.

3.3 Fringe Numbering

A strategy for numbering of interference fringe-fields must include the pertinent rules for such fringe field, discussed in sec. 1.2, in an algorithm. In addition, it should use 'a priori' known properties of the particular object in order to arrive at a fringe numbering correctly describing the present case. But at this place we should remark that a numbering which only uses information from the fringe profile, is not clear in every case.

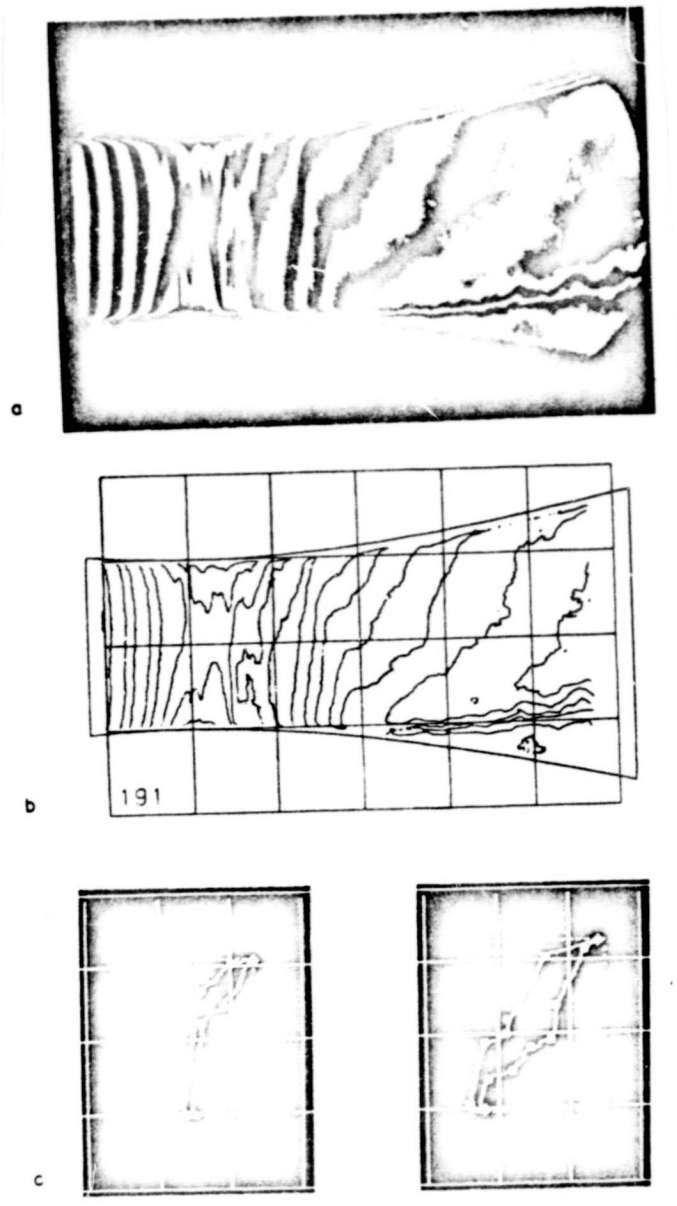

Fig. 15: Example for the Recognition and Elimination of Fringe Interruptions (Interferogram of a flat Laval-jet flow)
a) Original paper print of 16 mm film
b) Polygon-segment representation of the interferogram
c) Two strips from the polygon-representation with fringe misconnections

Strategy 1

A simple strategy for numbering of error-free extracted fringe fields which was applied in the presence of continuous object functions, consists first in assigning the individual lines to specific line systems. For closed, circular fringes, this step is obvious; for fringes ending at the edge, it is done through consideration of sequential edge intersections.

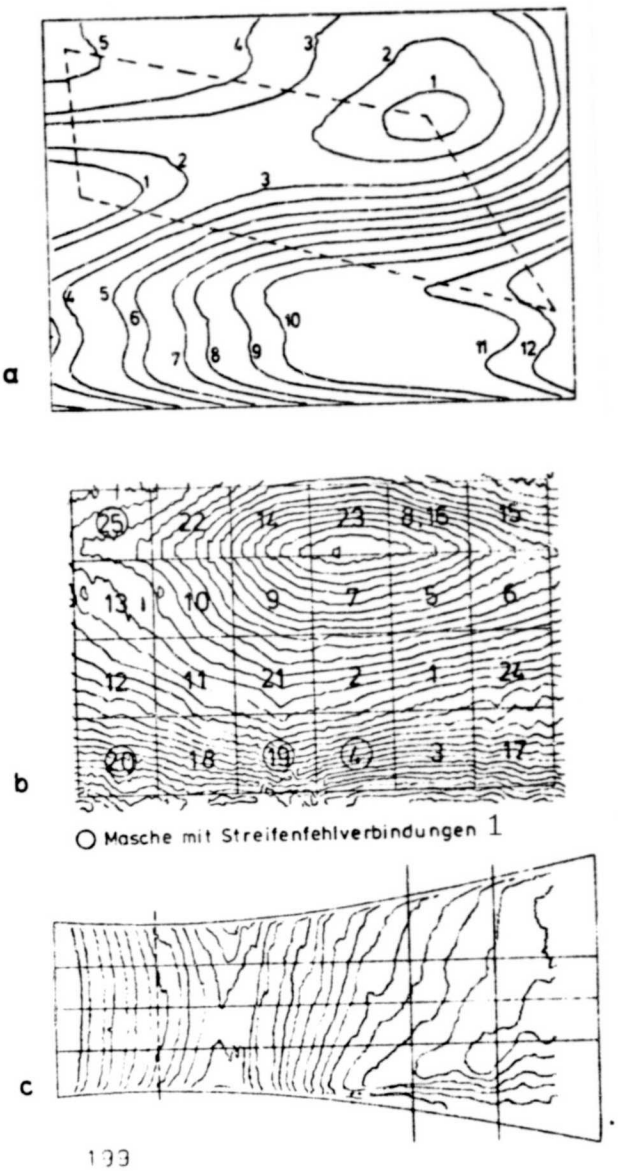

Fig. 16: Fringe Numbering (see text)
Key: 1-mesh with fringe misconnections

Now after this, the area centers of the internally closed lines or of lines ending internally at the edge, are linked so that no edge intersections of other lines lie between the edge intersections of the systems touching the edge, or so that the curvatures of the outer lines of both systems have the same sense of curvature in the region of intersection with the connecting lines. Now the lines along the connecting lines are numbered equivalently so that they are consistent with any line numbers already issued. If a line is cut twice in sequence, then the numbering direction is reversed.

The introduction of the continuity of the object and of a certain minimal principle (monotony of the object function) into the numbering strategy corresponds to this method, since the numbering direction

is changed only by double cutting of the same line or by two lines with the same number, and not between lines belonging to one fringe system, or which run similarly in the boundary region of two systems. Fig. 16a shows the example of a fringe field numberable with this strategy, in which the linkage lines of the line systems and the line numbers are included.

Now in order to number fringe fields with lines recognized as defective, and to correct them as necessary--which would have led to an inordinant amount of programming effort with the above method--a second numbering strategy was developed.

Strategy 2

An important finding which led to this strategy is that weak contrast and high line densities which can lead to disturbance of the line profile and of the line cohesion in the extracted fringe fields, frequently occur only at a few places of the picture (mostly in the edge region of the holograms), whereas the line profile outside these places is recognized satisfactorily.

To localize these inferference points, the line picture of the interferogram is split up by a suitably selected mesh grid into individual segments. For numbering of a mesh, the sequence of fringe intersections with the edge of this mesh is considered and used so that in an interference fringe field, the sum of the ordering differences along a close curve must be equal to zero. For each mesh a number (confidence) is determined which provides information about the numberability of the particular mesh. The confidence number is composed of the number of different lines in the mesh and the number of places where the direction of line numbering is reversed. This introduces the principle of beginning the numbering in a monotonous region of the object function. As starting point for the numbering, that mesh is selected which has the fewest reversal centers and the most lines. If this mesh has exactly two reversal centers, then it is assured that we are dealing with a defect-free mesh. Now the numbering is continued at one of the four neighboring meshes having the greatest confidence of those meshes and in which the numbering can be continued, i.e. the one with the first mesh having at least two interfections of different lines with unequal ordering number in common. The numbers of the other neighboring meshes are placed in a stack from which the mesh numbers to be numbered next, are taken.

Once this stack is worked off, but all meshes have not yet been numbered, then proceeding from the numbered mesh with the best confidence, so-called Large Meshes are formed which consist of two or more neighboring meshes and the numbering is continued. If the numbering method encounters a contradiction for one mesh, then it is first reset. After working off all other meshes, the defective mesh is worked on. Now the numbers known at the edge of the mesh from the numbering of neighboring meshes, are taken over, provided they are compatible with the line profile in the mesh. All fringes which had to be provided with two different numbers, are separated in the mesh and each individual segment is provided with the line number from the neighboring mesh. Through this strategy, disturbances in the line profile do not affect the numberability of the whole line system, but only affect the near neighborhood.

Figure 16b shows the mesh division for numbering the hologram. The numbers in the meshes tell the sequence which was used by the algorithm for processing them (for this particular example). The determined, relative numbering must now be adapted to the actual conditions by addition of a constant and any needed reversal of fringe counting-direction for the entire picture; this can be done e.g. by specification of the absolute value and a direction at any random point. This numbering can be different for interferograms of the same type, depending on the location of the starting mesh and the local fringe conditions there.

Strategy 3

The last strategy presumes a consistent fringe field for the numbering, where no fringes end in the interior of the mesh and where the numbering can continue in all regions of the fringe field if one begins at any random point.

Both assumptions are not generally applicable for the numbering of interferograms of instationary transsonic flows, since discontinuities of the object function can occur here due to the appearance of compression shocks which lead to the fact that the principle of the disappearance of the sum of the ordering-differences over a closed curve--which is generally valid for interferograms--is no longer valid for the extracted fringe fields here, since the fringes cannot be resolved in such regions of discontinuity and thus either disappear or occur as incomplete fringe bridges (see also sec. 4.2).

The numbering strategy of such interferograms must thus include the property of minimum change from picture to picture of an interferogram series, mentioned in sec. 1.2, for chronological development of the object.

Test lines placed through the strip field (see fig. 16c) are determined by numbered interference function N(x,y) interferograms*.

In the first run-through of the numbering algorithm, the numbers of the fringes of the preceeding interferograms are written on those lines of the fringe field to be numbered, which clearly overlap on the test lines with them. "Clearly" means in this regard, that the fringes of the old picture overlap with those of the new picture, at all test lines having intersections with them; but no overlaps occur with other fringes. This means that only the numbers of those lines whose shift and change of shape no longer equal one-half fringe width, are transferred into the new fringe field.

*T.N.: Sentence unintelligible.

In the second passage of numbering, an attempt is made to number the as yet unnumbered fringes along the test lines so that they on the one hand are consistent with these numbers taken directly and at the same time exhibit no significant deviations from the profile of the interference ordering function N(x,y) along the test lines in the preceeding picture. In order to do this, the interference orderings along the test lines are illustrated by means of a rational spline function, which has the advantage here, of exhibiting no overshoots at discontinuities. After this passage, any still-unnumbered fringes, e.g. those having no intersections with the test lines, are numbered by consideration of their fringe neighbors.

In this manner one attains an automatic continuation of a manual interferogram numbering over fringe fields which were not numberable with the methods discussed before.

An improvement of the numbering strategies and thus a better and faster application to distorted fringe profiles and a more secure resolution of fringe misconnections would result from the introduction of a fringe similarity scale which had been present in a weak form in the numbering strategies through one or more secondary conditions. In this case, a more rigid form would be needed, perhaps as defined over fringe sections where the principle of unchanged numbering direction between neighboring, similar-running fringes, would be taken more into account.

To accelerate the numbering strategies furthermore, a storage of fringe points is desired in a form which makes it possible to perform such operations like search for fringe neighbors at a certain place of the picture, calculation of fringe spacing etc. first on a set of points roughly representing the fringe field, and then to work with more accurate resolution on a quantity of points reduced accordingly.

3.4 Polynomial Presentation

The execution of a transformation of the interference ordering function present in polygon-segment form into a representation of the form $z = f(x,y)$ is equivalent to the problem of regenerating a function from its contour lines (lines where $f(x,y) = \text{const.}$; see sec. 1.2).

The needed interpolation to a surface specified by randomly set support points (field points) is more difficult to perform then if the field points of the surface were placed on a regular grid or at least on parallel lines. For these regular field-point distributions there are practical, acceptable methods which use orthogonal polynomials [31-33] or spline functions [22, 34]. A method used by Hayes and Halliday [34] can handle any distribution of field points and in a regular grid laid over the field points with m x n lines, so-called [illeg.] splines are computed and this leads to an unacceptably long computer time since an excessive equation system of quantities $(m+4).(n+4) \times N$ where N is the number of field points, has to be solved by a Householder reduction.

According to the methods used here, the field points near the interpolation point are weighted according to their spacing and are approximated by a polynomial of low order. The value at the interpolation point is now obtained through evaluation of this polynomial [35]. This method of local polynomial approximation was selected for the presentation of interferograms, since is needs relatively short computation times and [illeg.]...information like places of large curvature of places of large gradients can be had. In addition, a simple elimination of superimposed [illeg.] is possible through modification of the corresponding coefficients.

In order to present the [illeg.] ordering function in closed form [illeg.] covered by a regular grid with the grid points $(\lambda_i, \mu_j = 1, .. m)$. At these grid points, polynomials of second degree are used (to save computer time):

$$P_{ij}(x,y) = \sum_{k=0}^{2} \sum_{l=0}^{2-k} c_{kl} x^k y^l \qquad (3.4.1)$$

The coefficients at point (λ_i, μ_j) are determined with the side-condition that the sum of the squares of the errors is minimum (Gaussian Method of least squares):

$$\Omega = \sum_{r=1}^{N} (P_{ij}(x_r, y_r) - z_r)^2 \, w\,((x_r - \lambda_i)^2 - (y_r - \mu_j)^2) \stackrel{!}{=} \text{Min.} \qquad (3.4.2)$$

The weighting function $w(d^2)$ weights the field points with greater distance d from the interpolation point (λ_i, μ_j) less than those closer by. Through the use of a quickly declining function for $w(d^2) = \exp(-\alpha d^2)$ we have the advantage of not having to account for all field points (x_r, y_r) to calculate P_{ij}; only the field values from a certain environ of [illeg.] are taken, where $\exp(-\alpha d^2)$ is greater than a preset bound. The values of the coefficients are changed insignificantly by this. The solution of the equation system (3.4.2) can be transformed through formation of the normal equations:

$$\frac{\partial}{\partial c_{rs}} \Omega = 0 \qquad (3.4.3)$$

into the solution of the linear, quadratic equation-system:

$$A^T A\, c = A^T z \qquad (3.4.4)$$

Here, A is a n x 6 matrix, c is the coefficient vector and z is the vector of function values at the field points. Since the field values which represent the evaluated interferograms, are sometimes irregularly distributed, it is advisable to specify the parameter α in the weighting function $W = \exp(-\alpha d^2)$ since otherwise in a region with few field points, a strong weighting of the more distant points might occur and they would have to be used in the calcualtion. The parameter α was thus made dependent on the field-point density:

$$\alpha = 4/r^2 \qquad (3.4.5)$$

Here, the radius r is a neighborhood of (λ_i, μ_j) containing at least 16 field points and r is greater than or equal to twice the average grid-point separation.

Figure 17a shows an example of polynomial approximation. The determined 2D polynomials of the hologram no. 16 are seen in cross-section with the x or y-plane. The location of the grid lines and interference lines also proceeds from fig. 18. We see that the determined polynomials overlap relatively well, which speaks for a correct selection of the mesh size.

To compute the function values z(x,y), all 4 corner-polygons of the mesh in which point (x,y) lies, are evaluated and weighted in accord with the location of the point. However, slight undulations occur at the places where the computed polynomials do not overlap, e.g. at the edge where few data points are available to determine the local polynomial. To achieve a smooth representation of the surface rising over the mesh limits in first and second derivative, the local polynomial presentation (3.4.1) can be converted into a spline function. This is possible now without great computation effort if, to compute the coefficient c_{oo} some of the coefficients c_{o1}, c_{10} and c_{11} from the polynomial representation (3.4.1) are used. In addition, the solution is unique [21]. The general equation for a bicubic spline function is:

$$f_{ij}(x,y) = \sum_{k=0}^{3} \sum_{l=0}^{3} a_{ijkl} (x - \lambda_i)^k (y - \mu_j)^l \qquad (3.4.6)$$

$$i = 1, \ldots, n-1; \; j = 1, \ldots, m-1$$

The surface is accordingly defined by the matrix a_{ijkl} with $16 \cdot (n-1) \cdot (m-1)$.

The calculation of the point z(x,y) of this surface occurs through evaluation of the 16 coefficients of the function f_{ij} in the mesh (i,j) where the point (x,y) lies. Two-dimensional Horner algorithms can be used for this; only 16 multiplications are needed to compute a point z(x,y) according to (3.4.6). The two intersection planes of fig. 17a are shown in fig. 17b after conversion into the spline representation.

Figures 18ff show a line picture of a hologram with the included grid lines in part b, and in part c the interference ordering function computed from the polynomial representation using grid-lines. If we compare the two pictures, we find that the grid lines of the polynomial representation reproduce the lines of the hologram and that a certain line smoothing has occurred. Through the selection of the grid distribution for calculation of the polynomials, a smallest resolvable structure of the surface is defined which causes a deep-pass filtering of the interference ordering function. This deep-pass filtering is absolutely desirable and can even be used for tire-fault recognition in the case of tire-test holograms (see sec. 3.5).

Another property of this presentation is demonstrated in fig. 19 and 22. The region of the hologram covered by a spacer lying in the

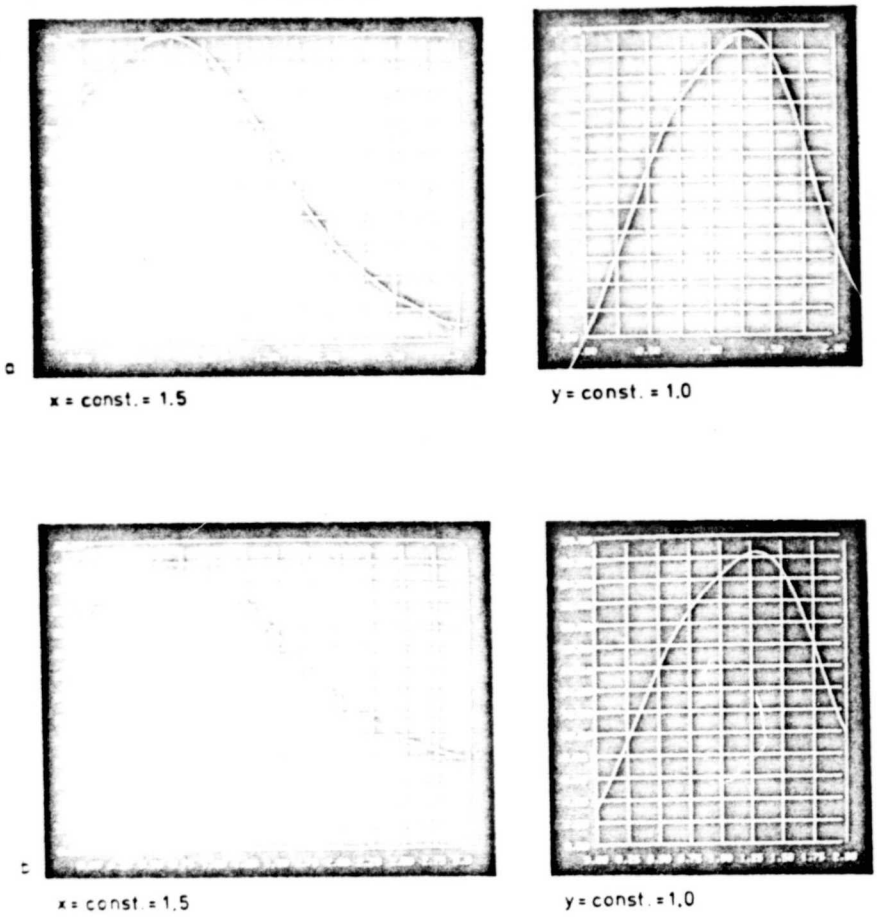

Fig. 17: The Polynomial Approximation (using interferogram no.16 in fig.18)

a) Axis cut through the local polynomial
b) Axis cut through the computed spline surface (the ordinate values are in units of half the wavelength of light (λ = 632.8 nm) with respect to an arbitrary zero point).

field of vision could not be evaluated here. Through an adaptation of the absolute numbering of the upper and lower picture section, the interference ordering function was described quite well in this covered region through the extrapolating property of the polynomial representation, as is immediately confirmed by a comparison with the hologram.

To compute the polynomial coefficients, the program PKF63 is used; for the representation of cut-curves of the polynomial surface on the video terminal, program PTST82 was used, and to compute geometric parameters like curvature and gradients of the polynomial surface, program PTST84 was used.

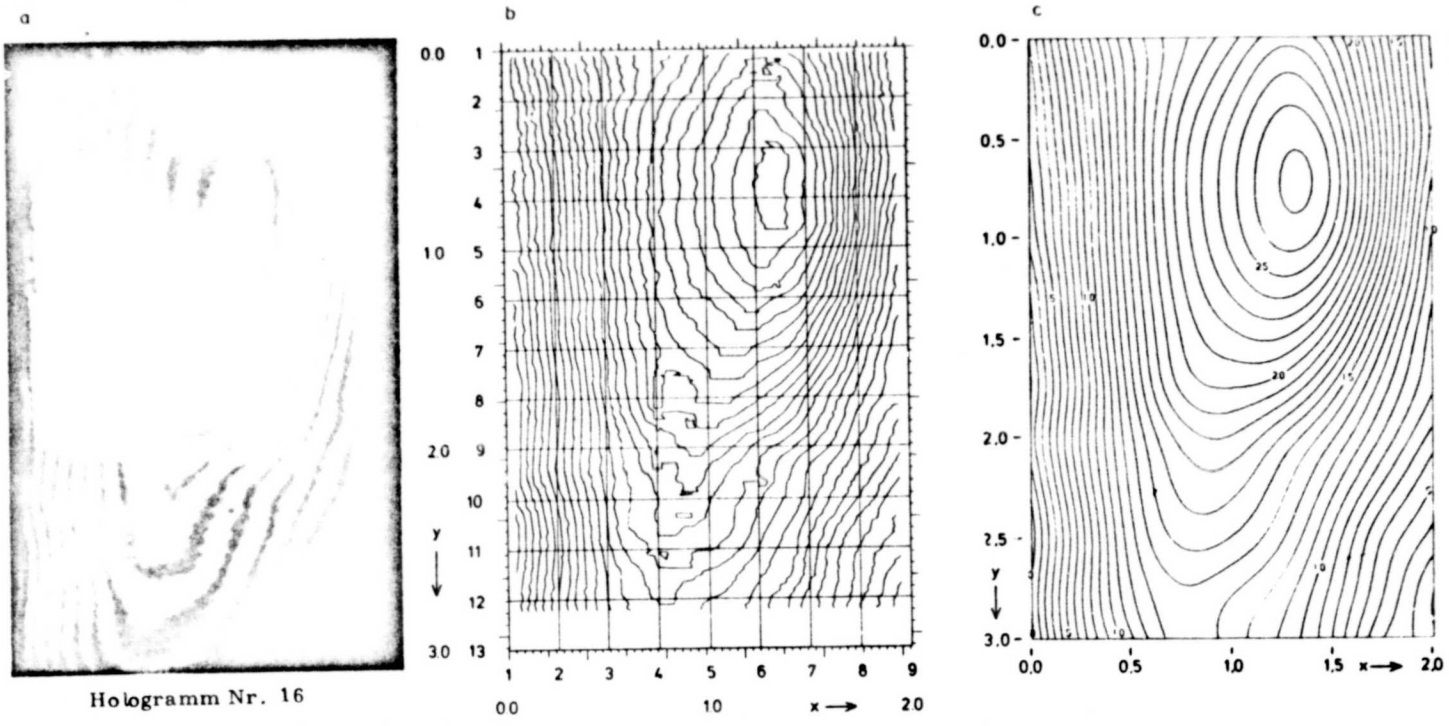

Fig. 18: Example for Interference Fringe Extraction and Polynomial Representation
a) Photo of the hologram to be evaluated (from video monitor of camera)
b) Polygonal representation of recognized fringe edges with coordinate system and grid lines for calculation of polynomial surface.
c) Elevation-line representation of the polynomial function computed from the numbered line picture b).

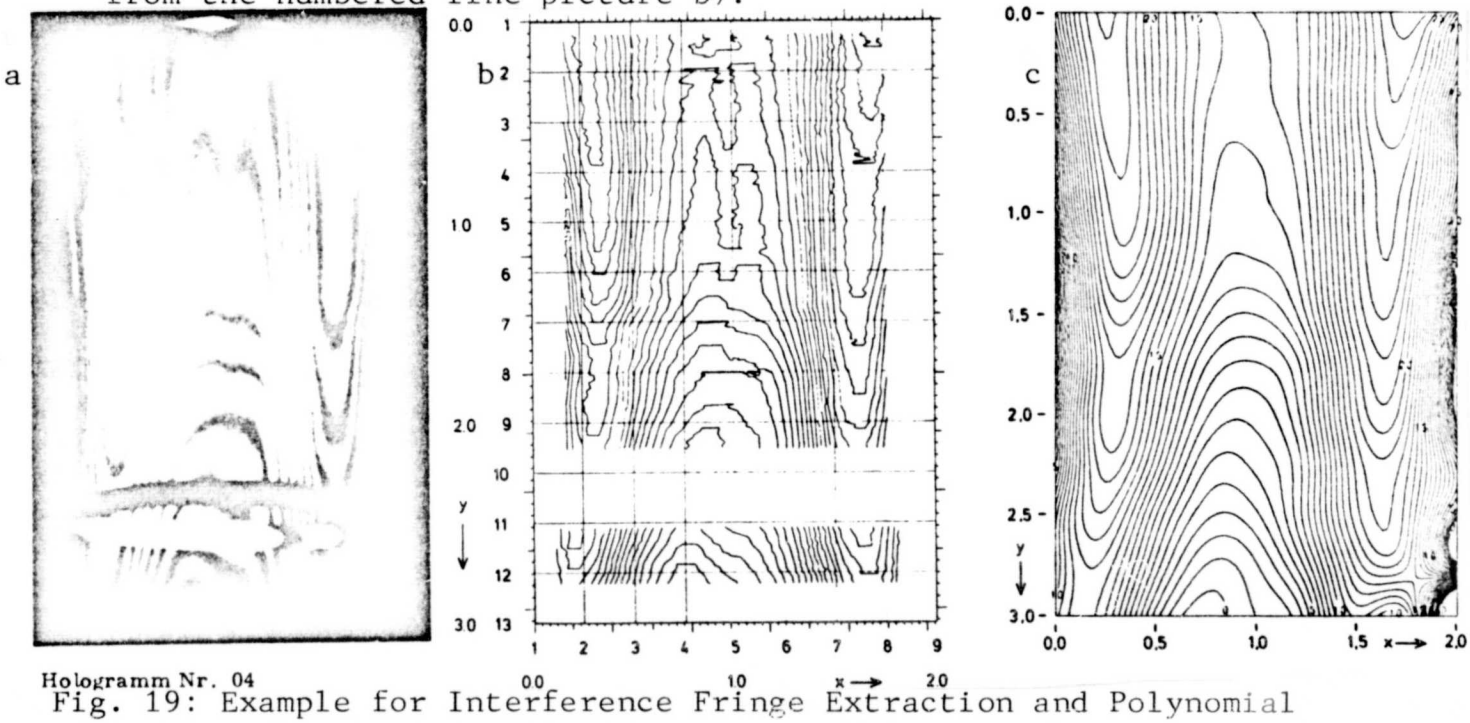

Fig. 19: Example for Interference Fringe Extraction and Polynomial Representation
a) Photo of the hologram to be evaluated (from video monitor of camera)
b) Polygonal representation of recognized fringe edges with coordinate system and grid lines for calculation of polynomial surface.
c) Elevation-line representation of the polynomial function computed from the numbered line picture b)

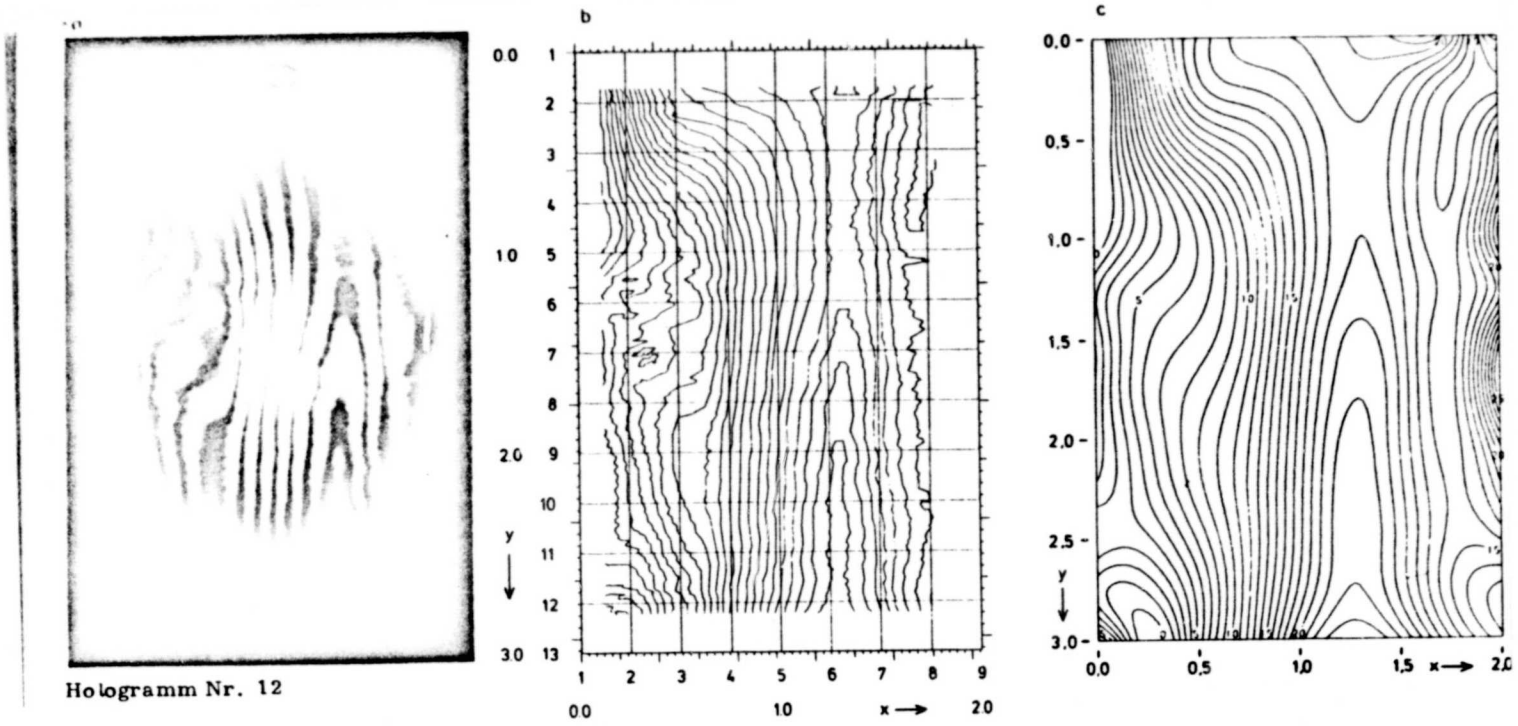

Fig. 20: Example for Interference Fringe Extraction and Polynomial Representation
a) Photo of the hologram to be evaluated (from video monitor of camera)
b) Polygonal representation of recognized fringe edges with coordinate system and grid lines for calculation of polynomial surface.
c) Elevation-line representation of the polynomial function computed from the numbered line picture b).

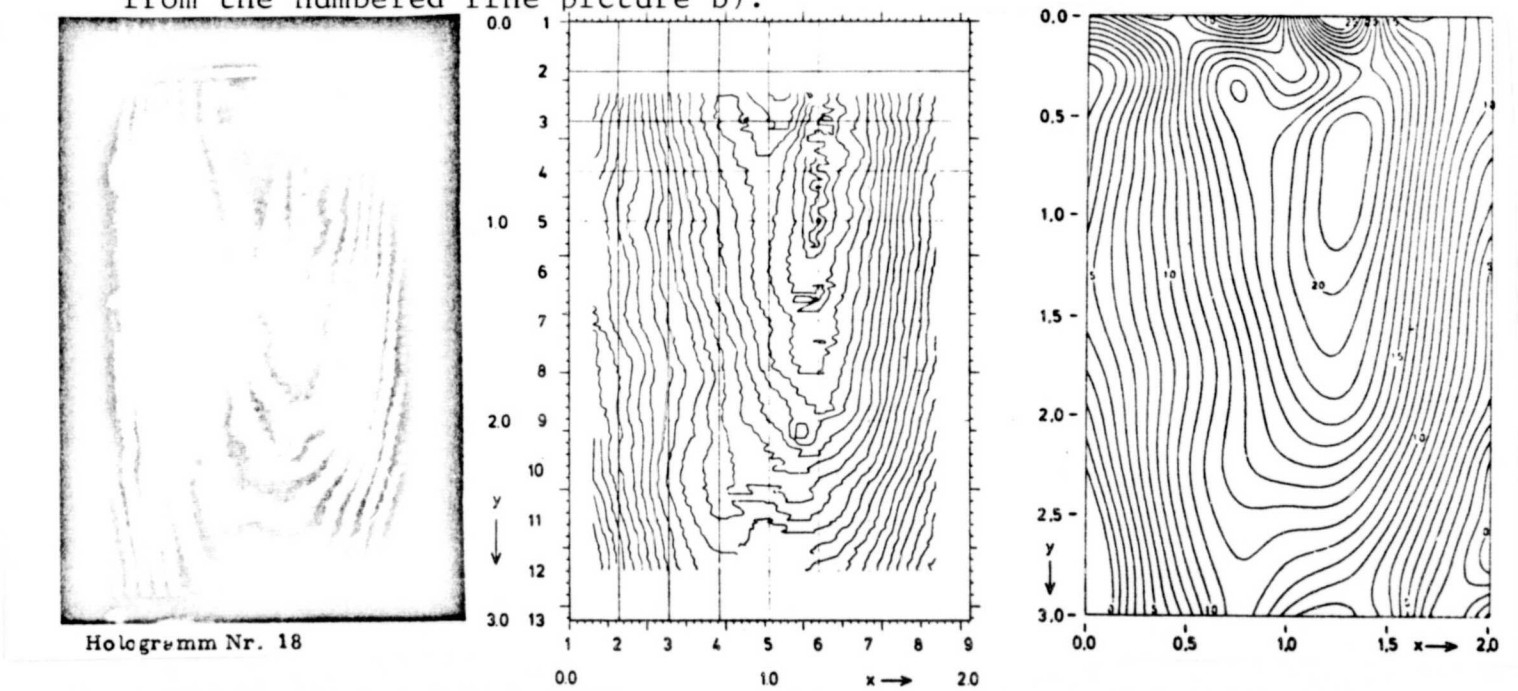

Fig. 21: Example for Interference Fringe Extraction and Polynomial Representation
a) Photo of the hologram to be evaluated (from video monitor of camera)
b) Polygonal representation of recognized fringe edges with coordinate system and grid lines for calculation of polynomial surface.
c) Elevation-line representation of the polynomial function computed from the numbered line picture b).

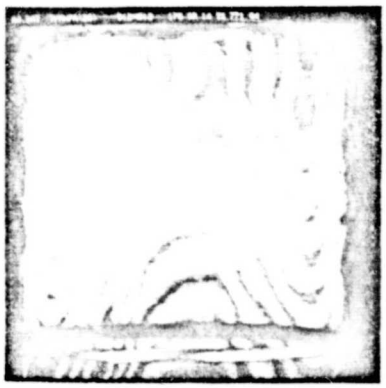

Hologramm Nr. A4

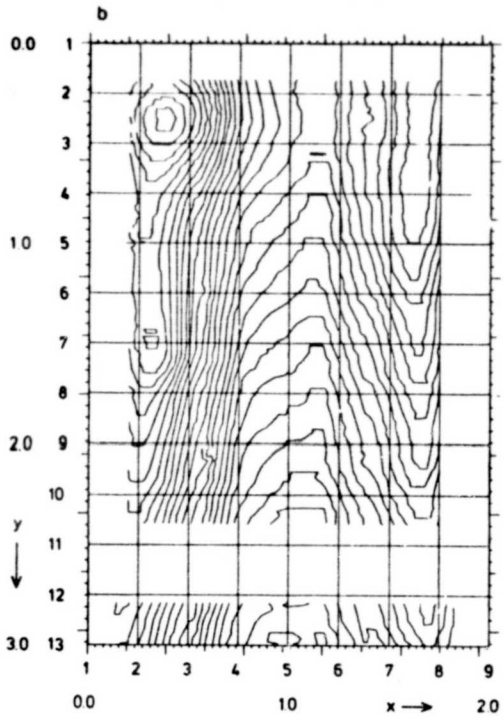

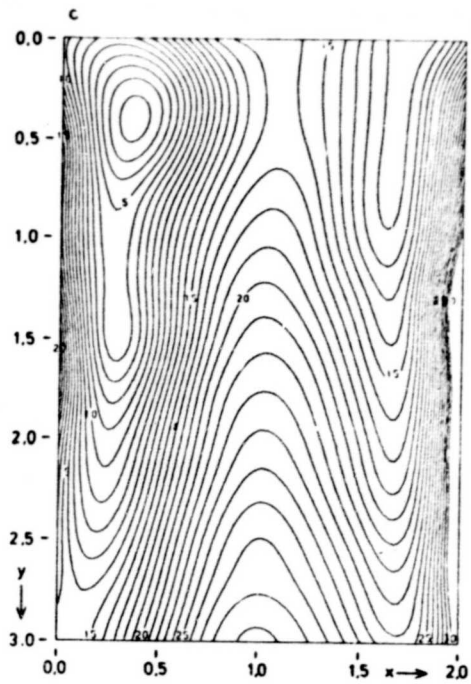

Fig. 22: Example for Interference Fringe Extraction and Polynomial Representation
a) Photo of the hologram to be evaluated (from video monitor of camera)
b) Polygonal representation of recognized fringe edges with coordinate system and grid lines for calculation of polynomial surface.
c) Elevation-line representation of the polynomial function computed from the numbered line pictrue b).

3.5 Sums and Differences of Interferograms

The polynomial representation described in section 3.4 for the interference ordering function can also be used for the computation of time series for the flow interferograms and for averaging over several interferograms. The polynomial coefficients of the appropriate interferograms are simply averaged and an elevation line representation of the resulting surface is examined.

Figure 23 shows an application to interferograms of a turbulent gas jet. In fig. 23b there is a typical polygonal representation, input with the program FAW2, of such a free-jet interferogram, whereas fig. 23c shows an interference ordering function averaged over 20 interferograms. We see that the turbulent fluctuations are generally averaged out and that the symmetry properties are clearly pronounced. Only in this form can the interferograms be compared with results of theoretical calculations [36].

In one application of the polynomial representation to fault recognition in the tire-test holograms, the deep-pass property of this representation is used to recognize small-area surface deformations which frequently means tire defects. For this purpose, the difference with the computed polynomial surface is formed on the points of the line picture. The surface deformations smaller than the mesh width

of the polynomial representation will be distinguished by greater values in this "high-pass fraction". Figure 27 shows two such difference pictures where the size of the deviations from the polynomial representation is made known by different symbols.

It turns out that at the "prominent" places, actual tire defects were concealed. But here, a structure investigation of the environ of these regions must be performed to solidify our information about the type of disturbance and reinforce the diagnosis (see also sec. 4.1).

Another application of the polynomial representation is the elimination of overlapped interference fields. In the tire-test holograms, an interference patterns is present, due to the type of tire-tension and the geometry of the photographic set-up, which cannot be computed from the deformation properties of such a complex material composite system as is a vehicle tire. To investigate the effect of production defects on this basic interference pattern, a so-called "standard hologram" will be found through averaging over a series of tire interferograms, in order to obtain by difference formation with an actual tire interferogram, the interference pattern generated by it based on its individual properties. Figure 28 shows an initial approximation of such a standard hologram averaged from five interferograms. Figure 28 shows some difference interferograms which were formed with this standard hologram.

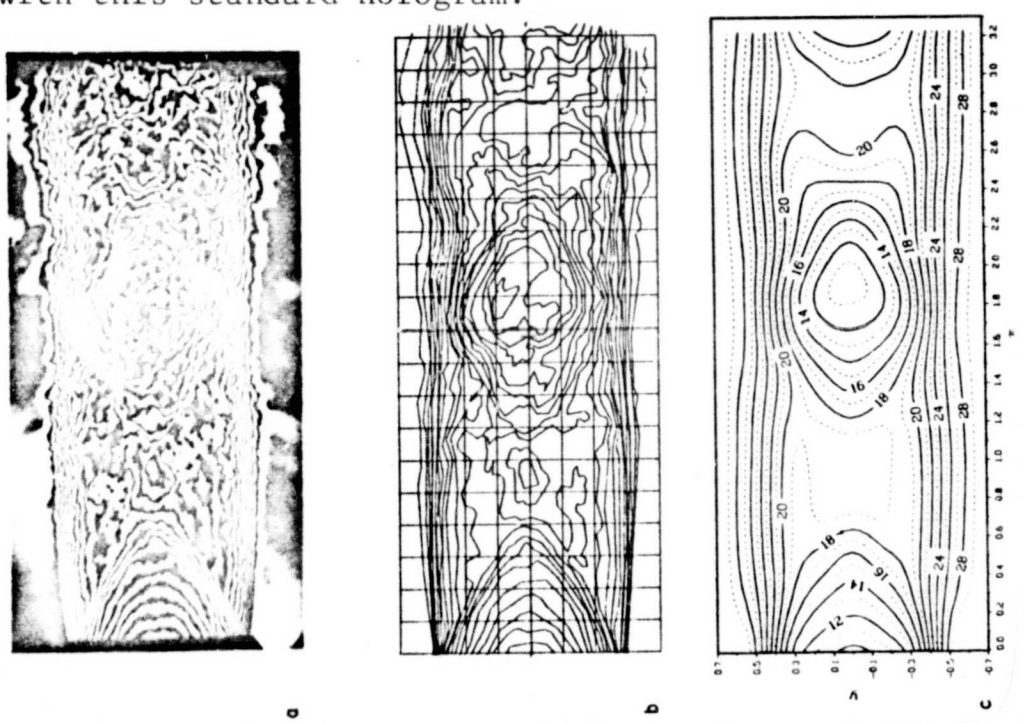

Fig. 23: Example of Interferogram Averaging
a) Photo of an interferogram of a supersonic free jet
b) Fringe profiles of the interferogram and grid lines input manually with the FAW2 program to calculate the polynomial representation.
c) Elevation-grid lines of a polynomial representation averaged over 20 interferograms

Notice here that a "useable" standard interferogram naturally cannot be obtained from an average over only five interferograms. But for reasons of time, a larger series was not considered. The examples here are presented only to demonstrate the properties of the polynomial representation.

3.6 Elimination of Distortion from Object Geometries

In many cases of calculation of the object function, it is necessary to perform a coordinate transformation after the interference ordering function of the object becomes available. For the flow interferograms this transformation is simpler as a rule, since only one coordinate manipulation is needed, and the interference allocation for 2D flows is converted by a linear relation and for rotation-symmetrical flows, by the solution of an integral equation of appropriate density.

For the tire-test holograms, an elimination of distortion from the local coordinates is also necessary in order to permit reversal of the transformation of object points due to the type of photo and reproduction of holograms, and the geometry of the object, and e.g. to specify the localization of certain structures in the holograms in tire-coordiantes. Figure 25 shows a sketch of the distortions occurring in a certain tire-format which are caused by the central projection of a torus in a plane. Since the re-transformation of this image is not possible in a mathematically closed manner, and due to the deviations of the tire from a torus shape, a more accurate accounting for this distortion would be attained through measuring off several points marked on the tire.

To compute a transformation of the plane for random pass points, the KTRANF program was developed. The picture of the digitized object is covered with a regualr grid, similar to the polygonal representation (sec. 3.3). At these grid points (x_i, y_i) are written coordinate values (x',y') of the point in the new coordinate system. In this manner we obtain two imaging functions x'(x,y) and y'(x,y) which are now presented analogous to the procedure in sec. 3.3 with two spline functions, which is why the calculation of the transformation of random intermediate points can be performed simply and quickly.

3.7 Computation Times

The computation time needed for the evaluation of an interferogram is divided into the time for digitizing the patterns, performance of any needed preparatory steps, fringe extraction and numbering of line pictures and finally, the time needed for further processing, like the calculation of the polynomial representation and for fault analysis in tire-test holograms.

The digitizing speed depends on the scanning frequency, i.e. on the resolution used. Due to the line-advance method for video systems of the CCIR-standard, after digitizing a line sequence, we have to wait 20 ms or 40 ms until the next line can be accessed (see sec.2.4).

For a picture with a resolution of 512 x 512 points, about 10 seconds results since two lines are digitized in one pass. As already pointed out in sec. 2.4, this time can be reduced to one-third if several line sequences were scanned in one TV-frame, which would be technically possible. If a chronological signal averaging has to be performed to improve the S/N-ratio due to low-light patterns, as is the case in particular for holograms, the time is multiplied by the number of averagings. If this signal averaging were performed in real time with special hardware (appropriate systems have recently come onto the market), then only one second would be needed for averaging of 25 pictures.

For the other picture preprocessing methods discussed in sec. 3.1, ca. 30 s computation time is needed for a picture size of 512 x 512 points (SMO8), ca. 60 s for the subtraction of the average intensity profile (SUBMF3) and ca. 60 s for the picture-halftone transformation (STREX3). These times contain no access times to external memory media (I/O-time), since for a combination of the methods through sequential processing, an interim-storage of data is not needed. Only the application of the program SUBMF3 requires a storage of data. Another ca. 20 s I/O-time would be needed here.

If two-dimensional filter operations are used for picture preprocessing (as described in sec. 3.1.3), then computation times of ca. 20 min. are needed for one transformation and re-transformation with Fast-Fourier-Transform methods, if the calculation is performed on the PDP 11 computer. The times for the following processing steps like extraction of fringe edges, numbering and polynomial representation depend on the number of fringes in the interference picture and for a typical hologram, amount to ca. 60 s for fringe extraction and redundance reduction of polygon segments (sec. 3.2.2), ca. 40 s for numbering (NUM1) and ca. 210 s for calculation of the polynomial surface (PKF63)(for 117 field points as in fig. 18ff for example). For a complete evaluation of a typical tire-fault hologram with a resolution of 512 x 512 points with time averaging over 20 pictures, spatial averaging, fringe extraction, calculation of the polynomial surface, of the difference hologram without tire-fault analysis, computation times on the order of 10 - 20 minutes are needed. For the evaluation of an interferogram without time and space averaging with calculation of the polynomial surface, about 5-10 minutes is needed. For the evaluation of a flow-interferogram (see sec. 4.2) with a resolution of 512 x 384 points, where a time average over 5 pictures was performed for picture preprocessing, an evaluation time of 2.5 min. was attained per picture up to the polygon-segment representation. These times are quite long for a series evaluation, especially if time-intensive picture preprocessing steps have to be performed for poor image quality, which is why the use of an array processor (AP) was considered for the system. In particular, in the picture preprocessing and calculation of the polynomial surface, the times can be reduced by a factor of 50 to 100 with the use of an array processor, as comparison calculations on an AP have shown. The time-intensive segments of the other programs should be shifted to the AP which will give a reduction in total evaluation time to ca. 20-40 s per interferogram or hologram. Through the use of the AP, methods of two-dimensional filtering can be used for picture preprocessing in series evaluation.

4. Application of Automatic Interferogram Evaluation

An application of the automatic evaluation to the fault analysis of industrial tire-test holograms and to the interferogram evaluation of plane, instationary transsonic flows in Laval jets is described below.

4.1 Evaluation of Industrial Tire-Test Holograms

To check vehicle tires for production defects, Continental Rubber Works Co. uses a holographic method where the tire is registered by a double-exposure method in a partly-evacuated chamber under two different external pressures [8]. One photograph shows one quarter of the tire with a view from the inside to the tire tread. A sketch of the photographic array is shown in fig. 24. The four views of a tire are stored on a hologram film which is advanced after each photo. The size of a hologram is 57 x 33 mm^2 or 55 x 18 mm^2. For reconstruction, the hologram is illuminated with an expanded He-Ne laser beam (Spectra Physics Model 120) and imaged through a wide-angle lens (lens 1:1.8, 4.8 mm (110°)) with a video camera (Philips HQ-LDH 26 with 2/3"-Newvicon XQ 1274). Digitizing occurs as in sec. 2.4 with a resolution of 25 MHz. Of the obtained 1600 points per picture line, 512 points in the line-middle are taken up by the computer and processed.

Figure 25 shows the location of the tire view on the TV monitor. When imaging with the 110°-wide angle lens, an angle range of ca. 85° is evaluable in a photo of 512 lines; when digitizing all 600 evaluable TV-lines, an angle range of 94° could be attained.

In fig. [illegible] the distorted view of the tire surface is presented as an angle network which was computed with the tire size 12 R 22.5 assuming a torus-shaped tire surface. From this presentation, the location-dependent resolution can be read off. In the middle of the picture it is ca. 5 picture points per degree in the tire running direction, or 3 points per degree diagonal to this direction, which corresponds to a picture point size of ca. 1.7 x 1 mm^2 on the tire surface (12 R 22.5).

Through a variation of the air pressure during the double exposure, the tire deforms globally and locally at the places having specific production flaws. The interference pattern thus consists of a more or less large fringe system, depending on tire type, which as a rule is quite narrow out to the tire edges, since a greater deformation occurs there due to existing, smaller material thickness.

Now as a rule, small-area disturbances like curl-shaped line systems with narrow line profile, bulges of parallel-running fringes (primarily in the shoulder region on a line in the tire-roll direction) or jagged fringe deflections are superimposed on this large pattern; these disturbances are attributable to the presence of certain tire production defects. Even fluctuations in fringe width due to an irregular deformation of the tire surface, should be indicative of faults in the tire. The interference pattern describing local tire

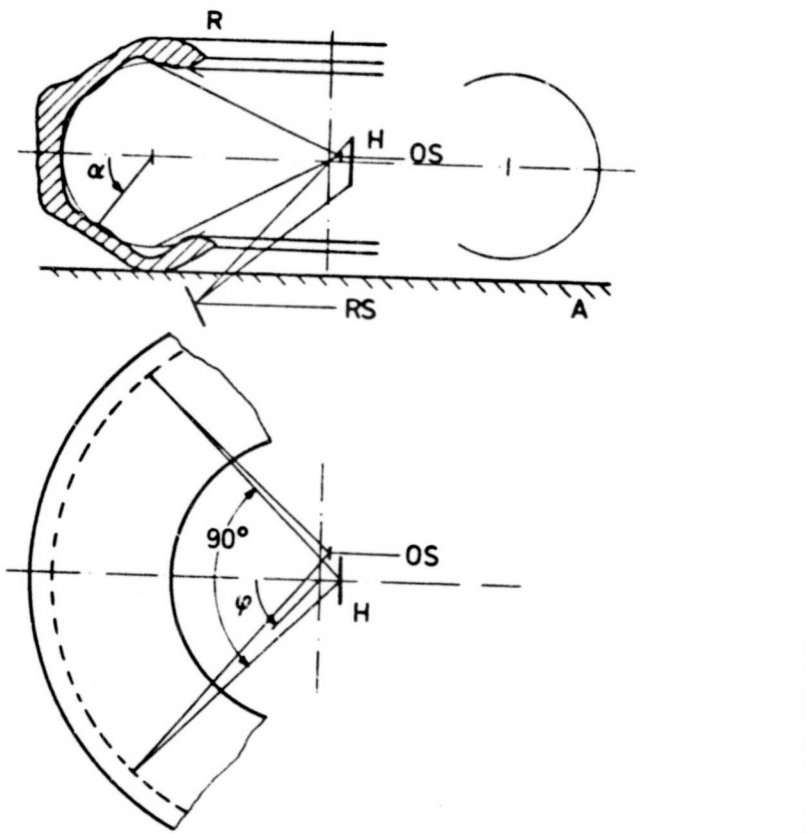

Fig. 24: Sketch of the Photo of a Tire-Test Hologram

R spread-out vehicle time
H Hologram film
OS Object illumination beam
RS Reference beam
A Tire support
α Meridian angle
φ Angle in the tire-running direction

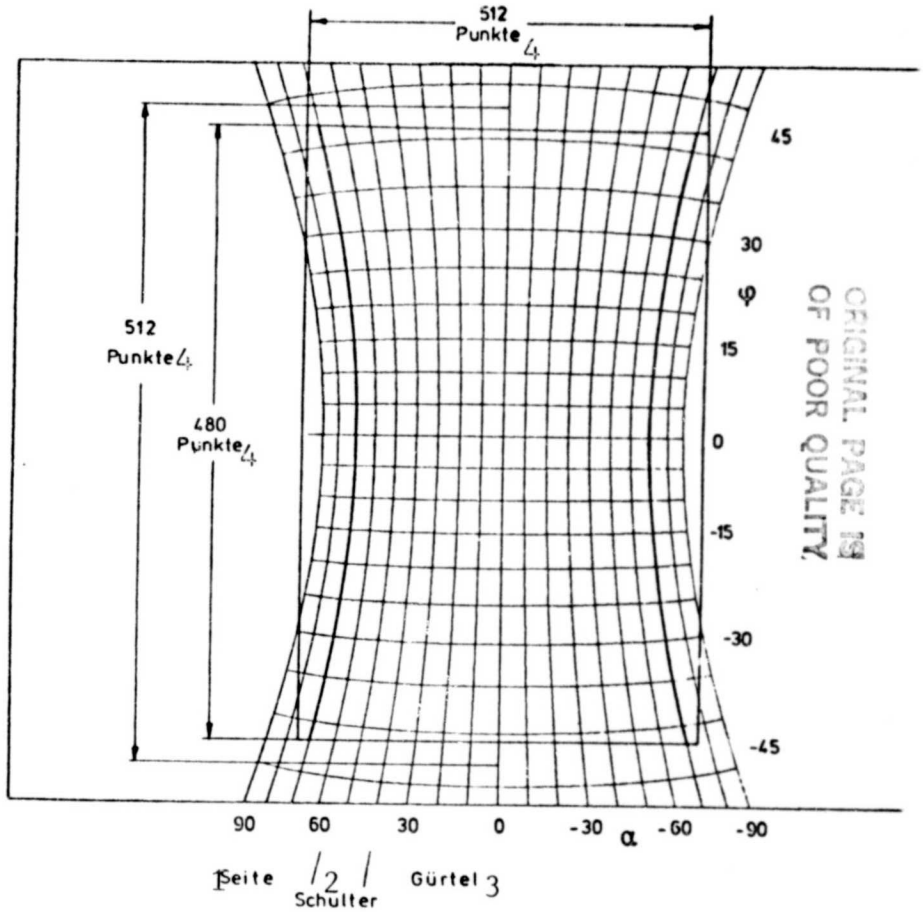

Fig. 25: Sketch of the Distortion of the Object Coordinates by a Hologram Photograph

φ is the angle in the tire-running direction and
α is the meridian angle in degrees

(φ and α are computed here for the tire size 12 R 22.5)
Key: 1-side 2-shoulder 3-belt 4-points

defects is however, not at all unique. For example, a circular fringe system with high line density is not in every case attributable to a tire fault, but only when it appears in an otherwise uniformly running line system. The zig-zags in the line profile of the fringe occur frequently but only under certain conditions represent tire faults (when they appear e.g. to extend over several fringes or are symmetrical to the tire rolling direction).

Some examples of such distortions attributable to tire defects are e.g. seen in fig. 18 (fringe deflection, small circular fringes), in the middle of the top half of fig. 21 (circular line system with high fringe density, small, cohesive line systems), in fig. 22 (small circular structure in the parallel-running fringe field) and in fig. 29 (in the shoulder region there are chains of small structures).

In the photography, reconstruction and digitizing of holograms, a series of disturbances affecting the automatic evaluability and error analysis occurs. Through irregular illumination of the object, due to irregular reflection from the tire surface and the granulation due to speckle formation always present in holograms, and due to scattering which leads to a certain blackening distribution of the hologram which of course, is also imaged due to the great depth sharpness of the wide-angle lens, there results a severe modulation of the background intensity. Furthermore, the hot-bellows impressions (diagonal to the tire-roll direction there are narrow compressions generated in the production process) are quite prominent. On the hot bellows impressions, the fringe system is partly shifted up to one-half a fringe width. In sec. 3.1 methods were presented for subtracting the background intensity and for elimination of the hot-bellows interference pattern through two-dimensional filtering techniques.

Another disturbance caused by the photography of the tire is the imaging of the "spreaders" (those bars holding the tire apart), and their shadows. The spreaders are covered by a fringe system, since they apparently shift somewhat between the two photos. Together with the shadow regions, the spreaders form regions of the picture field where every fringe recognition process fails if the location of the spreader is not known 'a prior'. Another system-induced difficulty consists in the limited resolution of the scan system and the sometimes very low contrast in the holograms. This can cause a severe local deformation in the evaluated line picture--not as a circular line system, but as an irregularity in the profile of the neighboring fringes.

4.1.1 Recognition of Special Structures and Tire Defects

A tire-fault analysis as is desired in automatic test operation, should definitely recognize tires with defects and also permit a classification of the defect by type, size and location; furthermore, the global deformation of the tire should be investigated, including a comparison with a standard type (see sec. 3.5).

One method for this tire-fault analysis was created in two steps. In the first step, the hologram is converted into the polygon-segment representation using the steps described in sec. 3 (with correction of fringe misconnections, sec. 3.2.3).

A simple error analysis can be done based on this data set; it aims at the recognition of certain structures and the computation of certain geometric parameters of the line field representing the fringe profile.

In the second step of error analysis, the numbering of the line field and the calculation of the polynomial representation (sec. 3.3, 3.4) is needed in order to obtain the "high-pass fraction" (sec. 3.5) as an additional potential for local fault analysis, through subtraction of the smooth polynomial representation with the original line picture, and secondly to permit an analysis of the global deformation and a comparison with a standard type.

The steps for implementation of the second stage of the error analysis, like numbering, computation of the polynomial representation, formation of the high-pass fraction and of the standard and difference interferograms, has already be described in sections 3.3, 3.4 and 3.5, so that only the local structural analysis will be discussed here.

For preselection of difficult-to-evaluate holograms, e.g. those with non-resolvable fringe density or with insufficient contrast, first some global quantities are computed, like the ratio of the number of closed lines to the number of unclosed lines, the average line density computed from the total length of all fringes, and the average number of points needed to represent a length unit of the redundance reduced polygon segments.

Difficult-to-evaluate holograms have a high percentage of individual, closed lines, since possibly only fringe-fractions or pseudo-structures are detected here, and can be sorted out by means of the geometric parameters mentioned above.

Regarding the calculation of the scope, area, emphasis and shape factor (3.2) of the closed lines, those lines were sorted out which are to be regarded as an index for tire faults due to their size, shape and location.

In order to make a statement about the fringe width fluctuation important for the tire-test analysis, at each point of a line normal to the average line profile, the distance to the left and right neighboring line is computed. If the ratio AV of the quotient of these distances AQ1 to the quotient of the distances AQ2 in the nearest polygon-segment point of this line which lies at one for parallel fringe profile, differs essentially from it, then a position with strong fringe-width variation exists (see fig. 26).

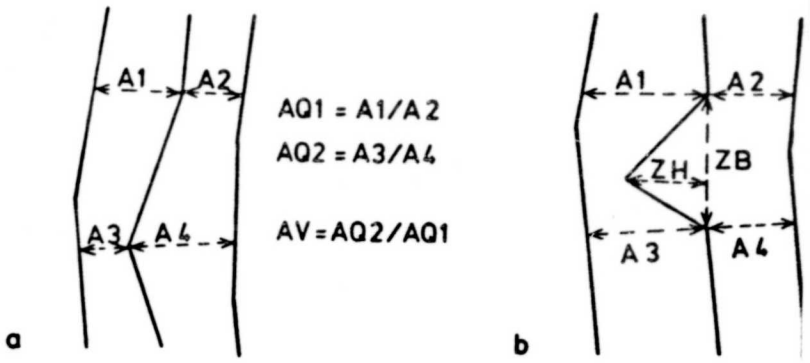

Fig. 26: Sketches for Calculation of
a) the ratio AV and
b) the zig-zag sizes.

Since this criterion responds in a meaningful manner only in regions with global parallel line profile, the local line spacing as the average of distances A_1 to A_4 (fig. 26a) is simultaneously compared with the average line spacing of the entire picture. If the local line spacing is large compared to the average line spacing, or if the point lies at the picture edge, then it is not interpreted as a tire defect.

To investigate zig-zags in the line profile, the change in direction of the polygon segments is considered. A zig-zag is recognized where a direction change $\varphi \cong 90°$ occurs and where the values of certain geometric quantities of the zig-zag, like the shape ZH/ZB and the relative height ZP are present (zig-zag height ZH normed with the average spacing A_1 to A_4; see fig. 26b).

As an example for this structure analysis, in figures 27 and 30 we see the places where a tire fault was found in the particular hologram due to variations in fringe width; these points are denoted by a square, and the places where the threshold values for detection of zig-zags were exceeded, are denoted by a circle.

Upon comparison with the corresponding holograms, we see that the tire faults were localized quite well, but that a fault classification was not possible, since at many places the sawtooth criterion is responsible and at other places, it is the spacing criterion, where actually another situation is present. Another problem is the selection of threshold values. If they are too small, even places not in regions of tire faults will respond.

Since tire faults look quite different in the polygonal picture, one natually cannot expect that only one method will detect all tire faults. Instead, the various methods like determination of severe variations in fringe width, zig-zags and the difference picture (see fig. 27) must be considered together. Because only through the linkage of these methods is a sure detection of tire faults possible.

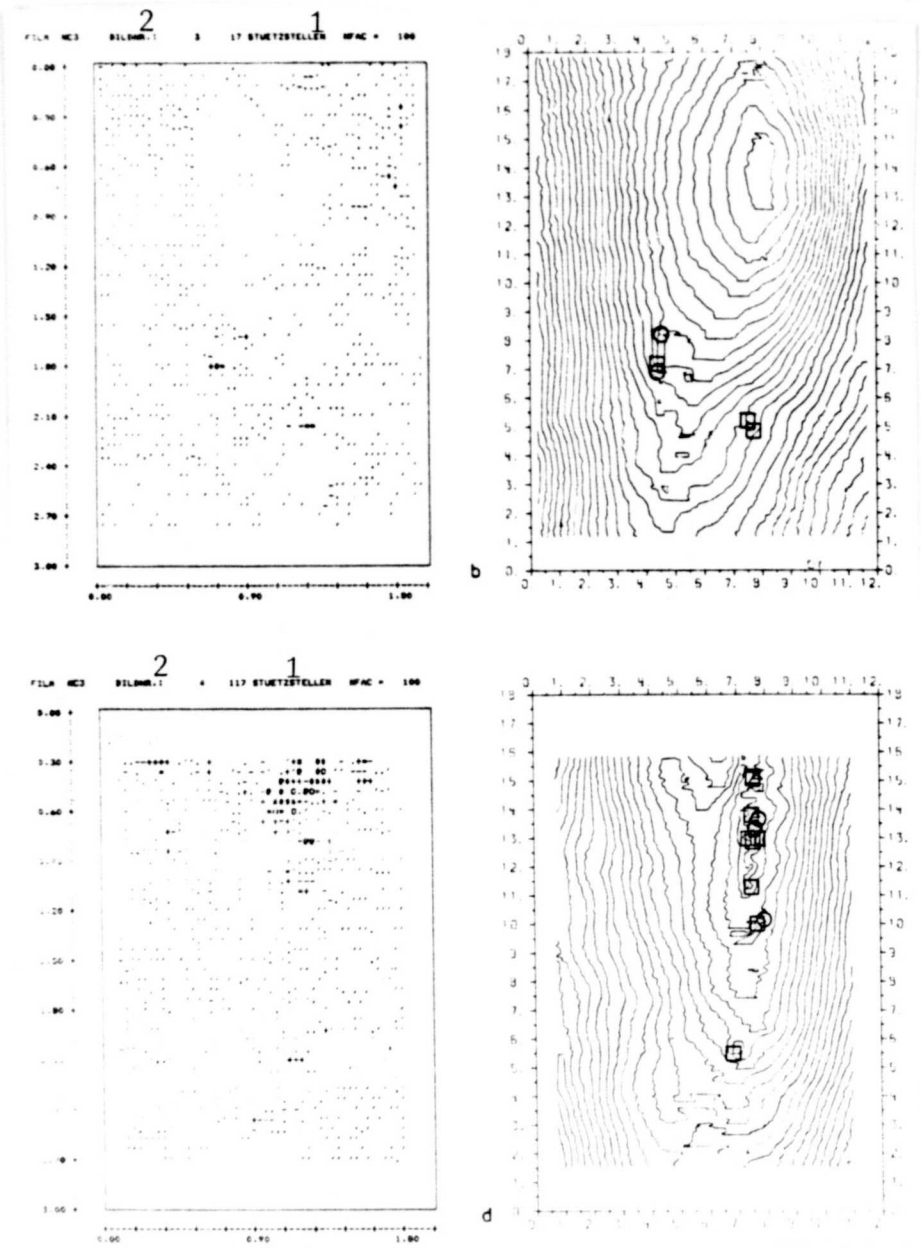

Fig. 27: High-Pass Portion and Examples for Structrue Analysis

a) and c): Differences of the polynomial surface of the hologram no. 16 or no. 18 at the line-points of the fringe field ("high pass portion")(the deviations are marked with the symbols '-+=0e*#, and ' corresponds to a difference of 0.075 and # to a difference of 0.75 fringe widths)

b) and d): Regions with tire defects detected by means of sutructural investigation.

Key: 1-field points 2-picture number

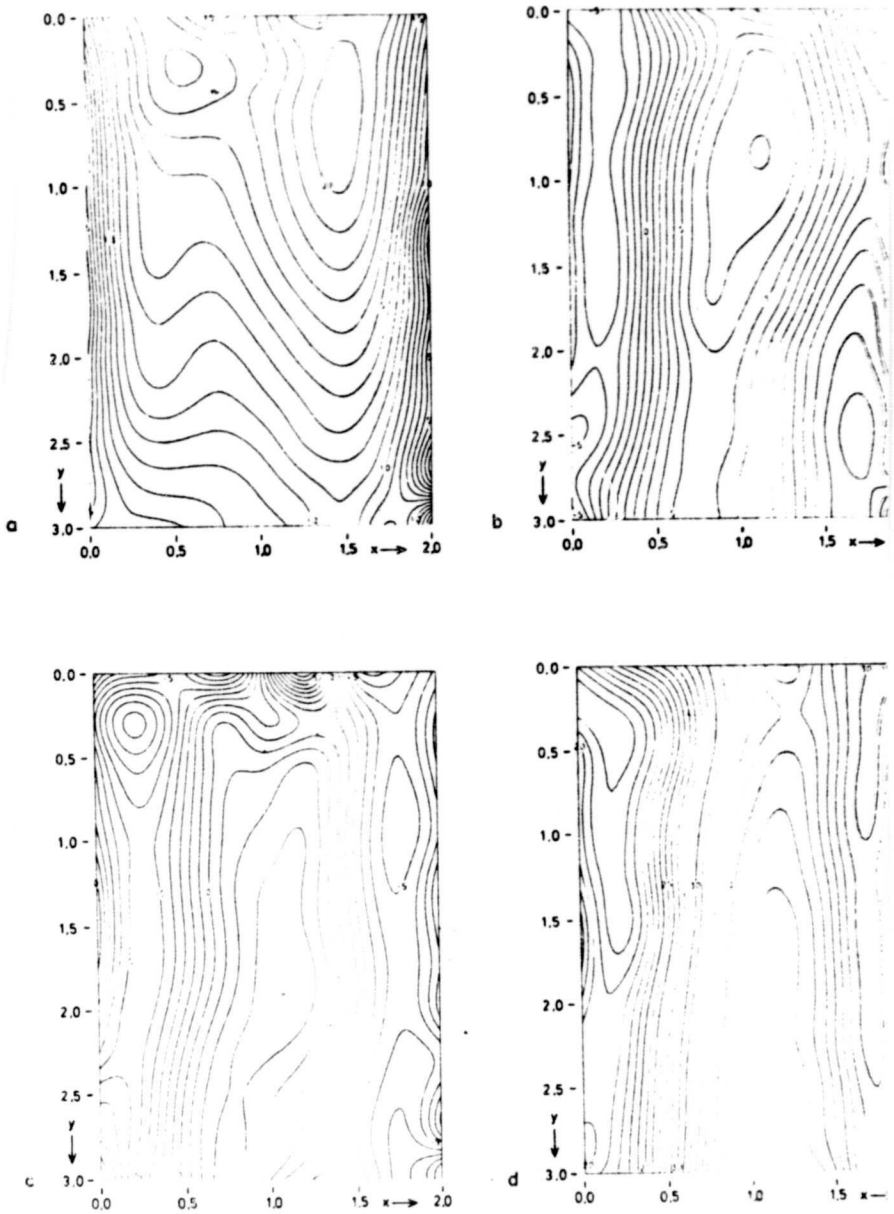

Fig. 28: Example for Difference Interferograms

a) Representation of the elevation lines of a "standard hologram" averaged from the holograms of figs. 18 - 22.
b) Elevation line representation of the difference of hologram no. 16 to the standard hologram a)
c) Like b), hologram no. 18
d) Like b), hologram no. A4

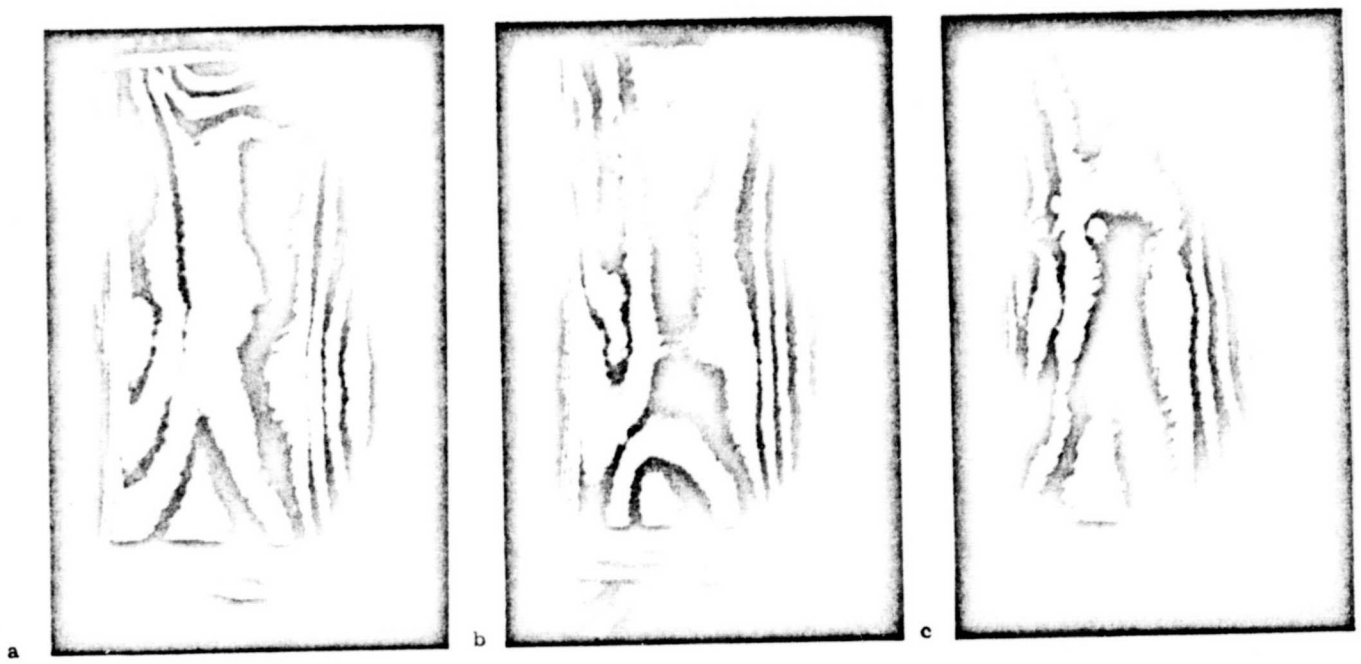

Fig. 29: Holograms No. 21, 22 and 23 for Comparison with the Fault localization in fig. 30. (Photos by video monitor of the camera).

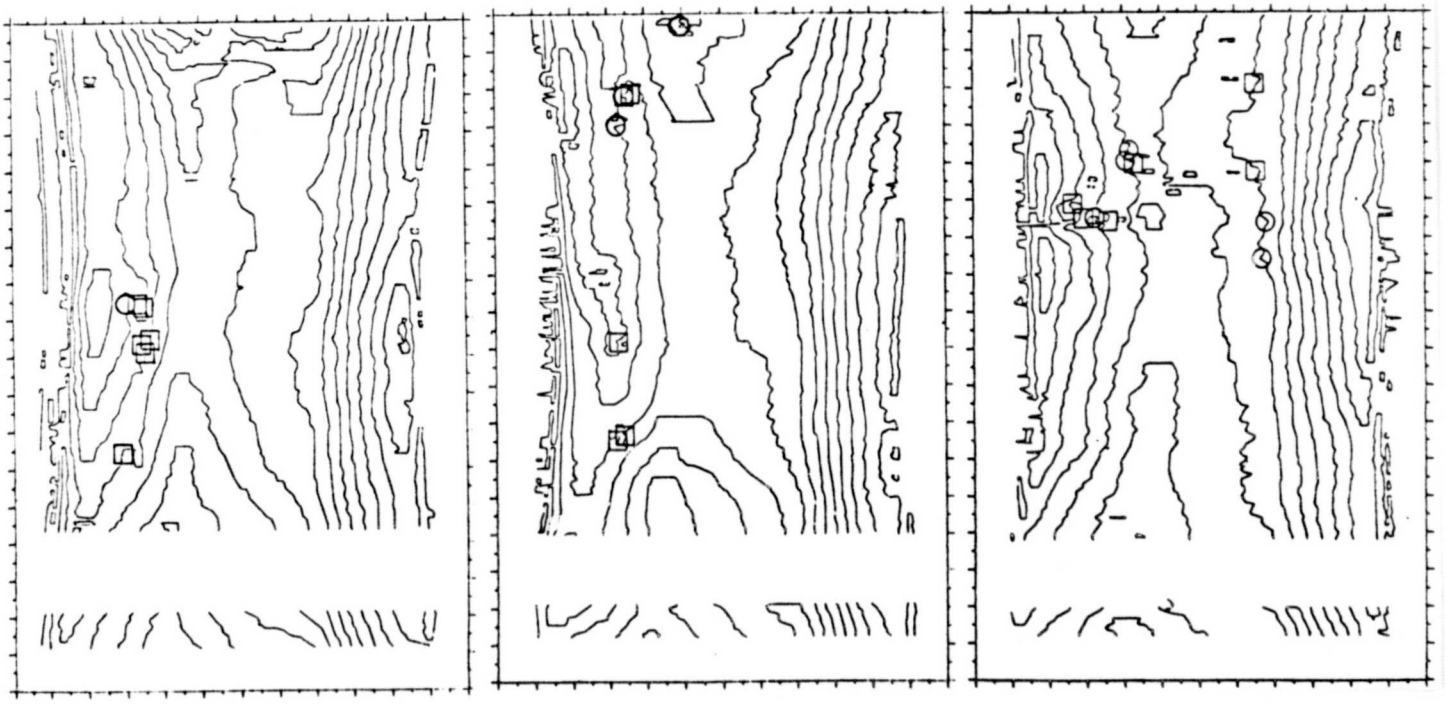

Fig. 30: Places Suspected of being Tire Faults Determined by Means of the Structure Analysis in the Holograms of Fig. 29.

The meaning of the global tire-deformation discussed above, on the tire-fault analysis is not yet clear; additional investigations on this topic are underway by Continental Co. An initial approximation of a standard hologram was obtained by averaging over the five holograms of figures 18 - 22. It is presented in fig. 28 in addition to several difference interferograms computed from it (see sec. 3.5).

4.1.2 Possibilities for Improving tire-Fault Recognition

A certain, automatic tire-fault analysis presumes a satisfactory fringe recognition, which in turn places certain requirements on hologram quality. If no photography-induced disturbances were present in the holograms, then the programs of structural analysis could be linked together more easily, so that they would not respond in regions without tire faults.

Basically, many problems could be avoided by undertaking some improvements to the hologram photograph; presently these problems of fringe detection, numbering and tire-fault analysis have to be solved by very time-consuming methods. We are thinking primarily of the hot-bellows impressions, illumination (contrast) and spreaders.

The hot-bellows impressions are often quite distinct in the holograms because the tire shifts between the two photos, which could be prevented by an improved tire seating. Through a better illumination of the object, where all stray light would be kept away from the hologram surface, the greatly variable brightness distribution in the holograms could be smoothed out. A disturbance due to the location of the spreader rods in the field of vision could be easily prevented by a spreader device which grasps the tires from the outside.

For the introduction of a picture evaluation system described here into automatic tire-fault recognition, the use of an array processor to accelerate the evaluation is urgently advised, as discussed in sec. 3.7.

4.2 Mach-Zehnder Interferograms of Flat Jet Streams

To investigate the instationary behavior of transsonic flows, at the Max Planck Institute for Flow Research, pressure was measured at selected points and velocity measurements with Laser-Doppler methods were used, but primarily interferometric methods were tested [9-11]. The planar test route stretching between two mirrors of a Mach-Zehnder interferogram has one of the split lightwaves passing through diagonally to the flow direction and undergoes here a path difference to the other beam proportional to the density of the flowing medium (see also sec. 1.1.1).

To observe dynamic processes, the interferograms are registered on film using high-frequency cinematographic methods. Figure 31 shows a sequence of some typical interferograms of the flow in a Laval jet.

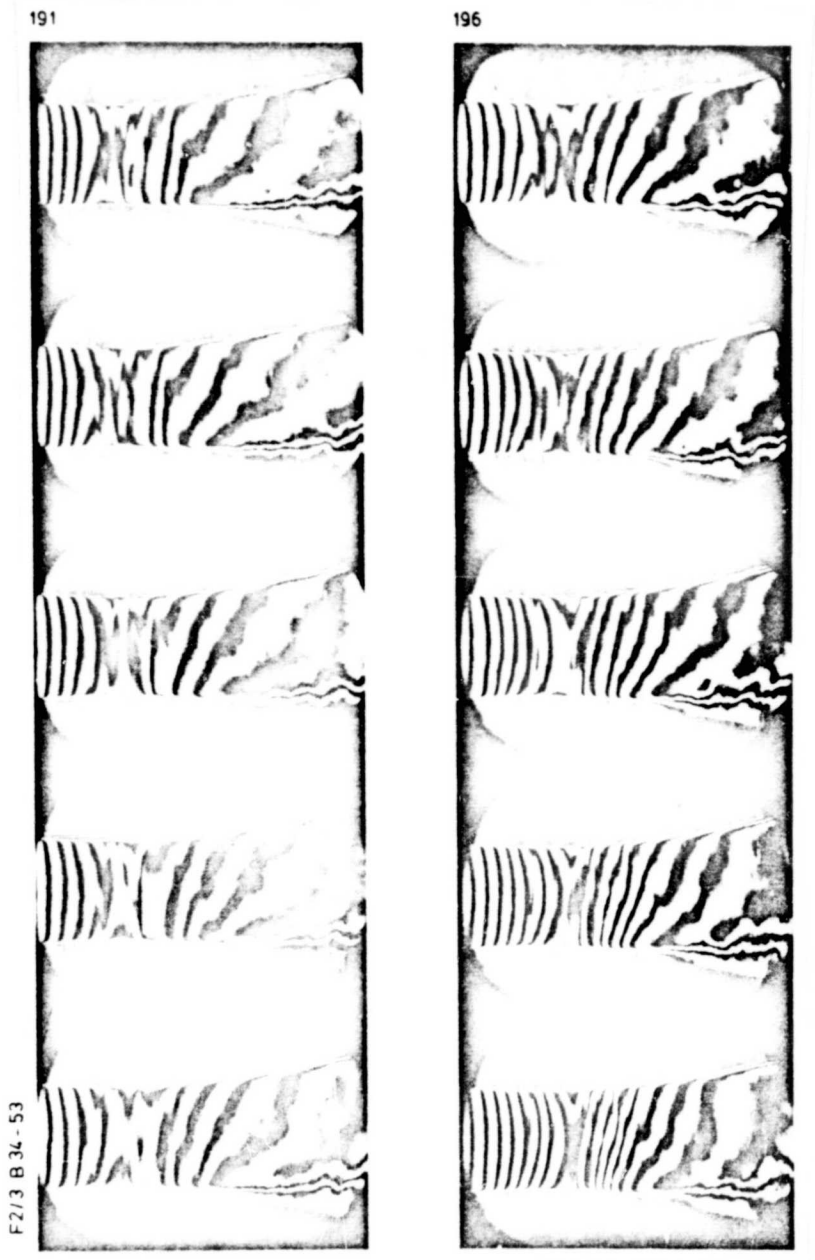

Fig. 31, part 1: Interferograms of a Planar, Instationary Flow in a Laval jet. Formation of a compression shock (chronological distance between the pictures: 0.1 ms, flow direction from left to right)

The chronological picture spacing is one-tenth of a millisecond here. The registration took place with a drum-camera (Strobokin, Impuls-physik Co.) and a spark light source (flash time 1 µs) on 16 mm film.

Typical for the interferograms of such flows is the relatively large-area fringe profile in the subsonic flow. Due to the set pressure difference, the flow accelerates which leads to a density drop, especially in the divergent jet-region, which increases the fringe density. After

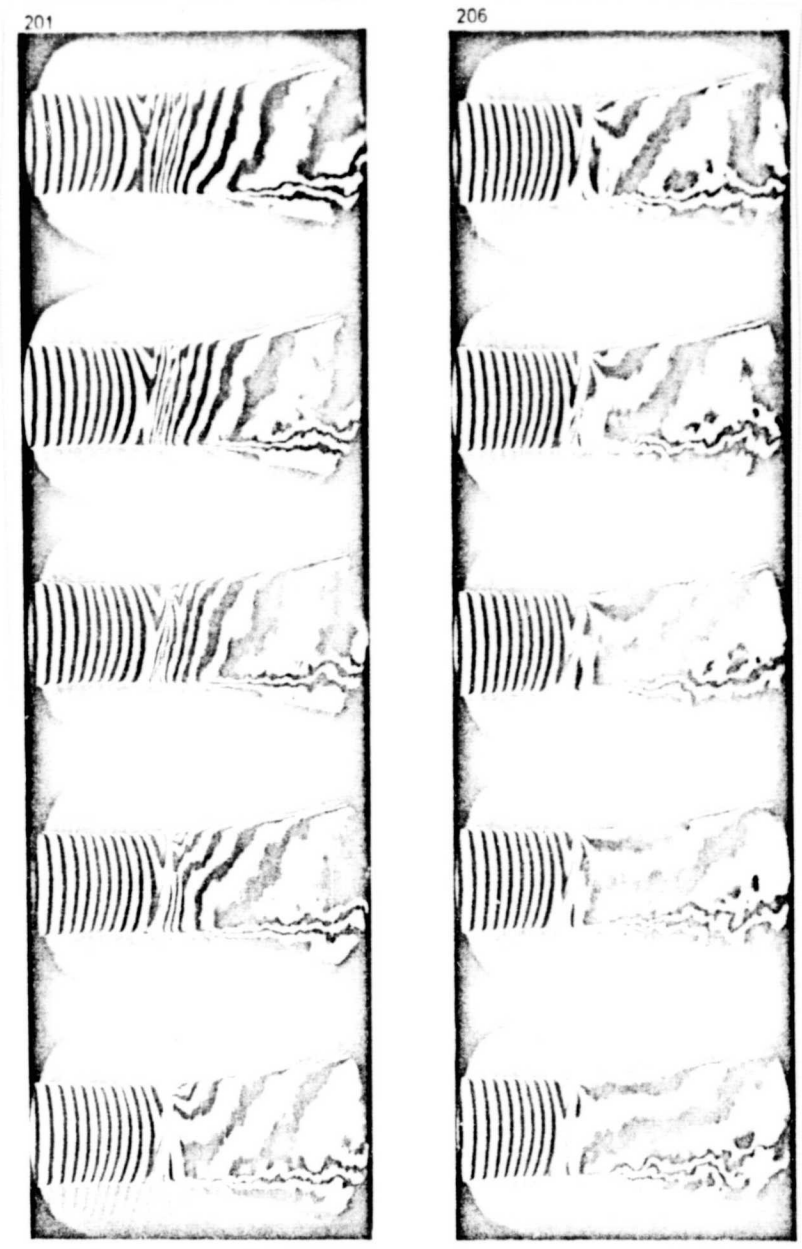

Fig. 31, part 2: Interferograms of a Planar, Instationary Flow in a Laval jet. Formation of a compression shock (chronological distance between the pictures: 0.1 ms, flow direction from left to right).

reaching the speed of sound at the narrowest cross-section (marked in the interferograms by a thin wire), the flow velocity in the divergent part of the jet goes back to subsonic due to a perpendicular compression shock. This shock is not stationary, but moves upstream by interaction with the wall boundary-layer in which a flow-cavitation is generated by the pressure gradient of the shock [11]. Since the shock includes the cavitation point of the wall boundary-layer, there is a self-sustaining instability which causes the shock finally to break down the entire supersonic region and to disappear upstream.

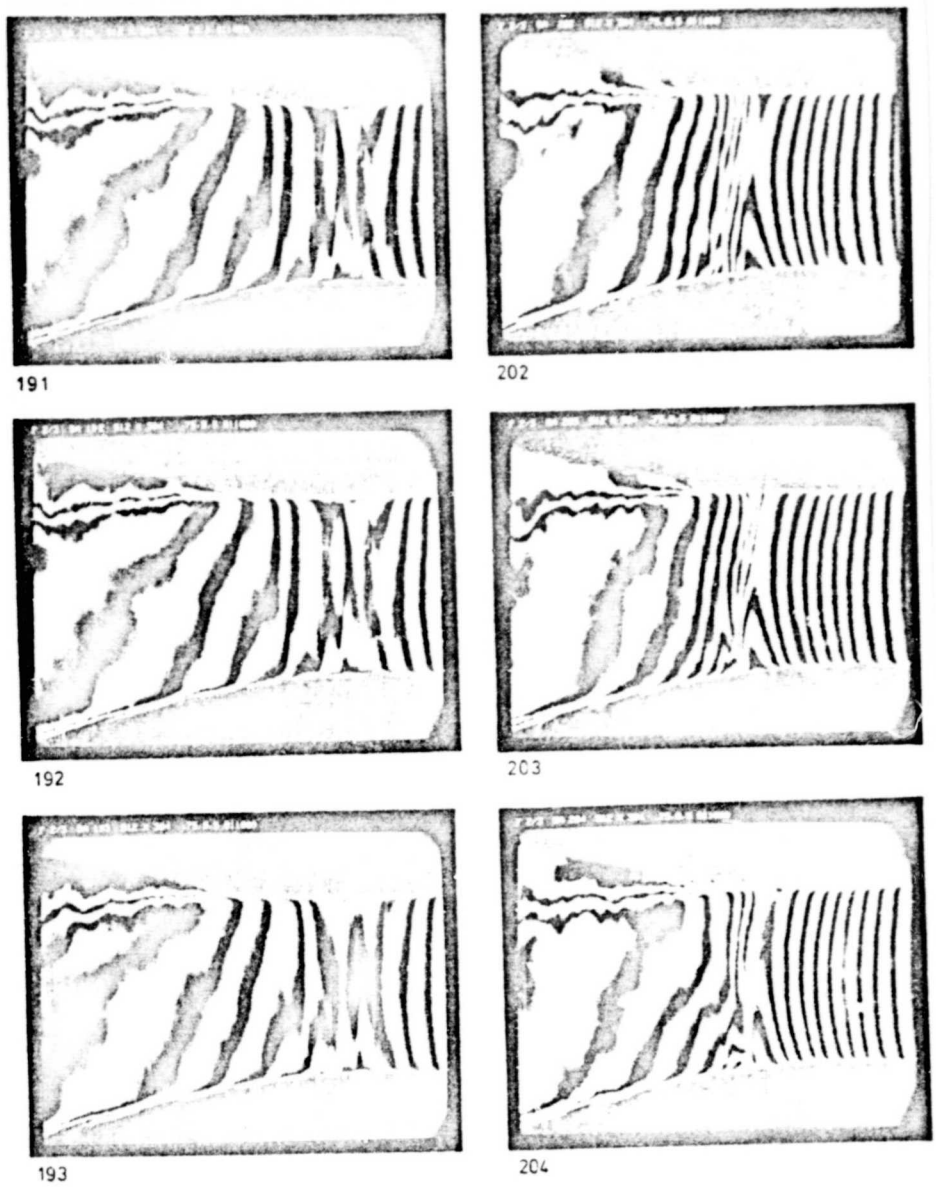

Fig. 32: Several of the Interferograms from fig. 31 after Digitizing
(Resolution 512 x 384 picture points, 8 bit)
(Presentation is distorted for reasons discussed in sec. 2.4).

In the area of the compression shock and in the area of the boundary layer, the fringe densities are so high that they can no longer be resolved by the film material or by the digitizing system. This leads to the appearance of fringe misconnections in an automatic evaluation, when several fringes run into such an area.

As an example to illustrate the resolution limits, figure 32 shows several of the interferograms from fig. 31 after digitizing, with a resolution of 512 x 384 picture points. The reproduction occurred as discussed in sec. 2.4 with a halftone resolution of 16 steps via the VT-11 video terminal. It should be remarked here, that due to an

increase of the scanning accuracy, the problem of fringe misconnections in the shock and in the boundary layer, cannot be solved. Only the location of such misconnections is shifted into a picture region with even denser fringe profile, which naturally increases the accuracy of fringe detection there, but could not prevent the appearance of fringe misconnections. An increase in scan accuracy with the same picture size would not only increase the quality demands of the optical sensor and digitizing system, but also increase the data quantities and thus the computation times to such an extent that the evaluation of interferograms would no longer be possible in the desired time and apparatus framework. The occurrance of such disturbances must therefore be taken into account by using the method of localization of fringe misconnections (sec. 3.2.3) and of fringe numbering (sec. 3.3).

For fringe numbering, two statements derived from the nature of the object can be used. First, we recognize the place where the speed of sound is reached (Ma = 1) in a supersonic flow. For the relative density, we have the following expression:

$$\rho/\rho_o \mid_{Ma=1} = \left(1 + \frac{\kappa-1}{2}\right)^{-\frac{1}{\kappa-1}} \qquad (4.2.1)$$

With $\kappa = 1.4$ (air) and equation (1.1.7) results the following expression for the interference order N at p = 760 Torr, T = 293 K and $\lambda = 575$ nm:

$$N|_{Ma=1} = 0.173 \cdot h, \qquad (4.2.2)$$

where h is the channel depth in millimeters. For a channel depth h = 100 mm, the fringe of order 17 sets in for a Laval jet at its narrowest cross-section (Ma = 1). Secondly, from the profile of the fringes in the boundary layer we obtain information about the direction of increasing or decreasing fringe order. Since in the boundary layer there is frictional heat and a heat exchange takes place with the wall, the flow here is no longer isentropic. Through differentiation of the isothermal equation of state for ideal gases, we obtain the relation:

$$\frac{dp}{p} = \frac{d\rho}{\rho} + \frac{dT}{T} \qquad (4.2.3)$$

With the fundamental theorem of boundary-layers, according to which the pressure from the outer flow remains unchanged in the boundary layer, normally for the wall we have $\partial p/\partial n = 0$ and:

$$\frac{d\rho}{\rho} = -\frac{dT}{T} \qquad (4.2.4)$$

Since there is heat addition to the boundary layer, the density must decrease near the wall. Now if an interference fringe represented in the interferometer setting at "fringe width infinite" by a line of constant density, is diverted into the boundary layer with or against the flow, then the interference fringe order decreases in this direction.

A difficulty occurring in the digitizing of interferograms consisted in the localization of the picture location on the film. Due to a small chronological discrepancy between the synchronization signal derived from the film perforation and the triggering of the

light flash, the vertical position of the film picture is inconstant and fluctuates up to ca. 20% from a central position. Due to an irregular winding of the film on the drum of the camera, a lateral shift of the film picture can occur, which varies slightly from picture to picture. A compensation of such picture shifts can be implemented practically only by the determination of the coordinates of certain, prominent fixed structures relative to the object. In order to be able to use the least object-dependent method which is applicable for all flow contours brought into the channel, the use of so-called fitting or reference points (e.g. by drilling into the wall contour) would be needed, whose location in object coordinates is known. These reference points should be quickly and easily recognized by a high contrast and by a location outside the measured field by the evaluation system. However, in the interferogram films available for the evaluation, such reference points do not exist, which is why the known flow contour must be used here as a reference. Theoretically, the current position of the picture would be obtained by a correlation of the digitized film picture with a mask of the flow contour. But since this procedure seemed uneconomical for reasons of anticipated computation time and programming effort, a simplified contour-search algorithm was developed which depends on the geometry of the investigated object and which may have to be modified for different flow bodies. In addition, it is assumed that besides any occurring, small initial rotation, no additional twisting of the interferogram on the film occurs.

With this method the average absolute deviation in the considered line section is first formed by a sliding line average of the preceeding line segments and compared with a bound. Since in the region of the jet-wall an average gray value prevails which is superimposed by inhomogeneities of the background and by noise from the electronic components, once the wall contour is exceeded in the region of the measured field covered with interference fringes, deviations from the average-value obtained above, will occur. In order that the method not be distorted by a film inhomogeneity, like a spot occurring in development, a dust grain on the film or a film scratch, the determined length of the narrowest cross-section is compared with the specified, known theoretical length. In case of a deviation from this theoretical length, the process of contour search is repeated with appropriately changed threshold, until the position is located with sufficient accuracy, or the evaluation of the picture is discarded if after a specified number of attempts, no convergence has occurred, which can be the case e.g. for a missing or improperly lighted picture. The formed bound is now used as the starting value for the next picture in order to achieve a faster convergence.

To determine the horizontal shift, in these interferograms a thin wire marking the narrowest cross-section and running diagonally over the measured field, is used. In order to do this, the columns within the measured field are analyzed in a region which must contain the position of the wire, based on preceeding pictures. The wire, like the wall regions, is illuminated only by one beam of the interferometer and thus has an average gray value of relatively uniform profile. The location of the wire is assumed to be at that

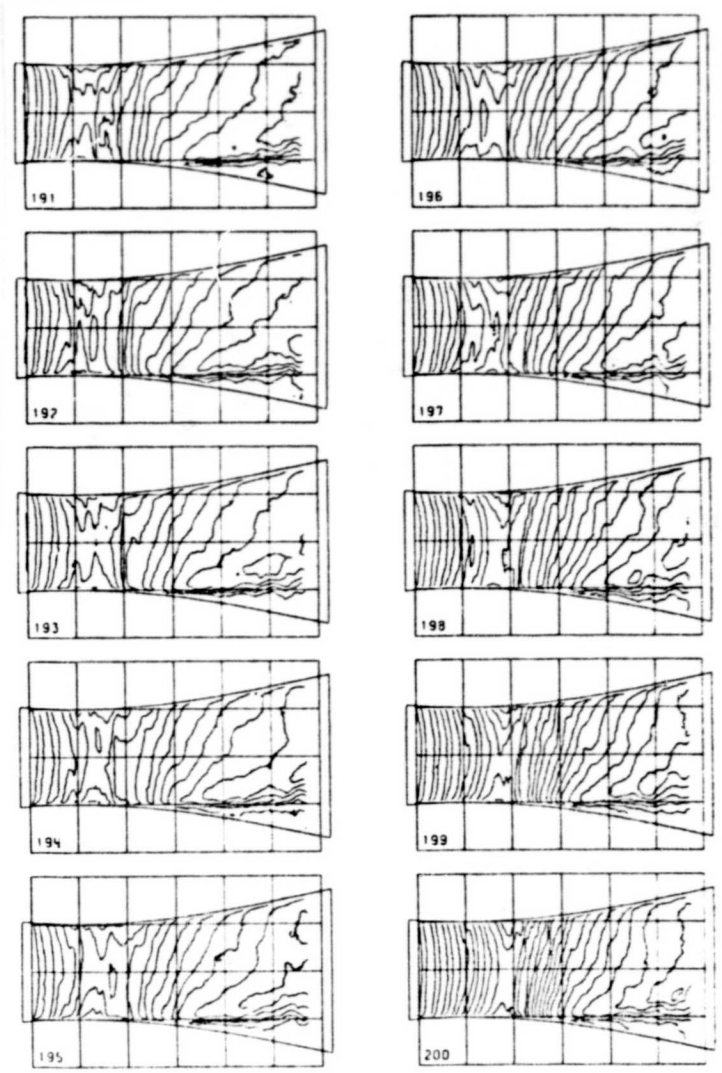

Fig. 33, part 1: Profile of the Flank Lines of the Interference Fringes from fig. 31, after segmentation.

place where the sum of the squares of the deviations from the average value, has its minimum. In order than any uniform interference fringe extending over the entire region will not disrupt the detection process, the newly-found value is compared with the old one and in case of an excessive deviation, it is replaced by the old value itself. In order that the wire does not disturb the following fringe recognition process, the gray values in the region of the wire are replaced by fitting a spline function in the line direction and extrapolation over the points lying in the neighborhood of the wire.

The discussed method of simplified contour position determination has proven to be excellent in practice. In ca. 1000 evaluated interferograms, the method failed only once because there was a relatively large spot in the region of a jet contour (probably caused by an air bubble in the development of the film). The times for contour position

determination are on average 5 seconds, which is hardly important considering a total evaluation time of 2.5 minutes per interferogram.

In figure 33, the polygon segments of the fringe edges are presented after fringe extraction and a coordinate transformation, corresponding to the interferograms of fig. 31. The averaging of gray values over the wire at the narrowest cross-section, was eliminated here in order to recognize the profile of the wire at the partly deflected lines there and to allow comparison with its theoretical position. In the illustration of the fringe edges, the profile of the edge contour and a grid network are presented in object coordinates for better comparison.

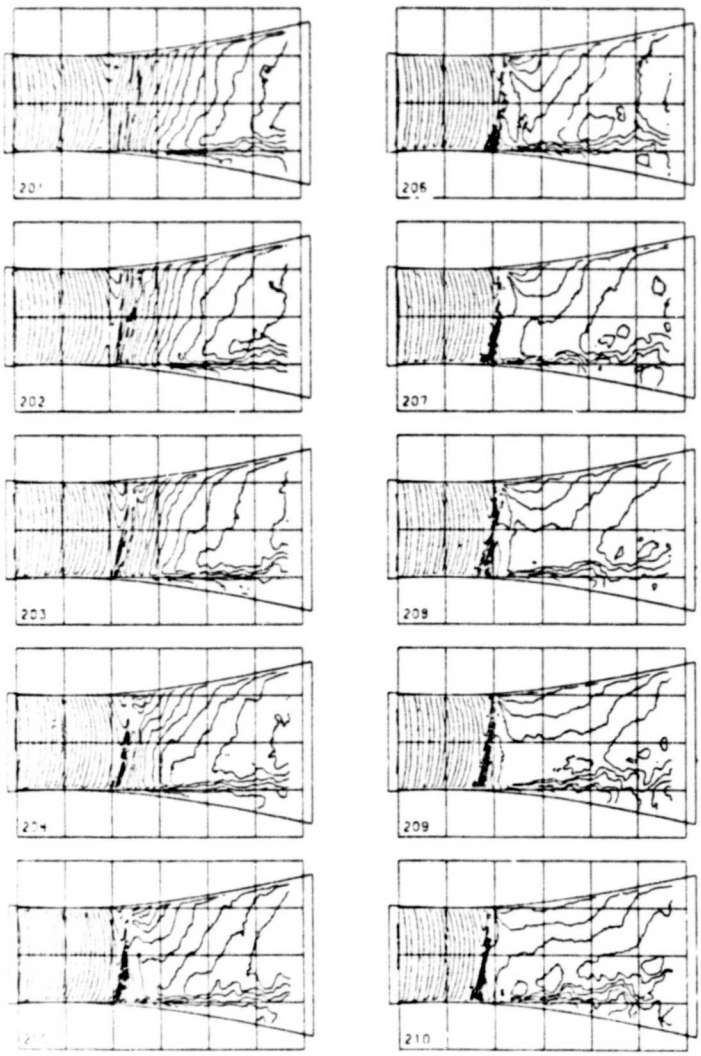

Fig. 33, part 2: Profile of the Flank Lines of the Interference Fringes from fig. 31, after segmentation.

5. Appendix

5.1 List of Programs

Listing of the main program segments for evaluation of interferograms with a brief description of function (a complete listing of most of these programs, and of the used routines, is found in greater detail in [37]).

Program segment	Description
BVSF BVSF2	Elimination of fringe misconnections and fringe interruptions
FAW*	Manipulation of graphic data: Input via curve digitizer, display and modification on graphic terminal
KON	Contrast determination
KOORT	Transformation of the polygonal points
MOSKO1	Generation of an edge mask from a polygonal representation of the edge
NUM NUM1A NUM3	Fringe numbering, strategy 1 " " " 2 " " " 3
PKF63	Polynomial approximation
PTST*	Spline representation; cut-representation on the screen; calculation of difference and standard holograms; calculation of curvatures
RFEL	Structure investigation, tire-fault analysis
SMO8	Spatial averaging
SOBMAX	Gradient formation with Sobel operator
STREX*	Halftone transformation with fixed threshold Halftone transformation with local-dependent threshold
STR2*	Polygonal representation of the interference fringes from a preprocessed, digitized picture or execution of digitizing and preprocessing for continuous evaluation.
SUB	Picture subtraction of two digital pictures
SUBMF3	Subtraction of background brightness
TRANSP	Transposition of a dig. picture
DS6 DS7A	Halftone output of digitized pictures via graphic terminal
HIS	Calculation and display of a gray-value histogram
MN6 MN7A	Digitizing of single pictures with different resolutions and averaging over several, single pictures
RD1	Display of sections of digitized pictures in isometric projection
TLE	Aux. program to display indiv. picture lines on the screen
LCT,F DAMP DCLR CFFT DRFT	Execution of a 2D Fourier transformation, back- & forth-transformation, calc. of amplitudes, filtering.

5.2 Structure Plan

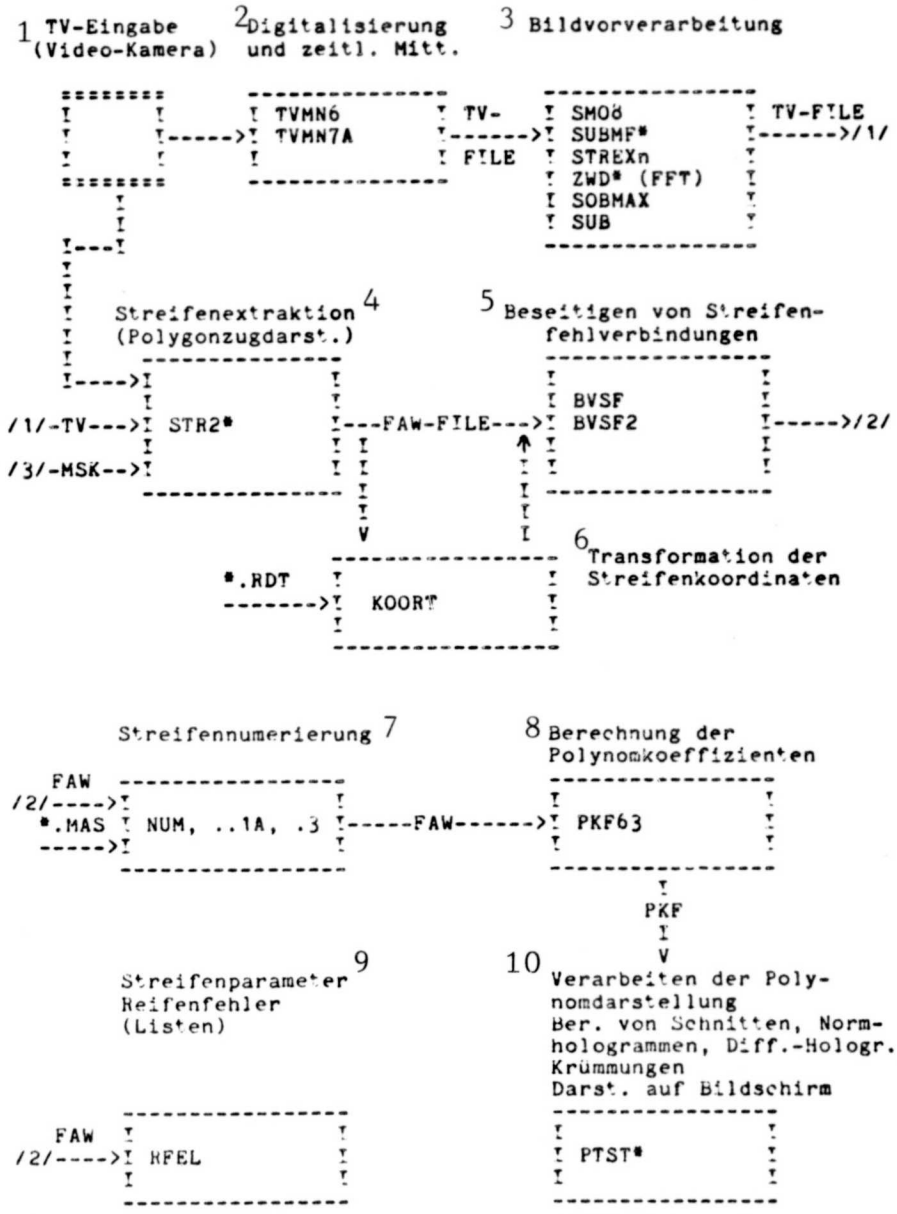

Key: 1-TV input (video camera) 2-digitizing and time-averaging 3-picture preprocessing 4-fringe extraction (polygonal rep.) 5-elimination of fringe misconnections 6-transformation of fringe coordinates 7-fringe numbering 8-calc. of polynom. coefficients 9-fringe parameter, tire-defect (lists) 10-processing of polynom. rep. Calc. of intersections, std. holograms, diff. holograms, curvatures Presentation on screen

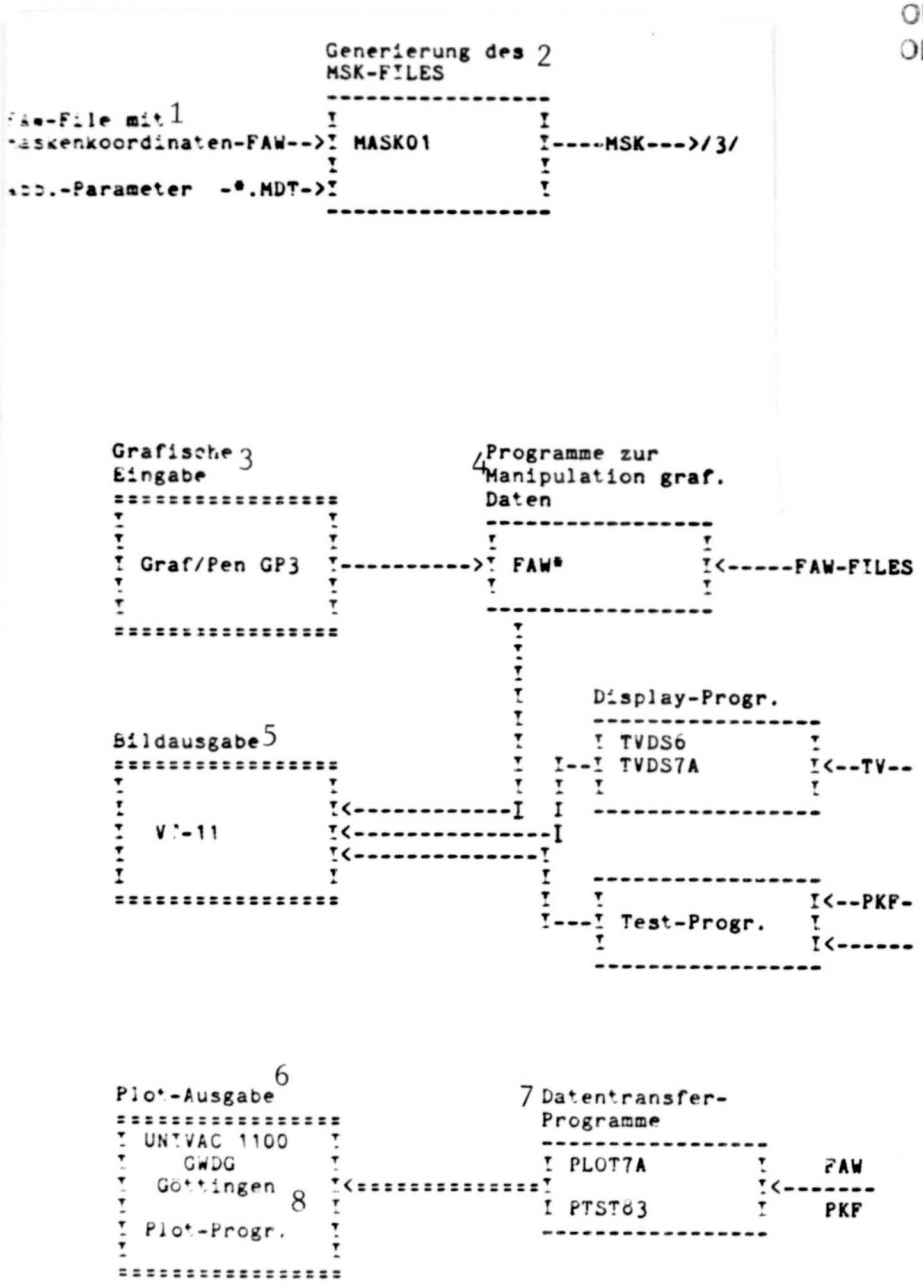

Key: 1-FAW file with mask coordinates 2-generation of MSK file
3-graphic input 4-programs for manipulation of graphic data
5-picture output 6-plot output 7-data transfer program
8-Goettingen Computer center, plot program

6. Bibliography

[1] Berggren, R.: Analysis of Interferograms. Optical Spectra (12, 1970), 22-25.

[2] Freniere, E.R., Toler, O.E., Race, R.: Interferogram evaluation program for the HP-9825A Calculator. Opt. Eng., V. 20, no. 2 (4, 1981) 253.

[3] Kreitlow, H., Kreis, Th.: Development of an Equipment System for automatic static and dynamic evaluation of holographic interference patterns. Laser 79 Opto-Electronics, Munich 2/6 July 1979, Conference Proceedings, IPC Science and Tech. Press, London 1979, 426-436.

[4] Fischer, B., Geldmacher, J., Jüptner, W.: Investigations on the automatic detection and processing of holographic interference patterns with the line-scan method. Laser 79, Opto-Electronics, Munich 2/6 July 1979, Conference Proceedings, IPC Science and Technology Press, London 1979, 412-425.

[5] Fischer, W.R., Crostack, H.A., Steffens, H.D.: Automatic Analysis of holographic interferograms for non-destructive testing. Laser 79 Opto-Electronics, Munich 2/6 July 1979, Conference Proceedings, IPC Science and Technology Press, London 1979, 404-411.

[6] Nukadate, S., Magome, N., Honda, T., Tsujiuchi, J.: Hybrid holographic interferometer for measuring 3D deformations. Opt.Eng. V. 20, no. 2 (4, 1981), 246-252.

[7] Schlüter, M.: Analysis of holographic interferograms with a TV picture system. Optics and Laser Technology 12, (1980) 93-95.

[8] Krüger, R.: Non-destructive tire testing with Double-exposure holography. ATZ Automobiltechnische Zeitschrift 79 (1977) 10, 439-442.

[9] Meier, G., Hiller, W.: High-frequency interferometer as the basis for statistical-numerical vibration analysis in instationary, planar, transsonic flows. High Speed Photography, Proc. 8th Int. Congr. (1968) Wiley and Sons.

[10] Meier, G.E.A.: Shock induced flow oscillations. AGARD Conference Proc. no. 168 (1974), 21-1 - 29-9.

[11] Meier, G.E.A.: An instationary behavior of transsonic flows. Reports from the MPI for flow research and the AVA, Göttingen, no. 59 (1974).

[12] Felske, A., Happe, A.: Vibration Analysis by Double Pulsed Laser Holography. Soc. of Automative Engineers, Paper no. 770030, Detroit (1977).

[13] Kohlrausch, F.: Praktische Physik (Practical Physics), vol. 1, 22nd Ed. p 408, Teubner Stuttgart 1968.

[14] Schumann, W., Dubas, M.: Holographic Interferometry, Springer Series in Optical Sciences, V. 16 (1979).

[15] Jacobi, M.: A Holographic interferometer for real-time high-speed photographs of extended phase objects. Graduate work, University of Göttingen 1978.

[16] Lanzl, F., Schlüter, M.: Video-Electronic Analysis of Holographic Interferograms. SPIE V. 136, 1st European Cong. on Optics Applied to Meteorology (1977) 166.

[17] Sollid, J.E.: Holographic Interferometry Applied to Measurements of Small Static Displacements of Diffusely REflecting Surfaces. Aplied Optics V. 8, no. 8 (1969), 1587.

[18] Dändliker, R., Ineichen, B., Mottier, F.M.: High Resolution hologram interferometry by electronic phase measurement. Opt. Commun. V. 9, no. 4 (1973), 412.

[19] Kohler, H.; Interference-line dynamics in the evaluation of holographic interferograms. Optik 47 (1977), 9-24.

[20] Ramer, U.: An Iterative procedure for the Polygonal Approximation of Plane Curves. Computer Graphics and Image processing, V. 1 (1972), 244-256.

[21] Becker, F.: The computer-supported evaluation of interferograms Graduate work, University of Göttingen, 1978.

[22] Späth, H.: Spline Algorithms for Construction of Smooth Curves and Surfaces. R. Oldenburg Pub., Munich, Vienna 1973.

[23] Hecht, E., Zajac, A.: Optics. Addison-Wesley Publishing Co. 1974 p 397.

[24] Pratt, W.K.: Digital Image processing. Wiley, New York, 1978.

[25] Brigham, E.O.: The Fast Fourier Transformation. Prentice Hall, 1974.

[26] Rosenfeld, A., Thurston, M., Lee, Y.H.: Edge and Curve Detection: Further Experiments. IEEE Trans. EC, V. C-21, no. 7 (1972) p. 677-714.

[27] Hueckel, M.H.: A Local Visual Operator Which Recognizes Edges and Lines. J. ACM. V. 20, no. 4 (Oct. 73), p. 634-647.

[28] Martelli, A.: An Application of Heuristic Search Methods to Edge And Countour Detection. Com. ACM, V. 19, no. 2 (1976), p. 73-83.

[29] Schindler, K.P., Lincoln, D.N., Flossdorf, J.: FRINGE Programs to Evaluate interferograms with an HTV-C 1000 Camera. Gesellschaft für Biotechnologische Forschung mbH, Braunschweig 1979.

[30] Agrawala, A.K., Kulkarni, A.V.: A Sequential Approach to the Extraction of Shape Features. Computer Graphics and Image Processing V. 6 (1977), 538-557.

[31] Clenshaw, C.W., Hayes, J.G.: Curve and Surface Fitting. J. Inst. Maths. Applics (1965), pp. 164-183.

[32] Cadwell, J.H., Williams, D.E.: Some orthogonal methods of curve and surface fitting. The computer Journal, V. 4 (1961/62), pp. 260-264.

[33] Cadwell, J.H.: A least-squares surface fitting program. The Computer Journal, v. 3 (1960/61), pp. 266-269.

[34] Hayes, J.G., Halliday, J.:The least squares fitting of cubic spline surfaces to general data sets. J. Inst. Maths. Applics 14 (1974), pp. 318-324.

[35] McLain, D.H.: Drawing contours from arbitrary data points. The Computer Journal 17, no. 4 (1974). pp. 318-324.

[36] Grabitz, G., Hiller, W.J., Meier, G.E.A.: The density distribution of rotation-symmetric supersonic free jets exiting against a slight overpressure and underpressure. In U. Müller, K.G. Roesner and B. jSchmidt (Ed.): Recent Development in Theoretical and Experimental Fluid Mechanics--Compressible and Incompressible Flows. Springer Verlag, Berlin-Heidelberg-New York 1979, p. 144-156.

[37] Becker, F., Meier, G.E.A., Wegner, H.: Programs for interferogram evaluation. Part II of the final report on research project Development of an instrument for Evaluation of Interferograms. BMFT 13 N 5083 (5, 1981).

Acknowledgement

Thanks are due Prof. E.A. Müller, Ph.D. for allowing me to perform this work at the Dept. for Applied Mechanics and Flow Physics and for obtaining access to the Max-Planck Institute for Flow Research and for his positive interest in promoting the work.

My special thanks are due my editor, Dr. G.E.A. Meier, whose continuing interest and numerous suggestions have contributed so richly to the success of the work, and for the application and support of the evolution of the BMFT project connected with this work.

Mr. H. Wegner deserves my gratitude for his efforts in programming, especially for the development of fault-search programs for the tire-fault analysis.

Mr. W. Krämer and R. Plotzki performed the installation and repair work to the computer system, Mr. R. Dvorak provided support in electronic problems and Mr. D. Knauer and H.W. Kompart helped with the implementation of software installations in the computer link. Miss B. Behre typed the manuscript.

The performance of this work was supported financially by the Federal Ministry for Research and Technology (BMFT Project no. 13 N 5083) and by Continental Gummiwerke Co., Hannover, who are due a special debt of gratitude.

In conclusion, I wish to thank my family, especially my wife, for her understanding and patience, especially in the final phase of the work.